

Towards Non-Abelian Quantum Signal Processing: Efficient Control of Hybrid Continuous- and Discrete-Variable Architectures

Shraddha Singh^{1, 2, *}, Baptiste Royer³, and Steven M. Girvin^{1, 2}

¹*Department of Applied Physics and Physics, Yale University, New Haven, Connecticut, USA*

²*Yale Quantum Institute, Yale University, New Haven, Connecticut, USA*

³*Département de Physique et Institut Quantique,
Université de Sherbrooke, Sherbrooke, Québec, Canada*

(Dated: April 29, 2025)

Robust quantum control is crucial for operations below the quantum error correction threshold. Quantum Signal Processing (QSP) transforms a unitary parameterized by θ into one governed by a polynomial function $f(\theta)$, a feature that underpins key quantum algorithms. Originating from composite pulse techniques in NMR, QSP enhances robustness against systematic control errors. We extend QSP to a new class – non-abelian QSP, that utilizes non-commuting control parameters, $\hat{\theta}_1, \hat{\theta}_2, \dots$, representing quantum harmonic oscillator positions and momenta. We introduce a fundamental non-abelian composite pulse sequence, the Gaussian-Controlled-Rotation (GCR) for entangling and disentangling a qubit from an oscillator. This sequence achieves at least a $4.5 \times$ reduction in circuit duration compared to the state-of-the-art abelian QSP pulse BB1 [1], while maintaining performance. Though quantum fluctuations in the control parameters are unavoidable, the richer commutator algebra of non-abelian QSP enhances its power and efficiency. Non-Abelian QSP represents the highest tier of QSP variants tailored for hybrid oscillator-qubit architectures, unlocking new possibilities for such systems. We demonstrate the utility of GCR in high-fidelity preparation of continuous variable oscillator states—including squeezed vacuum, Fock states, cat states, GKP states — using fully analytical schemes that match numerically optimized methods in fidelity and depth while enabling mid-circuit error detection. Furthermore, we propose a high-fidelity QSP-based end-of-the-line GKP readout as well as a measurement-free and error-corrected gate teleportation protocol for logical operations on GKP bosonic qudits, bridging the gap between the idealized theoretical and experimentally realistic versions of the GKP codespace. Finally, we showcase a GCR-based phase estimation algorithm for oscillator-based quantum computing. These results lay the groundwork for a constructive theory of non-abelian QSP with utility in robust, fault-tolerant control of hybrid continuous- and discrete-variable quantum systems.

I. INTRODUCTION

The continuous-variable (CV) quantum information resources available in hybrid oscillator-qubit systems enable us to harness quantum advantage at a lower overhead relative to discrete-variable (DV) systems that rely solely on qubits. In this paper, we present new techniques to harness this quantum advantage by extending the concept of quantum signal processing (QSP) [2–5] from the DV domain with classically controlled qubit rotations to the CV domain where the qubit rotations are controlled by the non-commuting position and momentum coordinates of quantum oscillators. We utilize the rich commutator algebra of such hybrid systems to build several experimentally practical and useful circuit ‘gadgets,’ thereby taking some first steps towards a constructive theory of *non-abelian quantum signal processing*.

CV systems can be constructed using propagating photons or static harmonic oscillators such as superconducting microwave resonators or the mechanical oscillations of trapped ions, which have large, formally infinite, Hilbert space dimension. In this work, we will focus on harmonic oscillators. These systems have long coherence

lifetimes but require auxiliary sources of non-linearity to achieve universal control [6–8]. Discrete-variable (DV) systems, on the other hand, are nonlinear systems with typically lower coherence times that can act as controllers to unlock quantum advantage within the CV framework [9]. For example, in the superconducting platform, the shorter-lived transmon qubits have proven to be a convenient source of fast universal control of microwave resonators [10]. In a hybrid superconducting-atom architecture, Rydberg atoms can be used to control a superconducting microwave resonator via the Jaynes-Cummings Hamiltonian [11–14]. In trapped-ion systems, the mechanical oscillation of the ions is controlled via lasers supplying forces that depend on the spin state of the individual ions [15–17]. Mechanical oscillations of cold atoms in trapping potentials are only just beginning to be explored as a quantum control/computation platform [8, 18, 19].

The hardware efficiency and power of hybrid oscillator-qubit systems has been recently demonstrated with quantum error correction for memory close to or beyond the break-even point using a variety of CV quantum error correcting codes in microwave resonators: the cat code [20], the binomial code [21], the truncated 4-component cat code [22], and the Gottesman-Kitaev-Preskill (GKP) code [23, 24]. Error correction with the GKP code has also been demonstrated in a trapped-ion

* Corresponding author: shraddha.singh@yale.edu

system [16, 17]. Another natural application for these hybrid systems is the quantum simulation of physical models containing bosons, for example, lattice gauge theories [25], simulating the physics of spin-boson systems [8], etc. Several recent experiments have explored the measurement of Franck-Condon factors in molecular photo-electron spectroscopy using efficient boson sampling in both the optical [26] and the microwave domain [27, 28] and also explored non-adiabatic dynamics near conical intersections in molecular energy surfaces [29]. These microwave boson-based simulations used quite modest hardware and achieved results that would have required circuit depths far beyond the capabilities of any currently existing qubit-only hardware systems.

Thus, the convergence of CV and DV systems in hybrid architectures opens new frontiers in quantum information processing, both theoretically and practically. However, a dearth of efficient bosonic control methods including state preparation and measurements poses a challenge for any useful computation from these quantum systems. Note that an *efficient circuit*, here, refers not only to the circuit with the shortest depth but also one that is robust in the presence of errors. Errors in the auxiliary control qubits while it is entangled with the oscillator can inhibit the advantages achieved by the hybrid architecture. Recent progress improving fault tolerance to ancilla errors in bosonic quantum error correction has been made through novel bosonic code designs [30] and use of multi-level ancillas [10, 31–36].

In this work, we present various analytical primitives for efficient optimal control of bosonic systems using DV systems. All our primitives belong to the class of non-abelian QSP, a term we introduce for the pulses discussed in this work which will serve as the key to optimal universal control of CV systems in the presence of errors. There has been some prior advancement in the direction of CV-DV control using QSP [5, 37]. However, these works correspond to the case of commuting variables. We introduce a fundamental composite pulse sequence using non-commuting quantum control variables which we dub Gaussian-Controlled-Rotation (GCR). The GCR sequence is designed to produce a well-defined rotation of the ancilla qubit that is robust against errors due to quantum fluctuations in the position and momentum of the oscillator, and we show that it achieves a minimum of $4.5 \times$ reduction in circuit depth compared to the best-known QSP pulses with commuting variables, such as BB1(90) that produces a 90-degree qubit rotation, an important example task for applications discussed in this work. Further, we show a concatenation of GCR with BB1 that produces a response function closer to a square wave compared to BB1 alone. This concatenation is generalizable to other abelian composite pulses as well.

The next part of our work is focused on highlighting the use case of non-abelian composite pulses in efficient control of bosonic systems using ancillary qubits. We have employed GCR to derive analytical circuits for efficient high-fidelity preparation of CV states, including cat

states, GKP states, and Fock states with fidelity and circuit depth comparable to numerically optimized methods in Ref. [10]. In addition, the circuits have a structure that yields an advantage in the presence of noise. These results are summarized in Sec. IV. Our work focuses on the phase space instruction set [8, 10], detailed in Sec. II A, due to its continuous variable formalism that makes it amenable to the new form of quantum signal processing that we utilize. This instruction set is particularly useful in the preparation of non-overlapping superpositions of Gaussian wave functions like those in two-legged cat states and GKP states.

To further this resource-overhead reduction in QEC, we provide primitives for efficient universal control of GKP bosonic logical qubits using an auxiliary DV control system, including high-fidelity state preparation and analytical explanations for numerically optimized readout protocols. With GKP codes, Ref. [23] achieved an error correction gain of $G \approx 2.3$ corresponding to a logical lifetime of 400 error correction cycles. A recent state-of-the-art experiment with qubit-only codes using 49 qubits [38, 39] has achieved similar memory gain. GKP bosonic codes have also enabled the first demonstration of beyond-break-even error correction with qutrits and ququarts, enabling higher dimensional qudits as the building block [40]. The versatility of our framework bridges the gap between the theoretically ideal and the experimentally realistic versions of the GKP logical code space, significantly enhancing the fidelity of practical logical gate operations. A key result in our work is a novel pieceable circuit sequence for non-Clifford gate teleportation that simultaneously corrects errors in oscillator-encoded GKP states. In the presence of oscillator and auxiliary qubit errors, we obtain improved fidelity, smaller circuit depth, and an analytical rather than numerical optimization for universal control of GKP qubits, surpassing current state-of-the-art schemes in [10, 41–43]. In addition, we present the first logical readout circuit for GKP codes specifically tailored to be efficient even in the presence of correctable errors. Importantly, our construction works not only for GKP qubit encoding but also for GKP-based qudit- and multi-mode encodings.

The unique feature of our results lies in the identification of a structure in these circuits which makes the state preparation and control circuits more fault-tolerant to ancilla errors. Such a structure is difficult to achieve via numerical optimization. Finally, as an application in the qubit-centric and oscillator-centric abstract machine model [8], we also give insights for how to use GCR in phase estimation as an application of ancillary oscillators in quantum algorithms.

The main ideas and structure of the paper are provided in Fig. 1. In Sec. II we give an overview of the concepts and hybrid instruction set required for this work. This includes a novel interpretation of a previously known instruction set, highly relevant for the results in this paper. Next, in Sec. III we introduce the non-abelian QSP pulses

GCR and BB1(GCR). We give their and analytical and numerical comparisons against BB1. In Sec. IV we provide analytical schemes for deterministic preparation of oscillator states, and show improvement by benchmarking them against state-of-the-art schemes in the literature. We cover the high-fidelity universal control of GKP codes in Sec. V. Finally, we give the compilation for quantum phase estimation using oscillators, and close the discussion with the summary and outlook of our work in Sec. VI. The numerous applications of our analytical understanding of error cancellation in non-abelian composite pulses suggests a prospective hierarchy of non-abelian QSP, delineating the challenges and framework necessary for efficient control of hybrid CV-DV quantum computing.

II. TECHNICAL BACKGROUND AND PRELIMINARIES

In this section, we first give preliminary information required for the construction presented in this paper. We briefly review the phase-space instruction set in Sec. II A and then introduce various novel constructions including the notion of composite pulses in phase space, rotation gadgets, and quantum operator valued control parameters in Sec. II B. We then give an overview of the main results with the help of a QSP hierarchy for the control of CV-DV architectures in Sec. II C.

A. Phase-Space Instruction Set

A hybrid system of oscillators and two-level systems can achieve universal control with different instruction sets. For this study, we will use the so-called phase space instruction set [8]. This instruction set is useful in the control of non-overlapping superpositions of Gaussian wave functions, such as squeezed states, cat states, and GKP states. The set comprises two parameterized gates: arbitrary qubit rotations (R) (about any axis in the equatorial plane of the Bloch sphere) and conditional displacements (CD), defined as,

$$R_\phi(\theta) = e^{-i\frac{\theta}{2}\sigma_\phi}, \quad CD(\beta, \sigma_\phi) = e^{(\beta\hat{a}^\dagger - \beta^*\hat{a}) \otimes \sigma_\phi}. \quad (1)$$

Here $\sigma_\phi = \cos\phi\sigma_x + \sin\phi\sigma_y$, \hat{a}, \hat{a}^\dagger are the annihilation and creation operators on the oscillator subspace, respectively, and $\sigma_x, \sigma_y, \sigma_z$ are the Pauli operators on the qubit subspace. The CDs are hybrid operations that displace the oscillator by $\pm\beta$ in phase space depending on the qubit state through the eigenvalue of σ_ϕ . Here $\beta = \Delta x + i\Delta p$ is a complex number parametrizing the phase space displacement. These gates have been realized in various superconducting circuits and trapped-ion experiments by means of dispersive interaction [10] and sideband interaction [16, 17], respectively.

For this work, we use so-called Wigner units [8] in which the oscillator quadrature operators are $\hat{x} =$

$\frac{\hat{a}+\hat{a}^\dagger}{2}, \hat{p} = \frac{\hat{a}-\hat{a}^\dagger}{2i}$. For these units, we have $[\hat{x}, \hat{p}] = \frac{i}{2}$ and the wave function of the minimum uncertainty vacuum state is given by, $\psi(x) = \left(\frac{2}{\pi}\right)^{1/4} e^{-x^2}$. See App. A for details on these units.

We note that while the qubit rotations $R_\phi(\theta)$ are only for axes lying on the equator of the Bloch sphere, they provide universal single-qubit control. As an aside, we also note that even if the natively available conditional displacement gate is controlled on σ_z , conjugation with qubit rotations allows easy synthesis of $CD(\beta, \sigma_\phi)$.

Importantly, we can alternatively interpret CD, not as a qubit-controlled displacement of the oscillator, but rather as an oscillator-controlled rotation of the qubit

$$CD(\beta, \sigma_\phi) = e^{i2\hat{v} \otimes \sigma_\phi} = R_\phi(-4\hat{v}(\beta)), \quad (2)$$

$$\text{where } \hat{v}(\beta) = \text{Im}(\beta)\hat{x} - \text{Re}(\beta)\hat{p} \quad (3)$$

where the qubit rotation angle \hat{v} is now a quantum operator acting on the oscillator Hilbert space. We will often use the notation \hat{v}_\perp to denote the perpendicular vector $\text{Re}(\beta)\hat{x} + \text{Im}(\beta)\hat{p}$. We will denote CDs with $\text{Re}(\beta) = 0$ as conditional momentum boosts. In addition, σ_ϕ for the case of $\phi = 0, \pi/2$ will be denoted by σ_x, σ_y , respectively. To distinguish states of the qubit from oscillator Fock states, we will use $|g\rangle, |e\rangle$ to represent the qubit ground $|0\rangle$ and excited $|1\rangle$ states.

B. Framework of Composite Pulses in Phase Space

Quantum states in an oscillator cannot have fixed position and momentum eigenvalues with infinite precision, as per the uncertainty principle. The simplest quantum state, a coherent state $|\alpha\rangle$, is given by a Gaussian wave function where the width of the Gaussian Δ gives the uncertainty in determining the position or momentum of the state. For example, in the position basis,

$$\langle x|\alpha_\Delta\rangle = \alpha_\Delta(x) = \left(\frac{2}{\pi\Delta^2}\right)^{1/4} e^{-\frac{(x-\alpha)^2}{\Delta^2}}, \quad (4)$$

is a state whose mean position is $\alpha \in \mathbb{R}$ with an uncertainty of $\delta x = \frac{\Delta}{2}$. This uncertainty is often just the natural uncertainty associated with the zero-point fluctuations of the oscillator ground state or vacuum (for which $\Delta = 1$), but may be smaller or larger in squeezed states (see Sec. IV A). For coherent states without squeezing, we will drop Δ from the notation and use $|\alpha\rangle$. For general squeezed coherent states, the most useful information related to $|\alpha_\Delta\rangle$ is (for our purposes) in the mean position and momentum determined by α , and (secondarily) in the squeezing Δ . We will use composite pulses inscribed in phase space using oscillator-controlled qubit rotations to access this phase-space information. As we will show, this technique is especially handy for the control of states represented by sums of non-overlapping Gaussian wave functions.

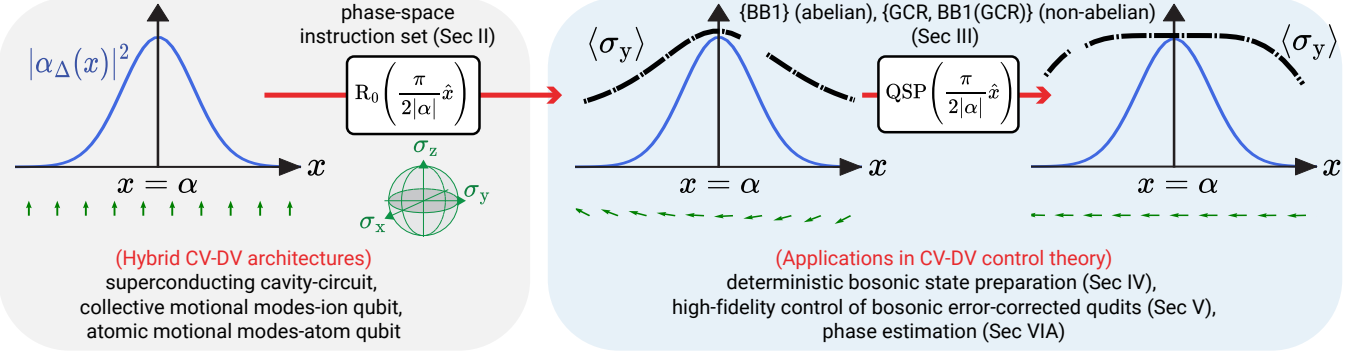


FIG. 1. **Framework of composite pulses in phase space and its applications.** Blue curves represent the Gaussian probability distribution $|\langle x|\psi \rangle|^2$ of the oscillator position. Green arrows indicate the spin orientation of the ancilla qubit as a function of the oscillator position for the state $|g\rangle \otimes |\alpha_\Delta\rangle$ (see Eq. (4)). The goal is to use only oscillator-controlled rotations to uniformly rotate the spin to its desired state $|g\rangle \rightarrow |\mp i\rangle$, given $\langle x \rangle = \pm\alpha$, independent of the position uncertainty of the oscillator. We utilize quantum signal processing pulses (QSP) to achieve this goal. The response function for these QSP pulses is given by the black dashed curves as the expectation value of the qubit operator $\langle \sigma_y \rangle$. The flatter this function is, the better the QSP pulse sequence. The gray panel depicts the hybrid CV-DV system in a product state that can be acted upon with a phase-space instruction set composed of conditional-displacements-cum-momentum-boosts (CD) and arbitrary qubit rotation (R) (see Eq. (1)). The conditional displacements $CD(\gamma, \sigma_\phi)$ give rise to oscillator-controlled qubit rotations denoted by $R_\phi(\gamma \hat{x})$. The blue panel discusses the premise of this work, the application of composite pulses in the phase space of an oscillator in the control of such hybrid systems. In particular, QSP corrects the errors introduced by R which are the result of over- and under-rotations of the spin associated with the position uncertainty of the Gaussian state. This is depicted by the left figure in the blue panel. We devise a non-abelian composite pulse sequence GCR and discuss its comparison against traditional composite pulses adapted for this purpose, such as BB1 [1], in Sec. III. The pulse BB1(GCR) is a concatenation of the pulses BB1 and GCR, recipe for which is also given in Sec. III. The right figure in the blue panel illustrates the resulting improvement in the fidelity of the qubit rotation and lists its several applications discussed in this work.

a. Rotation Gadgets. Let us first consider the task of extracting a single bit of information about a CV state, the sign of the mean value of the position operator (i.e., distinguish between $|+\alpha_\Delta\rangle$, $|-\alpha_\Delta\rangle$), using a DV auxiliary qubit. For convenience, we will focus on the case where α is a real number, with a straightforward generalization to arbitrary vector \hat{v} in phase space with complex α discussed in App. C 5. That is, given the knowledge of $|\alpha|$, the final DV qubit state should be independent of Δ . For large enough $|\alpha|/\Delta$ where $|+\alpha_\Delta\rangle$ and $|-\alpha_\Delta\rangle$ are nearly orthogonal, this task can be achieved if we manage to rotate the qubit in state $|g\rangle$ by an angle $R_0\left(\frac{\pi}{2} \frac{\alpha}{|\alpha|} \hat{x}\right)$, or equivalently $R_0\left(\frac{\pi}{2} \text{sign}(\hat{x})\right)$, and measure the qubit in the Y-basis of the auxiliary Bloch sphere. In short, we aim to find a unitary transformation \hat{U} such that

$$\hat{U} |g\rangle \otimes |\pm\alpha_\Delta\rangle \approx |\mp i\rangle \otimes |\pm\alpha_\Delta\rangle. \quad (5)$$

To address this problem, we derive a rotation gadget that executes a good approximation to $R_0\left(2\theta \frac{\alpha}{|\alpha|}\right)$ for arbitrary θ in the large $|\alpha|/\Delta$ limit¹. With this goal in mind, let us study the effect of a conditional momentum

boost

$$R_\phi\left(-\frac{\theta}{|\alpha|} \hat{x}\right) = e^{i \frac{\theta}{2|\alpha|} \hat{x} \otimes \sigma_\phi} \quad (6)$$

applied using the phase space instruction set in Eq. (1). In the position basis, the position-controlled rotation by $\hat{\theta}(\hat{x}) = \frac{\theta}{|\alpha|} \hat{x}$ applies a qubit rotation linear in the position of the oscillator. However, this operation suffers fluctuations due to uncertainty in the position of the oscillator, yielding a distribution of the spin polarization on the oscillator position x as depicted by Fig. 1 for $\theta = \pi/2, \phi = 0$. Our goal is to develop a QSP sequence that (approximately) converts \hat{x} to $f(\hat{x}) = \text{sgn}(\hat{x})$ (or more precisely to a periodic square-wave function of \hat{x}) that is antisymmetric in \hat{x} and has period 2α so that the flat tops are centered on $\pm\alpha$.

If we define $\hat{\epsilon} = \frac{\hat{x} - \alpha}{\alpha}$ then the qubit is erroneously rotated by,

$$R_\phi\left(-\frac{\theta}{|\alpha|} \alpha(1 + \hat{\epsilon})\right) = R_\phi\left(-\frac{\theta}{|\alpha|} \alpha \hat{\epsilon}\right) R_\phi\left(-\frac{\theta}{|\alpha|} \alpha\right), \quad (7)$$

since $\epsilon(x) \equiv \langle x|\hat{\epsilon}|x\rangle = 0$ only at position $x = \alpha$. Because of the Gaussian envelope of the wave function, the probability of finding the oscillator in a region of large $\epsilon(x)$ is small. This reduces the effect of over- and under-rotations at $x \neq \alpha$ for large $\alpha/|\Delta|$. This idea has been

¹ The case of small $|\alpha|/\Delta$ is discussed in Sec. IV A and App. E 2

used in several works [41, 44] to achieve the disentanglement of qubit and oscillator after a hybrid operation.

The errors associated with the quantum fluctuations in position need to be corrected in a QND manner, to learn information about the oscillator accurately. In this work, we show that these errors can be strongly reduced using composite pulse QSP sequences. Previous works [10, 41, 44, 45] have achieved similar improvements using numerical optimization on circuits composed of CDs to prepare oscillator states using DV systems. Our construction, on the other hand, is completely analytical and intuitive. This intuition gives rise to novel protocols discussed in Secs. IV–VI. But first, we ask if one can employ traditional pulses from the classical NMR spin control literature to achieve such error cancellations, removing the over- and under-rotation errors due to quantum fluctuations ($\hat{\epsilon}$) in the position.

b. Composite Pulses. Note that, the above-defined task amounts to executing a pulse sequence after which the spin-polarization (more importantly, the expectation value $\langle \sigma_y \rangle$) resembles a square waveform as a function of the position of the oscillator. This waveform should have a flat top near the peak of the Gaussian function representing the oscillator state (see Fig. 1). The NMR community has developed classical error-canceling pulse sequences for DV-only architectures that can produce a corrective rotation to compensate for the presence of systematic errors in control variables, say $\theta_\epsilon = \frac{\theta}{|\alpha|}\alpha(1+\epsilon)$. In the absence of any correction, the infidelity in achieving the target rotation $R_\phi(\theta)$ by such an erroneous rotation $R_\phi(\theta_\epsilon)$ is given by, $\sim \epsilon^2$. To reduce this infidelity, the composite pulses $f_\phi(\theta_\epsilon)$ apply,

$$f(\theta_\epsilon) = R_\phi \left(-\frac{\theta}{|\alpha|}\alpha\epsilon \right) + \mathcal{O}(\epsilon^n), \quad (8)$$

such that $f(\theta_\epsilon)$ cancels all $\mathcal{O}(\epsilon^{n-1})$ error terms, improving the fidelity of rotation to $\mathcal{O}(\epsilon^{2n})$. Some of the best-known composite pulse sequences, for classical (scalar) control variables θ_ϵ , include BB1 [1], SCROFULOUS [46], TYCKO [47], etc. Among these, the BB1 pulse sequence demonstrates the best error cancellation (or the flattest square waveform), and so, we shall use this scheme as the standard for comparisons.

c. Quantum Control Variables. Remarkably, for hybrid control, we can replace the classical control variables θ_ϵ in traditional QSP pulses with quantum control variables $\hat{\theta} = (\theta/|\alpha|)\hat{x}$, provided that all the quantum arguments for all rotations in a composite pulse commute. This replacement can be used conveniently with any signal designed using ideas of univariate QSP with commuting variables [48, 49]. For example, the BB1 pulse to

achieve a target rotation of $R_0(\theta)$ is given by,

$$\begin{aligned} \text{BB1}(\theta) &= R_{\phi_1} \left(\frac{\pi}{\theta} \theta_\epsilon \right) R_{3\phi_1} \left(\frac{2\pi}{\theta} \theta_\epsilon \right) R_{\phi_1} \left(\frac{\pi}{\theta} \theta_\epsilon \right) \\ &\times R_0(\theta_\epsilon), \quad \phi_1 = \cos^{-1} \left(-\frac{\theta}{4\pi} \right). \end{aligned} \quad (9)$$

We can adapt the sequence to achieve the corresponding correction of the oscillator-controlled qubit rotation $R_0\left(\frac{\theta}{|\alpha|}\hat{x}\right)$ using the following sequence,

$$\begin{aligned} \text{BB1} \left(\frac{\theta}{|\alpha|} \hat{x} \right) &= R_{\phi_1} \left(\frac{\pi}{|\alpha|} \hat{x} \right) R_{3\phi_1} \left(\frac{2\pi}{|\alpha|} \hat{x} \right) R_{\phi_1} \left(\frac{\pi}{|\alpha|} \hat{x} \right) \\ &\times R_0 \left(\frac{\theta}{|\alpha|} \hat{x} \right), \quad \phi_1 = \cos^{-1} \left(-\frac{\theta}{4\pi} \right) \end{aligned} \quad (10)$$

$$\begin{aligned} &= \text{CD} \left(-\frac{i\pi}{4|\alpha|}, \sigma_{\phi_1} \right) \text{CD} \left(-\frac{i\pi}{2|\alpha|}, \sigma_{3\phi_1} \right) \\ &\times \text{CD} \left(-\frac{i\pi}{4|\alpha|}, \sigma_{\phi_1} \right) \text{CD} \left(-\frac{i\theta}{4|\alpha|}, \sigma_x \right). \end{aligned} \quad (11)$$

In the last equation, we have used $\sigma_0 = \sigma_x$ for clarity. By using these extra conditional momentum boosts to create a composite pulse sequence, we can boost the fidelity of the target rotation against the quantum error $\hat{\epsilon}$, and more accurately relay information about the mean value $\pm\alpha$ of the oscillator position distribution to the control qubit. We discuss the exact performance metrics for this sequence in Sec. III.

C. Non-abelian QSP for Quantum Control of Hybrid Systems

Table I presents a summary of QSP techniques developed in the literature as part of a hierarchy of gate operation classes toward universal oscillator control. (See further details in App. B and in Ref. [8]). In this section, we formalize the requirements for QSP to achieve universal state preparation and control, and summarize helpful results for each class in the hierarchy and their applicability towards our goal of universal oscillator control.

We combine ideas and formalisms presented in [3, 5, 8, 37, 50] and this work to obtain the following general non-

Types of CV-DV QSP	Conditions	Use-case	Refs.
Univariate QSP	$[\hat{v}_i, \hat{v}_j] = 0$	Adaptation of traditional QSP methods [2, 3, 48] to quantum control variables	[37]
Multivariate QSP w/ commuting variables	v_1, v_2, v_3, \dots s.t. $[\hat{v}_i, \hat{v}_j] = 0$	Control of multiple oscillators	[5, 50]
Bivariate QSP w/ non-commuting variables	$[v_i, v_j] \neq 0$	High-fidelity control of single oscillator with low circuit-depth	This work
Multivariate QSP w/ non-commuting variables	$[\hat{v}_i, \hat{v}_j] = 0$ for at least one pair of variables $i \neq j$	High-fidelity control of multiple oscillators with low circuit-depth	N/A

TABLE I. **Hierarchy of CV-DV QSP Framework.** Overview of different types of QSP techniques, with commuting and non-commuting quantum variables, found in literature, developed towards universal oscillator control. The bottom two rows belong to the largely unexplored territory of non-abelian quantum signal processing (or NA-QSP; see Ref. [8] for a formal introduction to NA-QSP). Its applications in various arenas of CV-DV control theory are listed in Fig. 1.

abelian QSP sequence for hybrid CV-DV architectures,

$$U_{\vec{\phi}}(\hat{v}_1, \hat{v}_2, \dots) = e^{i\phi_0\sigma_z} \prod_{j=1}^k \text{CD}(\beta_j, \sigma_0) e^{i\phi_j\sigma_z}, \quad (\vec{\phi} = \{\phi_0, \phi_1, \dots\}) \quad (12)$$

$$\equiv e^{i\phi_0\sigma_{\phi_0}} \prod_{j=1}^k \text{CD}(\beta_j, \sigma_{\phi_j}) \quad (13)$$

$$= \text{R}_Z(\phi_0) \prod_{j=1}^k \text{R}_{\sigma_{\phi_j}}(\hat{v}_j), \quad (14)$$

where $\hat{v}_j = \hat{v}(\beta_j)$ as defined in Eq. (3). Note that, in traditional QSP where $\hat{v}_j \equiv \theta$ would correspond to a fixed rotation ('quantum signal') about the x axis of the Bloch sphere. In contrast, here the rotation angle also depends on the index j and is an operator on the oscillator Hilbert space that may not commute with other operators $\hat{v}(\beta_k)$. It is useful to note that the QSP sequence $U_{\vec{\phi}}$ defined above can be written in the form of a 2×2 operator acting on the DV qubit,

$$U_{\vec{\phi}}(\hat{v}_1, \hat{v}_2, \dots) = \begin{pmatrix} W_{gg} & W_{ge} \\ W_{eg} & W_{ee} \end{pmatrix}, \quad (15)$$

where each of the W blocks is a CV operator acting only on the oscillator, for example, $W_{ge} = \langle g | U_{\vec{\phi}}(\hat{v}_1, \hat{v}_2, \dots) | e \rangle$, etc.

For each problem below, the goal is that the qubit should be completely unentangled from the oscillator after $U_{\vec{\phi}}$ is applied to the starting state $|g, 0\rangle$ (qubit in $|g\rangle$ and cavity in vacuum $|0\rangle$). That is, we want $U_{\vec{\phi}}$ to be block diagonal and W_{gg} to perform a specified target (unitary) operation U_t on the oscillator. If these conditions are not perfectly satisfied, then we have several important measures of fidelity. First, how close is W_{gg} to U_t ? This is the fidelity, F_{ps} , of the operation post-selected on measuring the qubit to be in $|g\rangle$. Second, it is useful to know the success probability for the post-

selection

$$P_g = 1 - P_e = \langle 0 | W_{gg}^\dagger W_{gg} | 0 \rangle = 1 - \langle 0 | W_{eg}^\dagger W_{eg} | 0 \rangle. \quad (16)$$

If the P_e is small relative to, given errors in other operations of the system, then we can completely ignore the qubit outcome or use it to detect ancilla errors. In this case, we care about a third quantity, the hybrid fidelity F_H ,

$$F_H = |\langle \psi | W_{gg} | 0 \rangle|^2, \quad (17)$$

where $|\psi\rangle$ is the target oscillator state, in case of state preparation. For universal control, this quantity will correspond to oscillator fidelity with the target operation V . There are additional fault-tolerance metrics one can consider in the case that the ancilla qubit can raise a flag indicating a leakage error has occurred [32, 51, 52] but this is beyond the scope of the present work.

If we allow $\mathcal{O}(\epsilon)$ upper bound on a qubit-oscillator entanglement error, then the problem statements are framed as follows:

(Problem 1) Universal State Preparation to realize an arbitrary oscillator state $|\psi\rangle$ starting from vacuum. We require a hybrid unitary $U_{\vec{\phi}}(\hat{v}_1, \hat{v}_2, \dots)$ such that:

- $1 - |\langle \psi | W_{gg} | 0 \rangle|^2 = 1 - F_H = \mathcal{O}(\epsilon)$, and
- $\|W_{eg} | 0 \rangle\| = \sqrt{P_e} = \mathcal{O}(\epsilon)$,

where $\|\cdot\|$ is the state norm.

(Problem 2) Universal Control to synthesize a polynomial Hamiltonian $\hat{H}(\hat{x}, \hat{p})$ that realizes an arbitrary oscillator unitary (e^{-iHt}): Defining $\|\hat{A}^\dagger \cdot \hat{B}\| = \frac{1}{d} \sqrt{\text{Tr}(\hat{A}^\dagger \hat{B}^\dagger)}$ as the operator fidelity between operators \hat{A}, \hat{B} on a d -dimensional space, we need $U_{\vec{\phi}}(\hat{v}_1, \hat{v}_2, \dots)$ to obey:

- $1 - \|W_{gg}^\dagger \cdot e^{-i\hat{H}(\hat{x}, \hat{p})t}\| = 1 - F_H = \mathcal{O}(\epsilon)$, and
- $\|W_{eg}\| = \mathcal{O}(\epsilon)$.

General QSP techniques for single qubit rotations were introduced in the context of classical θ variables in [48]. These were extended to multi-variable QSP schemes [5, 50] where the polynomial is a function of more than one variable $\theta_1, \theta_2, \dots$. Note that, multi-variate or multi-variable does not necessarily refer to having many oscillators each with their own \hat{x}, \hat{p} , but rather (for the case of a single oscillator at least) to having multiple directions in phase space along which displacements can be made. The class of QSP techniques that use only conditional displacements and momentum-boosts (or any other orthogonal displacement generators in phase space) along with qubit rotations is universal. However, the availability of displacements using an arbitrary number of generators $\hat{v}_i = \alpha_i \hat{x} + \beta_i \hat{p}$ can yield more efficient circuits for the universal control of oscillators. An important addition of the present work is the attempt to generalize these schemes towards universal control of bosonic systems. Here the target polynomials, $\hat{f}(\hat{x}, \hat{p})$, are in general a function of two non-commuting variables. While a full constructive theory of this generalization remains an open problem, we suggest a hierarchy of QSP schemes in Table I that can yield insights into the developments of novel techniques with readily available QSP methods. See App. B for details.

Non-abelian QSP offers a powerful resource for hybrid quantum systems that will be a broadly useful tool for the realization of quantum advantage in continuous-variable quantum computing. The composite Gaussian Controlled Rotation (GCR) pulse scheme introduced in the next section is a first step in this direction.

III. GAUSSIAN-CONTROLLED-ROTATION (GCR): A NON-ABELIAN COMPOSITE PULSE

In this section, we introduce an analytic non-abelian QSP composite pulse sequence, the Gaussian-controlled-rotation, GCR(θ). This is an instance of a rotation gadget for the control problem defined in Sec. II B. We prove here that GCR(90) achieves a target rotation with similar error cancellation as the abelian QSP protocol BB1(90) but with a reduction of circuit duration by a factor of at least 4.5. We shine light upon the usefulness of GCR sequences in Secs. IV-VI.

Using the additional freedom afforded by NA-QSP, we define a Gaussian-Controlled-Rotation,

$$\text{GCR}(\theta) |g\rangle \otimes |\alpha_\Delta\rangle \equiv e^{i\frac{\theta}{2|\alpha|}\hat{x}\sigma_x} e^{i\frac{\theta\Delta^2}{2|\alpha|}\hat{p}\sigma_y} |g\rangle \otimes |\alpha_\Delta\rangle \quad (18)$$

$$= R_0 \left(-\frac{\theta}{|\alpha|} \hat{x} \right) R_{\frac{\pi}{2}} \left(-\frac{\theta\Delta^2}{|\alpha|} \hat{p} \right) |g\rangle \otimes |\alpha_\Delta\rangle, \quad (19)$$

$$\approx R_0 \left(-\theta \frac{\alpha}{|\alpha|} \hat{x} \right) |g\rangle \otimes |\alpha_\Delta\rangle. \quad (20)$$

The above sequence works equally well if the qubit operators are rotated by angle ϕ about the z axis such

that $\sigma_x \rightarrow \sigma_\phi, \sigma_y \rightarrow \sigma_{\phi+\pi/2}$. Similarly, the sequence is also generalizable to accommodate rotations conditioned on arbitrary (but perpendicular) displacements in phase space such that $\hat{x} \rightarrow \hat{v}$ and $\hat{p} \rightarrow \hat{v}_\perp$ in the CV phase space.

For a CV quantum state $|\alpha_\Delta\rangle$ with wave function given in Eq. (4), the composite pulse GCR(θ) performs a rotation of the qubit state $|g\rangle$ about an arbitrary axis on the equator of the qubit Bloch sphere by a fixed angle $\pm\theta$ whose sign is determined by the sign of α . Here, the momentum-controlled rotation (or, conditional displacement) applies a pre-correction to first-order in the uncertainty of $\hat{\theta}(\hat{x})$. Below we give a proof of correctness and an error analysis for this construction, computing the quantities P_e and F_H (see Eqs. 16-17) for GCR, and compare it against the case no QSP correction and BB1. The post-selected fidelity F_{ps} is also computed in App. C3.

A. Proof of Correctness

To understand the effect of a conditional displacement in Eq. (18) in the position basis, we note that the momentum operator acts as the derivative operator ($p = -\frac{i}{2} \frac{d}{dx}$) on $\alpha_\Delta(x)$ yielding powers of $(x - \alpha)$. This observation indicates that this operation could be used to correct for rotation errors proportional to $(x - \alpha)$ as follows,

$$|\psi\rangle = e^{i\frac{\lambda}{2}\hat{p}\otimes\sigma_y} |g\rangle \otimes |\alpha_\Delta\rangle \quad (21)$$

$$= [\cos(\lambda\hat{p}/2)I + i\sin(\lambda\hat{p}/2)\sigma_y] |g\rangle \otimes |\alpha_\Delta\rangle \quad (22)$$

$$\approx [I + i\frac{\lambda}{2}\hat{p}\sigma_y] |g\rangle \otimes |\alpha_\Delta\rangle, \quad \lambda \rightarrow 0. \quad (23)$$

$$\therefore \langle x|\psi\rangle \approx [I + \frac{\lambda}{4} \frac{d}{dx} \sigma_y] e^{-\frac{(x-\alpha)^2}{\Delta^2}} |g\rangle \quad (24)$$

$$= [I - \frac{\lambda}{2} \frac{x-\alpha}{\Delta^2} \sigma_y] e^{-\frac{(x-\alpha)^2}{\Delta^2}} |g\rangle. \quad (25)$$

$$= [I - i\frac{\lambda}{2} \frac{x-\alpha}{\Delta^2} \sigma_x] e^{-\frac{(x-\alpha)^2}{\Delta^2}} |g\rangle \quad (26)$$

$$|\psi\rangle \approx R_0 \left(\frac{\lambda}{\Delta^2} (\hat{x} - \alpha) \right) |g\rangle \otimes |\alpha_\Delta\rangle. \quad (27)$$

Through these steps we have converted a momentum-controlled qubit rotation, about the y -axis of the ancillary Bloch sphere, to a position-controlled qubit rotation, about the x axis of the ancillary Bloch sphere. The key step of this derivation is based on the second to last equation where we use $\sigma_y |g\rangle = i\sigma_x \sigma_z |g\rangle = i\sigma_x |g\rangle$. Therefore, this scheme only works if the initial qubit state is $|g\rangle$.

To first order in $\lambda\hat{p} \sim \frac{\lambda}{\Delta}$, this equality changes the expression into a unitary rotation gate. Thus, a small conditional displacement can be seen as a rotation on $|g\rangle \otimes |\alpha_\Delta\rangle$ which cancels the erroneous rotation $R\left(-\frac{\theta}{|\alpha|}\alpha\hat{e}\right)$ up to first order in $\epsilon(x)$, provided

$$\lambda = \frac{\theta\Delta^2}{|\alpha|}. \quad (28)$$

This quantity also decides the back action on the oscillator due to the pre-correction. If the initial qubit state were instead $|\psi\rangle \otimes |e\rangle$, the pre-correction requires reversing the sign of λ . Thus, the momentum-controlled rotation cannot yield the desired cancellation if applied to a qubit state that is not an eigenstate of σ_z .

While this is a case of bivariate QSP, studied in [5], it is different in that the two variables under consideration are non-commuting ($[f(\hat{x}), g(\hat{p})] \neq 0$) and this feature has favorable implications on reducing circuit-depth for error cancellations, as we will prove below. QSP for non-commuting variables is briefly outlined in [50] but no explicit instance of a pulse sequence is presented. Our composite pulse GCR(θ) is an example of bivariate QSP using non-commuting variables which we will refer to as ‘non-abelian QSP’. We will now quantify the advantages of our scheme. Our main goal in this analysis is to justify the reduced circuit depth by bounding the error of the scheme and its back action on the oscillator state for the reduced circuit duration achieved here.

B. Error Bounds

Here, we will talk about the correctness of our scheme for $|\alpha_\Delta\rangle$. Since we use non-commuting control operators, the back action on the conjugate basis should be studied to check the validity of the framework. To calculate the error in the process we will, at first, only consider a single basis state $|\alpha_\Delta\rangle$. Defining, $U = e^{i\frac{\theta}{2|\alpha|}(\hat{x}-\alpha)\sigma_x}$, $V = e^{i\frac{\lambda}{2}\hat{p}\sigma_y}$, $\lambda = \frac{\theta\Delta^2}{|\alpha|}$, Eq. (18) can be rewritten as

$$\text{GCR}(\theta)|g\rangle|\alpha_\Delta\rangle = R_0 \left(-\theta \frac{\alpha}{|\alpha|} \right) UV|g\rangle|\alpha_\Delta\rangle. \quad (29)$$

In the position basis, the action of U and V is given by the following equations.

$$\langle x|U|\alpha_\Delta\rangle|g\rangle = \sum_{m=0}^{\infty} \frac{[i\theta(x-\alpha)\sigma_x]^m}{2^m|\alpha|^m m!} \alpha_\Delta(x)|g\rangle = \sum_{m=0}^{\infty} r_m|g\rangle \quad (30)$$

$$\begin{aligned} \langle x|V|\alpha_\Delta\rangle|g\rangle &= \langle x| \sum_{n=0}^{\infty} \frac{(i\lambda\hat{p}\sigma_y)^n}{2^n n!} |\alpha_\Delta\rangle|g\rangle \\ &= \sum_{n=0}^{\infty} \left(-\frac{\lambda\sigma_y}{4\Delta} \right)^n \frac{1}{n!} H_n\left(\frac{x-\alpha}{\Delta}\right) \alpha_\Delta(x)|g\rangle \\ &= \sum_{n=0}^{\infty} s_n|g\rangle \end{aligned} \quad (31)$$

where $H_n(x)$ denotes the n^{th} physicist’s Hermite polynomial. Note that, in the absence of the corrective operation (‘pre-rotation’) V , the qubit rotation error caused by U is small when the uncertainty of $\frac{\theta}{4|\alpha|}\hat{x}$ is small. For conciseness, we will give expressions in terms of twice this

uncertainty,

$$\chi = \frac{\theta\Delta}{2|\alpha|}. \quad (32)$$

The corrective operation V cancels the rotation errors to the first order in χ , and so the fidelity of the process is proportional to χ^4 . We need to compute the distance between our approximate correction V and the exact cancellation operator U^\dagger for the initial state $|g\rangle \otimes |\alpha_\Delta\rangle = |g, \alpha_\Delta\rangle$.

Note that, throughout the analysis below we are only interested in the deviation of GCR(θ) from the desired operation. To do this, we focus on the deviation of UV from the identity operation on the hybrid oscillator-qubit space. The hybrid infidelity $1 - F_H$ increases as the implemented operation deviates further from the identity on the oscillator-qubit space. The failure probability P_e is non-zero iff the operation is not an identity on the qubit subspace. See Fig. 2. The details of the analytical calculations quoted below can be found in App. C3.

Failure Probability. The probability of incorrectly rotating the qubit (i.e., ending up in $|e\rangle$) is only affected by $\mathcal{O}(\chi^3)$ and $\mathcal{O}(\chi^5)$ terms in the expansion of UV , and hence,

$$P_e(\text{GCR}) \sim 0.1\chi^6 + \mathcal{O}(\chi^8), \quad \chi \ll 1. \quad (33)$$

Thus, the probability of making an erroneous rotation has been proved to scale as χ^6 . As $\chi \rightarrow 0$, the probability goes to 1, that is, the delta-function limit $\Delta \rightarrow 0$ or zero-rotation limit $\alpha \rightarrow \infty$ yield a unit probability of success, as expected. The approximation is not well-suited for $\alpha \rightarrow 0$ since higher-order terms come into play while in $\Delta \rightarrow \infty$ limit the momentum-basis is more suitable for the peak-dependent rotation of the qubits.

In the case of no QSP correction, the failure probability in the asymptotic limit of large α is given by, $P_e(\text{no-QSP}) = 0.25\chi^2$ (see App. C2). Improving upon which, the failure probability for BB1 is given by,

$$P_e(\text{BB1}) = 1.85\chi^6. \quad (34)$$

See App. C4 for details of this calculations and contrast this with the case no QSP correction and GCR. Note that this success probability scales with the same power of χ^6 and a $\times 10$ worse prefactor compared to GCR (see App. C4).

Hybrid Infidelity. If the failure probability is low enough, we can afford to ignore the outcome of the qubit and let it reset. In this case, the hybrid state fidelity is important.

$$1 - F_H(\text{GCR}) = \chi^4/8 + \mathcal{O}(\chi^6), \quad (35)$$

We see that hybrid state infidelity has a lower scaling of $\mathcal{O}(\chi^4)$ for our scheme due to unwanted back action from the conditional displacement $e^{i\frac{\lambda}{2}\hat{p}\sigma_y}$. The BB1 correction, on the other hand, has the same scaling as failure probability, and thus, a smaller back action

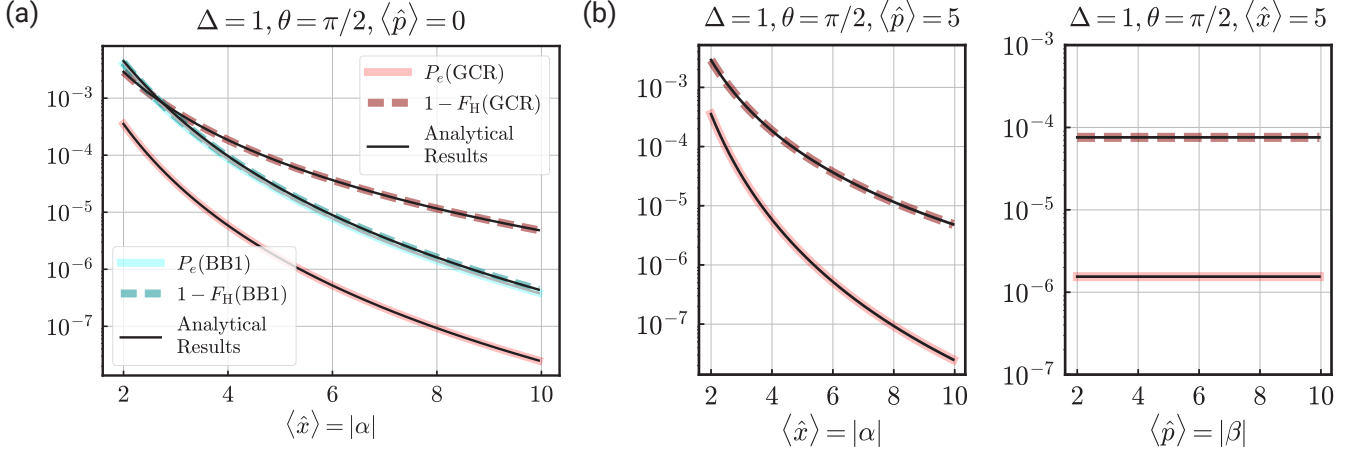


FIG. 2. **Performance of non-abelian composite pulse sequence GCR(θ) in quantum phase space.** (a) Comparison against BB1(θ) for a special case of $\chi = \frac{\pi}{4|\alpha|}$. The colored lines denote the various merits of correctness (failure probability: solid, infidelity: dashed) obtained from simulations using QuTiP [53] and the black lines denote the corresponding analytical expressions quoted in Eqs. 33-35. See App. C for derivation. The infidelities of GCR(θ) scale as χ^4 while the failure probability of both schemes scales as χ^6 . (b) Performance of GCR(θ) for the coherent basis $\{|\alpha_\Delta + i\beta_\Delta\rangle\}$ where $\alpha \neq 0, \beta \neq 0$. (Left) For varying $|\alpha|$ and fixed $|\beta| = 5$, the simulated failure probability (solid) and infidelity (dashed) show that this variation of GCR(θ) also improves upon the rotation errors with the same efficiency as confirmed by the black lines, again plotting Eqs. 33-35. (Right) For varying $|\beta|$ and a fixed $|\alpha| = 5$, we show that this improvement does not depend on $|\beta|$ as suggested by Eq. (C72) since it just requires a simple rotation to keep the anomaly coming from this state with center at $\langle \hat{x} \rangle \neq 0$ and $\langle \hat{p} \rangle \neq 0$ in check.

$(1 - F_H(\text{BB1}) \sim P_e(\text{BB1}) = 1.85\chi^6)$, because the scheme is composed of only conditional momentum boosts.

Circuit-depth: In terms of general gate counting methods to quantify circuit complexity, BB1 uses four gates while GCR uses only two gates. However, the duration of the hybrid gates scales with its amplitude ($T_{\text{CD}(\alpha, \sigma_\phi)} \propto \alpha$), and hence, we believe that the correct way to quantify the circuit depth is by comparing the total magnitude of conditional displacements and momentum boosts used in Eqs. (11) and (18). Using this figure of merit, the circuit duration for our non-abelian scheme is proportional to $T_{\text{GCR}} \propto \frac{\pi}{4|\alpha|}(1 + \Delta^2)$. For the case of BB1 correction, the total duration of conditional momentum boosts that we apply is $T_{\text{BB1}} \propto \frac{2\pi}{|\alpha|} + \frac{\pi}{4|\alpha|} = \frac{9\pi}{4|\alpha|}$ (see Eq. (11)). The duration of our scheme decreases for squeezed states ($\Delta < 1$) whereas it does not have any effect on the circuit duration of BB1. For the worst-case scenario of $\Delta = 1$ for our scheme,² our circuit depth is still shorter than BB1(90) by a factor approaching

$$\frac{T_{\text{GCR}}}{T_{\text{BB1}}} = 4.5 \quad (36)$$

² Note that for $\Delta < 1$, the correction pulse is smaller than the case of $\Delta = 1$. For the case of $\Delta > 1$, the position fluctuations are anti-squeezed and the momentum fluctuations are squeezed. Hence we should use the GCR sequence with $\hat{x} \rightarrow \hat{p}$, $\hat{p} \rightarrow -\hat{x}$ in which case Δ is replaced by $1/\Delta$. Hence, in this case as well the correction is smaller than the case of $\Delta = 1$. A larger amplitude for correction yields a larger back action on the oscillator, and thus, $\Delta = 1$ is the worst-case scenario for GCR.

in the limit of large $|\alpha|$. This is an appreciable improvement when it comes to high-fidelity performance in the presence of non-deterministic (random) errors such as DV ancilla decay. This is the dominant source of error in hybrid CV-DV architectures, where a longer circuit would induce more errors in the system and hence would be less suitable for high-fidelity outcomes. Thus, in the presence of such errors, our scheme's shorter circuit depth would take precedence if the failure probability P_e and hybrid infidelity $1 - F_H$ scaling are comparable.

We confirm our analytical results using numerics. In Fig. 2(a), we plot $1 - P_e(\text{GCR})$ and $1 - F_H(\text{GCR})$ against $|\alpha|$ for the special case of $\Delta = 1$. We find that the analytical results match with the numerical results for both GCR and BB1. The figure (along with detailed expressions in App. C) also implies that for the case of coherent states without squeezing ($\Delta = 1$) and $\theta = \pi/2$, we need $\alpha > 2$ to obtain any advantage from GCR or BB1. Thus, we have justified the correctness and validity of our scheme. Importantly, we have shown that the failure probability is low enough for most $|\alpha|$ values to be negligible. Hence, absent qubit or cavity decay errors, the scheme is effectively deterministic and does not need to rely on ancilla measurements. As a result, ancilla measurements can be used to herald the failure of the gate due to extrinsic factors such as detect qubit and cavity decay errors.

Our scheme has comparable performance to one of the best-known composite pulse sequences BB1(90). Comparing the plots in Fig. 2(a), we note the following: The failure probability of both schemes scales as χ^6 but the

prefactor of BB1 is an order of magnitude worse. The reset fidelity, on the other hand, scales as χ^6 for BB1 while it scales as χ^4 for GCR. Thus, the back action of GCR on the oscillator is worse than BB1 for large α . However, it is important to note that our scheme achieves this performance despite being shorter by a factor of at least 4.5 (more if $\Delta \neq 1$) in circuit duration. Thus, in the presence of loss as well in terms of time cost, our non-abelian-QSP-inspired sequence can be a better alternative to BB1 type correction for CV-DV control.

C. Composing Abelian and Non-Abelian QSP:BB1(GCR)

While the non-abelian QSP sequence GCR corrects for errors due to Gaussian uncertainty, it will be rendered less efficient if the state were to experience a small displacement error such that $\langle x \rangle \neq \pm\alpha$. We can solve this problem by concatenating GCR with BB1(90) which is designed to be resilient to such displacement errors. The net result for this QSP response function will be an approximate square wave that corresponds to a modular position measurement that is encoded into the ancilla qubit. Let us call this pulse BB1(GCR). The incorporation of GCR brings the response function somewhat closer to an ideal square wave, relative to just using BB1.

We can achieve the desired concatenation by converting each rotation in the BB1 (see Eq. (11)) into a Gaussian-controlled rotation.

$$\begin{aligned} \text{BB1}(\text{GCR}(\theta)) : & \text{GCR}_0\left(\frac{\theta}{|\alpha|}\hat{x}\right) \text{GCR}_{\phi_1}\left(\frac{\pi}{|\alpha|}\hat{x}\right) \\ & \times \text{GCR}_{3\phi_1}\left(\frac{2\pi}{|\alpha|}\hat{x}\right) \text{GCR}_{\phi_1}\left(\frac{\pi}{|\alpha|}\hat{x}\right), \end{aligned} \quad (37)$$

with the same expression for ϕ_1 as given in Eq. (11). We have presented a Gaussian-controlled version of the reversed BB1 sequence³. This order was chosen to match the order of pre-correction required for GCR. Here, for example,

$$\text{GCR}_{\phi_1}\left(\frac{\pi}{|\alpha|}\right) = e^{i\frac{\pi}{2|\alpha|}\hat{x}\sigma_\phi} e^{i\frac{\pi\Delta^2}{2|\alpha|}\hat{p}\sigma_\gamma}. \quad (38)$$

It is important to note that the pre-correction for $\text{GCR}_{\phi_1}(\pi/|\alpha|)$ is conditioned on the qubit Bloch sphere axis σ_γ , to be determined as follows. After the previous rotation $\text{GCR}_{3\phi_1}(2\pi/|\alpha|)$, we compute the state to which

qubit is rotated in the ideal case of no errors. Let us call this state $|\zeta\rangle$. Then,

$$\sigma_\gamma |\zeta\rangle = i\sigma_\phi |\zeta\rangle. \quad (39)$$

In the reverse BB1 case, σ_γ for GCR_0 depends on the state after the BB1 correction, which in the ideal case of no errors is the same as the starting qubit state $|g\rangle$. This makes the pre-corrections less intrusive and more efficient.

Remember that the goal here is not just to distinguish between $\langle x \rangle = \pm\alpha$ anymore. We would like to take advantage of the BB1(GCR(90)) and extract the following bit-wise information about oscillator position [54],

$$\frac{\langle x \rangle}{|\alpha|} \bmod 2. \quad (40)$$

- We start in the hybrid state $|g\rangle \otimes |\pm\alpha'\rangle$ where $\alpha' = m|\alpha|, m \in \mathbb{Z}$.
- If $m \in +\mathbb{Z}$, odd (even) m will yield $| -i \rangle$ ($| +i \rangle$) outcome.
- Else if $m \in -\mathbb{Z}$, odd (even) m will yield $| +i \rangle$ ($| -i \rangle$) outcome.

See Fig. 3 for numerical results for this protocol. For a coherent state with $\Delta = 1$, this sequence doubles the pulse length but also gives a better response. In addition, the more squeezed the state is, the shorter the additional pre-corrections are. From Fig. 3, we find that for $|\alpha| = \sqrt{\pi}/2, \Delta = 0.34$ the BB1(GCR) performs better in both metrics, defined in App. C1, terms of failure probability P_e as well as fidelity F_H . The improvement is same for both qubit measurement outcomes (± 1). This is an important requirement for measurement pulses, otherwise, it is not straightforward to say that the measurement fidelity (see App. C1) has been improved. Note that improvements for both bins are identical. Our choice of $|\alpha|, \Delta$ will be useful in Sec. V when discussing efficient end-of-the-line readout of logical GKP codewords. This composition is generalizable to all existing composite pulse sequences in the literature designed for qubit-only architectures [46, 47].

IV. DETERMINISTIC BOSONIC STATE PREPARATION

Conditional displacements and single-qubit rotations are a universal set of instructions that can map an oscillator in vacuum to an arbitrary CV state. It can also implement arbitrary quantum channels. This tool is a very powerful resource as Ref. [10] shows that these operations can be done extremely fast even in weak dispersive regimes, which is not the case for other qubit-based universal instruction sets. The weak-dispersive regime is key to reducing errors from higher-order terms like Kerr effects. Now, we will demonstrate how the composite

³ The BB1 correction can be run backward with the same performance. This sequence is equivalent to pre-pending the three corrective rotations. Note that BB1 correction can be appended at the beginning, end, or even in the middle of the target rotation.

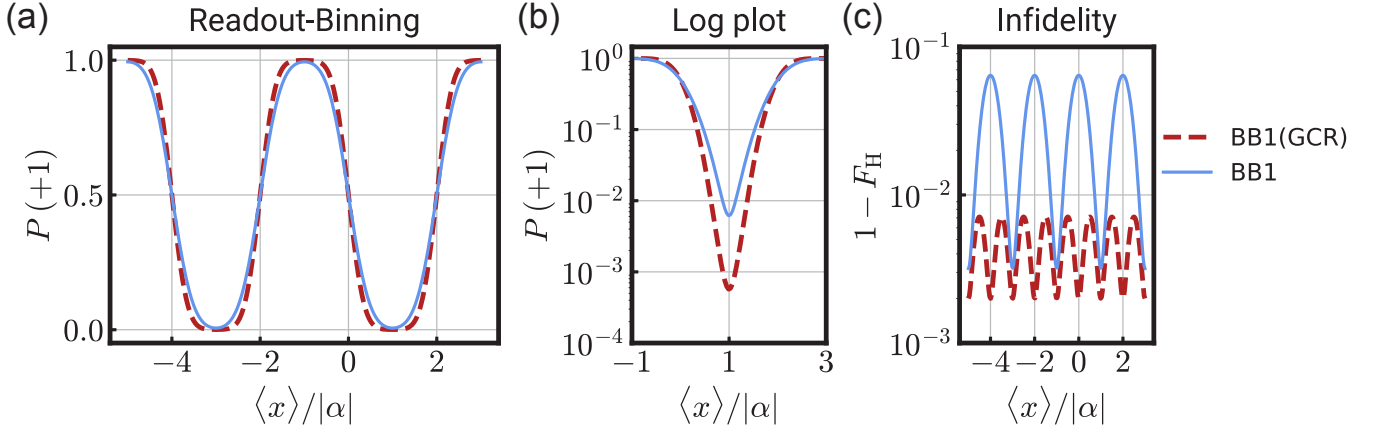


FIG. 3. **Readout binning using Gaussian-controlled-BB1 pulse sequence, BB1(GCR).** All plots follow the same legend. (a) Readout binning for the case of $|\alpha| = \sqrt{\pi}/2$. The plot gives the probability to measure a +1 outcome upon σ_y measurement, post the BB1(GCR) and BB1 in red and blue respectively. The x-axis represents the initial oscillator state with mean modular position value $\langle x \rangle / |\alpha|$ on which this pulse was applied. Note that a binning readout tells us whether the oscillator is in a specific bin (of size $2|\alpha|$) or not using qubit measurement outcome. Note that BB1(GCR) yields a flatter response function compared to BB1. (b) Logarithmic scale for plot (a) to quantify the advantage of BB1(GCR) precisely, for bins which support opposite qubit measurement outcomes. Note the order of magnitude improvement in BB1(GCR) compared to BB1 at the peaks of the target square wave response. (c) The hybrid fidelity F_H after each pulse. Interestingly, the BB1(GCR(90)) pulse has better fidelity as well.

pulse sequence designed in Sec. III can achieve deterministic preparation of states that are superpositions of non-overlapping Gaussian wave functions. Towards this direction, using our non-abelian QSP sequence GCR, we first give gadgets to squeeze an oscillator in Sec. IV A, entangle and untangle qubit from oscillator states which are represented as non-overlapping Gaussian wave functions in Sec. IV B.

With the help of these gadgets, we design preparation schemes of these simplest non-Gaussian states which can be represented as a superposition of non-overlapping finite-energy basis states $\{|\alpha\rangle_\Delta\}$ in the phase-space representation. This includes squeezed vacuum (Sec. IV A), two-legged cat states [55] (Sec. IV B), and GKP code-words [56] (Sec. IV C). Then, we will discuss the preparation of rotationally symmetric states in Sec. IV D. We explain why it might be better to use an abelian sequence like BB1 for N -legged cat states with high rotation symmetry (i.e., $N > 2$). We also present an amplification gadget to prepare the rotationally symmetric Fock states, setting the floor for future works to pursue universal state preparation for completeness.

For this section, we use the tensor product ordering $|\text{osc}\rangle \otimes |\text{qubit}\rangle$ for the joint Hilbert space. We will the total amplitude of CDs as the circuit duration (quoted in μs). The exact conversion into the runtime of circuit is given in App. D.

A. Squeezed States

We present a novel approach for generating squeezed states, marking a significant advancement in oscillator control. This result is comparable to state-of-the-art schemes in Refs. [10, 44] without the need for any numerical optimization tools. In addition, the structure identified by our scheme gives a more versatile approach to optimize the fidelity with respect to circuit duration. Our protocol has a basic unit composed of GCR. This basic unit follows an alternate explanation of $\text{GCR}(\theta)$ as a deterministic small-even-cat preparation circuit for small θ . The squeezing gadget uses the back action of GCR on the oscillator state to yield a squeezing gadget. Let us understand this effect in more detail for the case of momentum squeezing.

a. Squeezing gadget $\mathcal{S}(\Delta, \Delta')$. We pose the first step of this problem as modifying the uncertainties ($\delta x = \Delta/2, \delta p = 1/(2\Delta)$) of an oscillator state,

$$\psi(x) = e^{-\frac{(x-\beta)^2}{\Delta^2}}. \quad (41)$$

Our protocol begins with the oscillator in vacuum, that is, $\Delta = 2\delta x = 1, \beta = 0$. After a conditional displacement $\text{CD}(\alpha) = e^{i\alpha p \otimes \sigma_x}$ is applied to the joint state $|0_\Delta\rangle \otimes |g\rangle$, the expectation values of qubit operators conditioned on the position of the oscillator is given by,

$$\langle \sigma_x \rangle_x = \sin(\theta) = \tanh \frac{4\alpha x}{\Delta^2} \quad (42)$$

$$\langle \sigma_y \rangle_x = 0 \quad (43)$$

$$\langle \sigma_z \rangle_x = \cos(\theta) = \text{sech} \frac{4\alpha x}{\Delta^2} \quad (44)$$

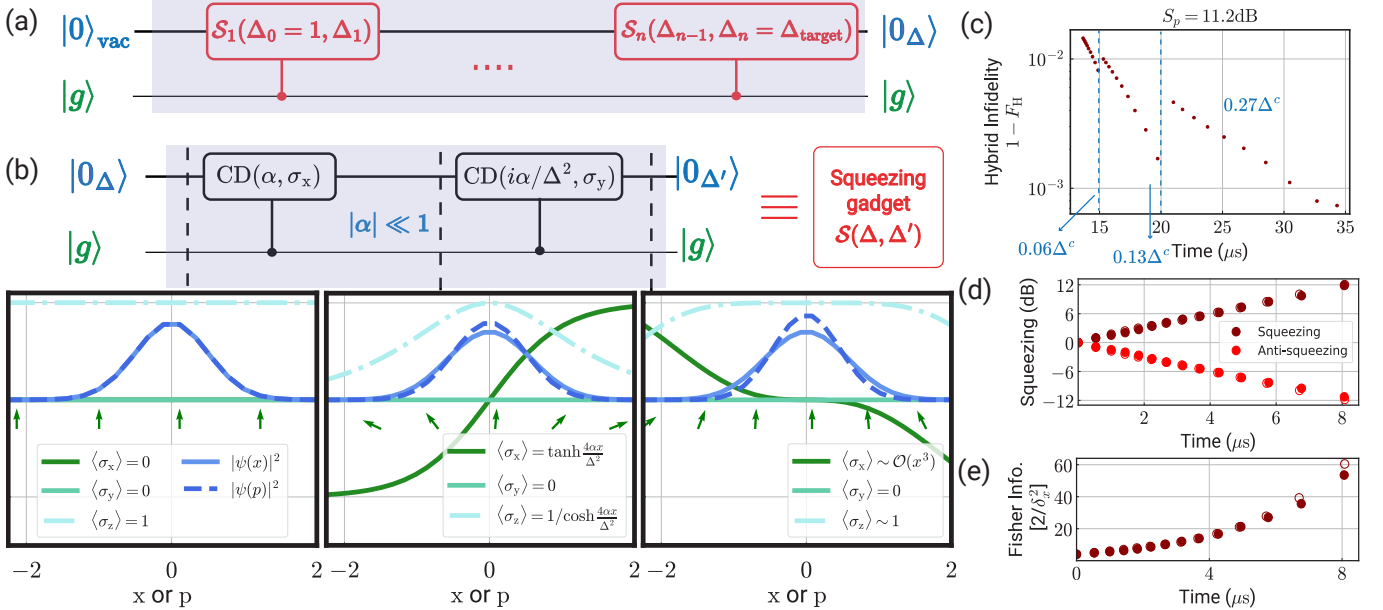


FIG. 4. **Deterministic Preparation of Squeezed States.** (a) Deterministic squeezing protocol with incremental GCR. (b) Narration of GCR as a squeezing gadget $S(\Delta, \Delta')$. The plots show how this sequence introduces a small amount of squeezing while unentangling the qubit from the final state for $\Delta = 1, |\alpha| = 0.25$. (c) Variation in fidelity and circuit duration with varying squeezing rate $|\alpha|_{k+1} = a\Delta_k^c$ where $c \in [-3, 0]$ and $a \in \{0.06, 0.13, 0.27\}$ for a target squeezing of 11.2 dB. (d) Squeezing (maroon) and anti-squeezing (red) are shown as a function of the circuit duration for the faster protocol with $c = 2$. See App. D for definitions of S_x, S_p in terms of Δ . (e) Fisher information for the faster protocol. The empty circles in (d,e) represent a plot of the results for the case when post-selection is activated.

where $\Delta/2 = \delta x$ is the position uncertainty of the input state for the units used in this work (see App. A). Note that, since the rotation axis was σ_x ,

$$\int_{-\infty}^{\infty} dx \langle \sigma_x \rangle = 0, \quad (45)$$

as should be the case. However, for a specific value of x , $\langle \sigma_x \rangle \neq 0$ is possible. Maintaining a small slope ensures that $\langle \sigma_x \rangle$ is proportional to x as long as $\psi(x)$ has significant amplitude. To un-entangle the qubit from the oscillator such that $\langle \sigma_z \rangle = 1$, we apply a rotation about σ_y by an angle $\theta = \sin^{-1}(\tanh \frac{4\alpha x}{\Delta^2}) \approx \frac{4\alpha x}{\Delta^2}$ (if $4|\alpha|x/\Delta^2 \ll 1$), i.e., $R_y(-4\alpha \hat{x}/\Delta) = e^{i \frac{2\alpha}{\Delta^2} \hat{x} \sigma_y} = \text{CD}(i\alpha/\Delta^2, \sigma_y)$. This corrects the linear part, setting

$$\langle \sigma_x \rangle \rightarrow 0, \langle \sigma_z \rangle \sim 1, \quad (46)$$

for the range where $x \ll \Delta^2/4|\alpha|$. This sequence equivalent to GCR in an alternate basis. In Sec. III we started with a conditional momentum boost and investigated the position basis, while in this case we started with a conditional displacement and investigated the position basis. The exact expressions of $\langle \sigma_x \rangle, \langle \sigma_z \rangle$ can be found in App. D.

Thus, for maximum un-entanglement of the oscillator and qubit, we need $|\alpha|/\Delta$ to be low enough, such that the

condition is satisfied. A larger⁴ $|\alpha|$ yields large squeezing but poor un-entanglement. Nevertheless, after a single application of this squeezing gadget, the position uncertainty δx of the state increases (see Fig. 4(a)), thus allowing for larger $|\alpha|$ in the successive round to obtain even larger squeezing. Note that, this in turn, also increases the range over which $\psi(x)$ has a significant amplitude. As we know, a small-even-cat state is nothing but a slightly squeezed vacuum, and thus, this narration leads to the preparation of squeezed oscillator states.

Protocol: In Fig. 4(a) we show that repeated application of the squeezing GCR circuit (\mathcal{S} , see Fig. 4(b)) yields the desired target squeezing. Careful selection of $|\alpha|_k$ for successive steps k is crucial for this purpose, as it dictates the convergence of squeezing with each cat step. For optimal squeezing, $|\alpha|$ should be as high as possible while ensuring that the slope of $\langle \sigma_y \rangle$ is linear over the range $|x| \leq 2\delta x$. Another important detail is that the even cat state is a sum of two highly overlapping Gaussian functions, posing a very high fidelity to a squeezed vacuum.

To determine the right correction for the next round $\frac{\alpha_k}{\Delta_k^2}$ we need to approximate it to the closest Gaussian function, that is, identify the resulting Δ after each

⁴ but small enough for the output state to resemble a Gaussian function

application of \mathcal{S} . This can be computed using various approximations/numerical methods. We derive that for a linear slope over FWHM of the oscillator state, $|\alpha|_{k+1} \ll 0.13\Delta^{1/2}$, see details in App. D.

To understand the relationship between convergence (which determines circuit duration) and un-entanglement (which determines hybrid oscillator-qubit fidelity) for various $|\alpha|_{k+1} = a\Delta^c$, we use this protocol to obtain a squeezing of $S_p = 11.2$ dB in Fig. 4(c). We note that, increasing a, c yields better fidelity but longer circuit duration. This behavior, however, is reversed for $c > 0$.

The upper bound on c is 2 since, for this value, the slope of $\langle \sigma_y \rangle$ is constant for varying Δ . This is the fastest rate of convergence one could choose. However, for the case of momentum-squeezing analyzed here, $\Delta \geq 1$. Thus, with each step k , $\langle \sigma_y \rangle$ will be now more nonlinear, making un-entanglement harder. So, we approximate corrections to the linear slope $4\alpha/\Delta^2$ numerically (see App. D). Using this faster protocol, we obtain Figs. 4(d,e). The squeezing efficiency, measured in dB, has a linear dependence on circuit duration⁵, as shown in Fig. 4. We note that this protocol results in faster convergence compared to Fig. 4(c).

Squeezed states often find use cases in measuring the net displacement or momentum boost in a state. The sensitivity of this measurement is usually determined via the Fisher information, which for a Gaussian state, like the momentum-squeezed state, is given by [57] $2/\delta_x^2$, where δ_x^2 is the variance of the position operator. Note that this is not the right formula to compare non-Gaussian states generated using conditional displacements; however, we still use this metric for comparison with results in Refs. [10, 44]. In addition, our final state is close to the desired Gaussian squeezed state compared to the state prepared in Ref. [44] that has more Wigner negativity. That is, the squeezed state prepared using our scheme is more suited to be used with this formula. Thus, quantifying the efficiency of this scheme in accurate position or momentum measurements, the highest Fisher information of $F = 2/\delta x^2 = 53.5$ is reported for the final state with squeezing $S_p = 11.2$ dB, $S_x = -11.9$ dB at infidelity of 0.008 in 8.06 μ s.

We also find that post-selection over qubit being in the state $|g\rangle$ (empty squares) does not improve results by much. This observation indicates that we are achieving optimal un-entanglement with the help of GCR for our choices of $|\alpha|_k$. In addition, each \mathcal{S}_k is small enough such that we can achieve better performance with the help of post-selection, in the presence of ancilla errors.

Discussion Our analytically derived circuit performs on par with the semi-analytical and numerically optimal methods in Refs. [10, 44]. We plot results against circuit duration instead of circuit depth, given the speed and errors in a conditional displacement gate depend

significantly on the length of the amplitude [10]. Our protocol achieves squeezing levels, with $S_p = 8.5$ dB of squeezing and $S_x = -8.4$ dB of anti-squeezing, alongside an infidelity of $\sim \mathcal{O}(10^{-3})$ in 5.8 μ s while Ref. [44] reports $\delta x = 8.5$ dB and $\delta p = -9.9$ dB with an infidelity of $\sim \mathcal{O}(10^{-2})$. The performance of our scheme is also on par with numerically optimized schemes [10], offering improved oscillator control. Details of the comparisons here can be found in App. D.

We briefly discuss the reason behind our improvement upon the results in Ref. [44]. In that work, authors use large conditional displacement in the first step in contrast to our approach of incrementing the amplitude of conditional displacements with increasing Gaussian width of the oscillator state. Due to this approach, the protocol requires numerical techniques to un-entangle the qubit. On the other hand, our protocol is completely analytical and yields squeezed states with better fidelity. Our protocol outputs states with fairly less interference (i.e., Wigner negativity), yielding higher fidelity with a squeezed state (which is a Gaussian state, and hence shows no interference/Wigner negativity).

B. Two-Legged Cat States

The superposition of two coherent states located at diametrically opposite locations in the phase space of an oscillator is known as two-legged cat states. The interference pattern at the origin is determined by the local phase of this state, also termed the ‘whiskers of the cat’.

$$|C_{+\alpha}\rangle \propto (|\alpha\rangle + |-\alpha\rangle) \quad \text{Even Cats} \quad (47)$$

$$|C_{-\alpha}\rangle \propto (|\alpha\rangle - |-\alpha\rangle) \quad \text{Odd cats.} \quad (48)$$

If the basis states $|\pm\alpha_\Delta\rangle$ with $\Delta \neq 1$ are used in this definition, then $|C_{\pm\alpha}\rangle$ are squeezed cat states.

A deterministic preparation of cat states will require the qubit to be unentangled from an oscillator after a large (equal to cat size) conditional displacement $CD(\alpha, \sigma_x)$ (see Fig. 5(a)) leading to the state $|C_{+\alpha}\rangle$ if the initial qubit state was in $|g\rangle$. That is, ignoring the normalization constant, we need

$$\mathcal{U}(|\alpha\rangle|+\rangle + |-\alpha\rangle|-\rangle) \approx |C_{+\alpha}\rangle|g\rangle. \quad (49)$$

So, the first question we address here is how to entangle or un-entangle oscillator states with qubits with minimal back action on the oscillator. This can be done with the help of GCR which we saw in Sec. III will rotate a qubit entangled with states $|\pm\alpha\rangle$ by $\pm\pi/2$. Thus, we now interpret GCR as *entangling-untangling gadgets* of the hybrid oscillator-qubit system, to be used repeatedly in the remainder of this work.

1. Entangling Oscillators and Qubits

The primary requirement to use the rotation gadgets (GCR or BB1) for entangling oscillators and qubits will

⁵ The conversion from amplitudes of CD to time is given in App. D

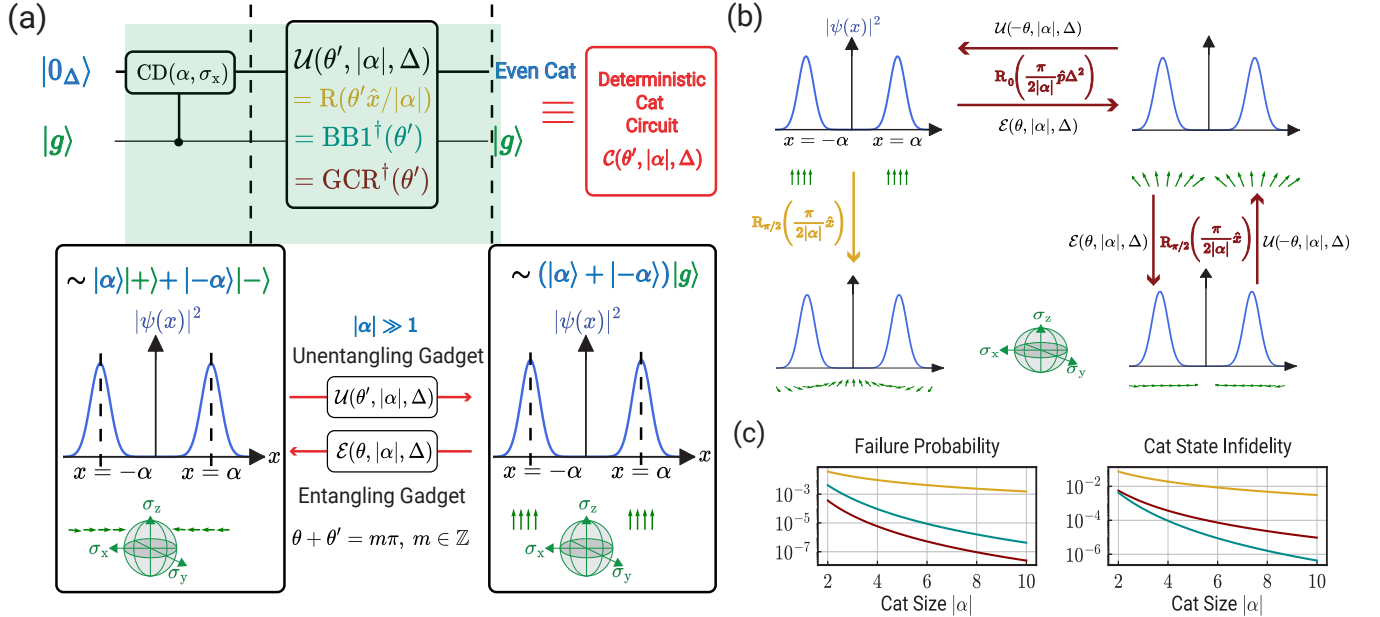


FIG. 5. **Deterministic Preparation of Two-Legged Cat States.** (a) Deterministic cat state preparation requires an un-entangling sequence given by \mathcal{U} . (b) Entangling-unentangling gadgets using GCR. (c) We show numerical results with options of no correction ($\mathcal{U} = R_y(\theta' \hat{x}/|\alpha|)$ in yellow), univariate or traditional QSP correction ($\mathcal{U} = BB1$ in cyan), bivariate (non-abelian) QSP correction ($\mathcal{U} = GCR$ in red). (Left) Success probability of ancilla ending in-state $|g\rangle$. (Right) Fidelity of output oscillator state with the desired cat state upon success.

be that the oscillator state be represented by a sum of non-overlapping Gaussian wave functions. Consider a state (ignoring normalization),

$$|\psi_\Delta\rangle \propto |+\alpha_\Delta\rangle \pm |-\alpha_\Delta\rangle, \quad (50)$$

with $\langle \alpha_\Delta | - \alpha_\Delta \rangle \rightarrow 0$, such that $|\psi_\Delta\rangle$ is a sum or difference of non-overlapping Gaussian wave functions. The entangling gadget \mathcal{E} and disentangling gadget \mathcal{U} are defined as (up to normalization constants),

$$\mathcal{E}|\psi_\Delta\rangle|g\rangle = |+\alpha_\Delta\rangle|+\rangle \pm |-\alpha_\Delta\rangle|-\rangle, \quad (51)$$

$$|\psi_\Delta\rangle|g\rangle = \mathcal{U}(|+\alpha_\Delta\rangle|+\rangle \pm |-\alpha_\Delta\rangle|-\rangle). \quad (52)$$

It can be trivially seen that $\mathcal{U} = \mathcal{E}^{-1}$ works, yet we will see next that this is not the only option available for the unentangling gadget \mathcal{U} .

a. \mathcal{E} : A Gaussian-peak-dependent entangling gadget can be defined as

$$\mathcal{E}(\theta, |\alpha|, \Delta) : GCR(\theta)(|\psi_\Delta\rangle \otimes |q\rangle), \text{ or } BB1(\theta)(|\psi_\Delta\rangle \otimes |q\rangle) \quad (53)$$

when the initial qubit state is $|q\rangle$. For the case of cat states in Fig. 5(a) or Eqs. 52, $\theta = \pi/2$.

b. \mathcal{U} : If we start in an entangled hybrid oscillator-qubit state, an unentangling circuit ensures that the qubit state at the end of the circuit is fixed (see Fig. 5(a)). Thus, we define the unentangling gadget as any circuit of the form,

$$\mathcal{U}(\theta', |\alpha|, \Delta) : GCR^\dagger(-\theta')|\phi_\Delta\rangle, \text{ or} \quad (54)$$

$$: BB1^\dagger(-\theta')|\phi_\Delta\rangle \quad (55)$$

where $|\phi\rangle$ represents a hybrid oscillator-qubit entangled state, such as the output of Eq 51. Note that, the parameters of the unentangling gadget can be different from that given by \mathcal{E}^{-1} , as noted from the periodicity of single-qubit rotations, only need to satisfy Eq. (52). The condition for $\mathcal{E} - \mathcal{U}$ for a specific oscillator state, is given by,

$$\theta + \theta' = m\pi \quad m \in \mathbb{Z}. \quad (56)$$

For example, for the case of cat states in Fig. 5(a), $(\theta, \theta') = (\pi/2, -\pi/2)$ is just one of the many choices. Now, we can summarize the cat state preparation protocol. For a pictorial representation of the cancellation of errors at $|\pm\alpha\rangle$ simultaneously, see Fig. 5(b).

Protocol: We assume that the Gaussian functions have negligible overlap, that is, $\alpha > 1$. We start with the hybrid oscillator-qubit state, $|0\rangle \otimes |g\rangle$ and perform a conditional displacement,

$$e^{-i2\alpha p \sigma_x}(|0\rangle_{\text{vac}} \otimes |g\rangle) \propto |\alpha\rangle|+\rangle + |-\alpha\rangle|-\rangle \quad (57)$$

This leaves the oscillator-qubit in an entangled state. At this point, if we were allowed to use measurements, we could probabilistically prepare even or odd cat states by measuring the qubit in the σ_z basis [11, 58, 59]. However, for a deterministic process, we need to avoid any measurement, and this is where the unentangling gadget \mathcal{U} can help. Therefore, the cat preparation circuit is

given by,

$$\begin{aligned} \mathcal{U}(\pi/2, |\alpha|, 1) e^{-i2\alpha\hat{p}\sigma_x} (|0\rangle_{\text{vac}} \otimes |g\rangle) \\ \propto \mathcal{U}(\pi/2, |\alpha|, 1) (|\alpha\rangle |+\rangle + |-\alpha\rangle |-\rangle) \end{aligned} \quad (58)$$

$$= e^{-i\frac{\pi}{4|\alpha|}\hat{p}\sigma_x} e^{i\frac{\pi}{4|\alpha|}\hat{x}\sigma_y} (|\alpha\rangle |+\rangle + |-\alpha\rangle |-\rangle) \quad (59)$$

$$\begin{aligned} \approx (|\alpha\rangle + |-\alpha\rangle) \otimes |g\rangle + O(\chi^2) |\psi'\rangle \otimes |g\rangle \\ + O(\chi^3) |\psi''\rangle \otimes |e\rangle, \end{aligned} \quad (60)$$

where χ is the error parameter defined in Eq. (32). This circuit requires no measurement and yields the even cat $\propto (|\alpha\rangle + |-\alpha\rangle)$ state in the cavity. Odd cats $\propto (|\alpha\rangle - |-\alpha\rangle)$ can similarly be prepared by starting in qubit state $|e\rangle$ or using

$$\begin{aligned} \mathcal{U}(\pi/2, |\alpha|, 1) e^{-i2\alpha\hat{p}\sigma_x} (|0\rangle_{\text{vac}} \otimes |g\rangle) \\ \propto \mathcal{U}(\pi/2, |\alpha|, 1) (|\alpha\rangle |+\rangle + |-\alpha\rangle |-\rangle) \end{aligned} \quad (61)$$

$$= e^{-i\frac{\pi}{4|\alpha|}\hat{p}\sigma_x} e^{-i\frac{\pi}{4|\alpha|}\hat{x}\sigma_y} (|\alpha\rangle |+\rangle + |-\alpha\rangle |-\rangle) \quad (62)$$

$$\begin{aligned} \approx (|\alpha\rangle - |-\alpha\rangle) \otimes |e\rangle + O(\chi^2) |\psi'\rangle \otimes |e\rangle \\ + O(\chi^3) |\psi''\rangle \otimes |g\rangle \end{aligned} \quad (63)$$

to end up in $|e\rangle$ with maximum probability. In these scenarios, the final state will have the highest fidelity with an odd cat of size α . As described in Sec. III B, the success probability and fidelity depend on the value of $\chi = \theta\Delta/2|\alpha|$, so the cat fidelity increases with increasing α and decreasing Δ .

Discussion In Figs 5(c,d) we vary α and plot for the worst case scenario of $\Delta = 1$, (1) $1 - P_e$ which is marked by the measurement of ancilla in $|e\rangle$ and (2) $1 - F_H$, the infidelity of the hybrid output state against the desired even cat state with the qubit in $|g\rangle$. Low P_e for GCR and BB1 indicate that ancilla measurement is not required for un-entangling the qubit here. As shown before in Sec. III B, the P_e for the un-entanglement gadget decreases with increasing $|\alpha|$ and as we move to $\Delta < 1$. We can see the same trend as given by the corresponding correctness metrics for our framework in Fig. 2. To study the effectiveness of QSP, we also show the respective curves for performing no correction with $\mathcal{U} = \text{CD}(\theta'/2|\alpha|, \sigma_y)$. The analytical expression $P_e = \mathcal{O}(\chi^2)$ for this curve has been derived in App. E 1. The analytical fidelity for the GCR and BB1 has been computed in App. C. Thus, we have shown orders of magnitude improvement achieved from our framework of using composite pulses in phase space when correcting continuous-variable rotation errors on qubits.

C. GKP States

GKP codes have applications for quantum sensing and bosonic error correction [17, 23, 24, 61]. In this section, we will only discuss the definition of logical codewords required for preparation, leaving all other details to Sec. V where we discuss universal control of these codewords. While we focus on the square GKP codewords to give explicit constructions for preparation, all our protocols are

easily generalizable to arbitrary lattices of hexagonal and rectangular GKP codes. Due to the completely analytical constructions, we note that our preparation schemes are easily generalizable to GKP qudits also. Such generalizations are not accessible to numerically optimized circuits, such as the ones shown in [10]⁶. The computational basis square-GKP codewords are defined as [56], ignoring normalization constants

$$|0\rangle_{\text{GKP}} \propto \sum_{m=-\infty}^{\infty} e^{-(m\sqrt{\pi})^2\Delta^2} D(m\sqrt{2\pi}) |0_{\Delta}\rangle, \quad (64)$$

$$|1\rangle_{\text{GKP}} = \propto \sum_{m=-\infty}^{\infty} e^{-(2m+1)\sqrt{\pi})^2\Delta^2} D([m+1/2]\sqrt{2\pi}) |0_{\Delta}\rangle, \quad (65)$$

where $m \in \mathbb{Z}$, $D(\alpha) = e^{\alpha\hat{a}^\dagger - \alpha^*\hat{a}} = e^{2i(\text{Im}(\alpha)\hat{x} - \text{Re}(\alpha)\hat{p})}$ denotes an unconditional displacement of the oscillator by $|\alpha|$ generated by the operator $\hat{v}(\alpha) = 2\text{Im}(\alpha)\hat{x} - 2\text{Re}(\alpha)\hat{p}$. Here, $|0_{\Delta}\rangle = |0_{2\delta x}\rangle$ are the position-squeezed states (see Eq. (4)). Note that, $|\pm\rangle_{\text{GKP}} = (|0\rangle_{\text{GKP}} \pm |1\rangle_{\text{GKP}})/\sqrt{2}$ states are exactly equal to the same superposition of finite-energy momentum-squeezed states $|0_{2\delta p}\rangle$.

There are various definitions of GKP states in the literature, in addition to the above equations, all of which are equivalent [62]. Note that the states we prepare in this work will closely resemble those described by the above equations. The most important task for a preparation routine is to prepare a state close to the GKP manifold such that the stabilization (i.e., subsequent rounds of error correction) can take care of the residual (yet correctable) small errors. Thus, in order to remove any non-uniformity in fidelity using various definitions, we will also compute the expectation values of the finite energy stabilizers [60],

$$S_{x,\Delta} = e^{i2\sqrt{2\pi}(\cosh \Delta^2 \hat{x} - \hat{p} \sinh \Delta^2)} \quad (66)$$

$$S_{p,\Delta} = e^{i2\sqrt{2\pi}(\cosh \Delta^2 \hat{p} - \hat{x} \sinh \Delta^2)} \quad (67)$$

Now, we present the first analytical measurement-free protocol, derived using non-abelian QSP, for the preparation of GKP codes. We give comparisons to other, numerically optimized schemes in Refs. [10, 41]. We also give a comparison against using the stabilization scheme which can cool any CV state towards the GKP manifold [16, 60]. The comparisons in this section discuss circuit depth. Our scheme has an additional advantage towards error correction which will be discussed in Sec. V A.

Protocol: GKP states are an extension of two-legged cat codes where the deterministic preparation scheme is now required to create superpositions of multiple

⁶ For each qudit codeword, a new optimization needs to be run since the circuit constructions are highly non-intuitive and provide no structure for any generalization.

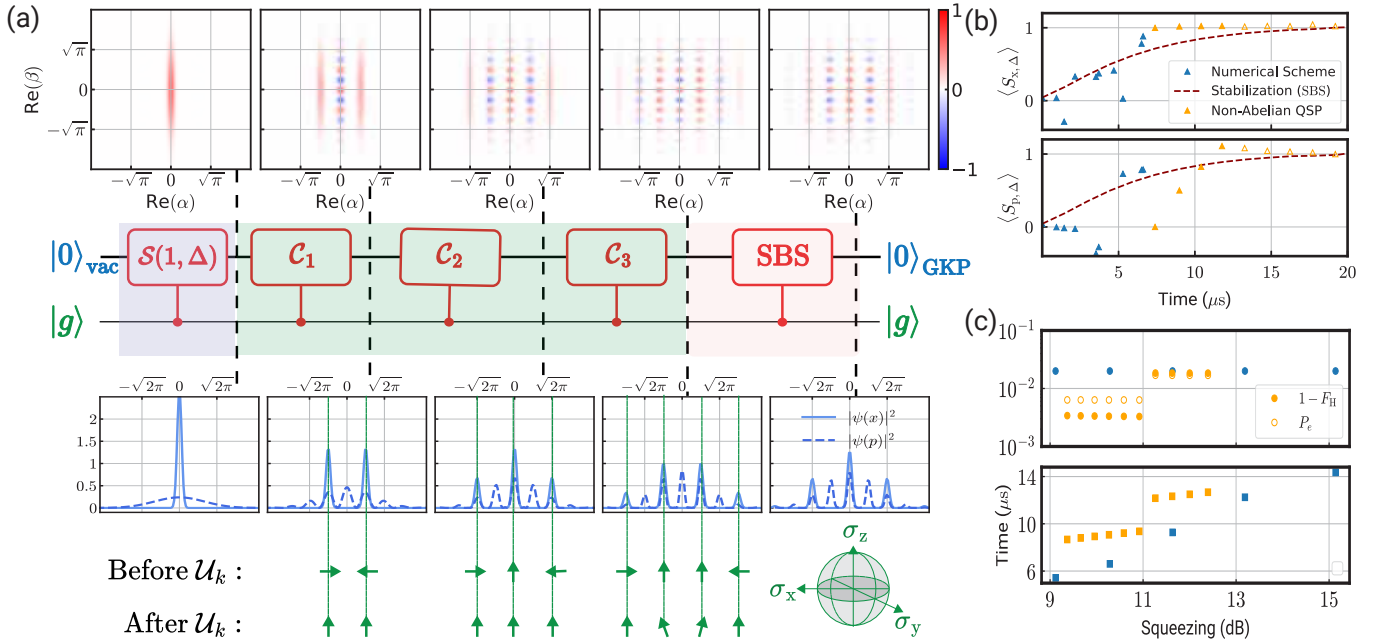


FIG. 6. **Deterministic GKP logical $|+Z\rangle$ state preparation.** (a) The circuit component (for $\Delta = 0.34$ used in recent experiments [10, 23]). \mathcal{S} represents the squeezing circuit from Fig. 4, and $\mathcal{C}_k = \mathcal{U}_k e^{-i\sqrt{2\pi}\hat{p}\sigma_z}$ represents the gate sequence given by Eq. (68) in the main text. Finally, SBS represents one round of the small-big-small protocol. See Table. II for justification of circuit-depth. (Top) We show the Wigner functions $\mathcal{W}(\alpha, \beta)$ [8] after each step of the protocol. Note the difference between the states before and after SBS. (Bottom) The wave functions show the GKP state and corresponding spin polarizations before and after each \mathcal{U}_k . Note that after \mathcal{U}_3 the qubit is still slightly entangled with the state such that $\langle \sigma_z \rangle = 0.9937$ and $\mathcal{F}_{\text{GKP}} = 0.9989$. (b) Convergence of various protocols. The evolution of states using the expectation value of finite energy stabilizers $\langle S_x \rangle, \langle S_p \rangle$ (see Eqs. 67,66). The non-abelian QSP protocol using GCR (via \mathcal{C}'_k 's) starts at $8.06\mu\text{s}$ to take into account the circuit-depth of achieving squeezing of 11.2 dB (see Fig. 4 and Sec. IV A). The empty triangles in our scheme denote the part where SBS is appended. Our protocol is on par or better than the numerical scheme [10] while being much faster than the stabilization scheme (using only SBS, see Fig. 9) [60]. (c) Hybrid infidelity, failure probability (top), and circuit duration (bottom) against squeezing (or, Δ) for the numerical scheme and the analytical circuit using a non-abelian QSP sequence via \mathcal{C}_k . Note that the fidelity and circuit duration of our scheme is on par with the numerical scheme while yielding a low failure probability. For all your numerical results in this figure, we have neglected any errors in the system, including damping, heating, and decoherence of both cavities and qubits. Simulations with errors are performed in Sec. V.

squeezed coherent states unentangled from the qubit. A sketch of the preparation scheme is given in Fig. 6(a). We now give the algorithm described by the circuit construction shown in Fig. 6(b) to prepare logical Pauli eigenstates of the GKP code.

We start with a squeezed vacuum (prepared using the protocol in Sec. IV A), and use the cat-state preparation circuit \mathcal{C}_1 (described in IV B) to prepare squeezed cats, leaving the ancilla unentangled. Circuits \mathcal{C}_k producing $k+1$ peaks represent the gate sequence,

$$\mathcal{C}_k : \mathcal{C}\left(\frac{\pi}{4k}, \sqrt{\frac{\pi}{2}}, \Delta_{k-1}\right) = \mathcal{U}\left(\frac{\pi}{4k}, \sqrt{\frac{\pi}{2}}, \Delta_{k-1}\right) e^{-i\sqrt{2\pi}\hat{p}\sigma_z}, \quad (68)$$

where we use the definition of the unentangling gadget $\mathcal{U}(\theta, |\alpha|, \Delta)$, conditioned on the input state, from Sec. IV B 1. In this case, the circuit components \mathcal{C}_k are decided by the lattice spacing ($\sqrt{2\pi}$ in Wigner units for square-GKP codes [56]), the finite-energy parameter Δ of the target GKP state and the previous state after $k-1$ snippet of the circuit. We first start with a squeezed state

which can be prepared using the protocol in Sec. IV A. Next, we create a squeezed cat state of size $\sqrt{\pi/2}$ where the non-abelian QSP correction is $\sqrt{\pi/2}\Delta^2$. This process is repeated to create a superposition of three Gaussian wave functions. Note that the information regarding integer multiple m is not required while designing the unentangling gadget. It is so because the gap between each peak is $\sqrt{2\pi}$ (in Wigner units), and that means each peak subsequently away from the origin rotates the qubit by an extra angle of $\sqrt{2\pi}|\alpha| = 2\pi$. Thus, each peak will rotate the qubit by the same amount (as 2π is the period of all trigonometric functions). Note that, in our scheme, expectation values exceeding unity in Fig. 6(b) are artifacts of the non-abelian pulse. This arises because the final state after \mathcal{C}_3 has not yet fully converged to the GKP code space; in particular, the most displaced squeezed states in the superposition lack the Wigner negativity characteristic of true GKP states. At this stage, applying a single round of SBS can effectively refine the state, bringing it closer to the ideal GKP form. Crucially,

using SBS at this point almost deterministically prepares the logical $|0\rangle_{\text{GKP}}$ state.

a. Fidelity and circuit-depth: The state prepared using this method yields a state whose Gaussian peaks have amplitudes that are binomial coefficients whereas the usual definition of GKP states uses a Gaussian envelope. Hence, we use the Newton-Raphson method to find the number of steps N required for a given Δ where the binomial coefficients reach a Gaussian distribution. This method is highlighted in App. F. With this circuit depth

Δ	Squeezing (in dB)	N	$1 - \mathcal{F}$
0.10	20	31	$\mathcal{O}(10^{-5})$
0.20	14	7	$\mathcal{O}(10^{-3})$
0.30	10.45	3	$\mathcal{O}(10^{-2})$
0.4	7.95	1	$\mathcal{O}(10^{-2})$

TABLE II. Circuit depth for different squeezing levels starting with the initial state $e^{-\frac{x^2}{\Delta^2}}$. Here, N is the optimal number of large conditional displacements ($\sqrt{\pi}$) are involved in preparing a $|0\rangle_{\text{GKP}}$ circuit for the desired finite-energy parameter, obtained using $N\Delta^2 = 0.32$ ^a as solved above.

^a Here, a state with $\Delta = 0.5$ is achieved with a very high fidelity because for states with such high finite-energy parameter, a GKP logical $|0\rangle_{\text{GKP}}$ state is a squeezed vacuum while a GKP $|1\rangle_{\text{GKP}}$ is the grid state which is similar to (not same as) a squeezed cat state.

we compare the fidelity of our GKP logical $|\mu = \{0, 1\}\rangle$ states using the definition,

$$|\mu\rangle_{\text{GKP}} = \mathcal{N}_\mu \sum_{m=-\frac{N+\mu}{2}}^{\frac{N-\mu}{2}+1} b_1 D([m + \mu/2]\sqrt{2\pi}) |0_\Delta\rangle, \quad (69)$$

where $m \in \mathbb{Z}$, $b_\mu = \binom{N}{m+\mu+\lfloor N/2 \rfloor}$ where $N = \lfloor 0.32/\Delta^2 \rfloor$ (see Table II). These equations are justified by showing the evolution of the prepared states in Fig. 6(b). Note that we have accounted for the circuit depth of squeezing in Fig. 6(b), as the first point for non-abelian QSP starts at $8.06\mu\text{s}$.

b. Success Probability: For the circuits C_k we need $\mathcal{U}(\theta', |\alpha|, \Delta)$ with $\theta' = \pi/4$ for $k < 3$. For $k = 3$, as can be seen in Fig. 6(a), the angle required to rotate the qubits at peaks on the farther end is $\pi/12$. Thus, the un-entanglement gadget \mathcal{U}_k at this point rotates the qubits by $\theta = \pm\pi/12$ at the two extreme peaks as required. However, it also rotates the qubits entangled with the peaks in the middle, ones that did not require any rotation. While the rotation at the central peaks is not significant, there is a different angle of rotation compared to $\pi/4k$ which could produce better un-entanglement for $k \geq 3$. We compute the optimal angle of rotation using the procedure given in App. F. With this protocol, we obtain Figs. 6(a,b) for $\Delta = 0.34$ (used in recent experiments [10, 23]). The fidelity after $k = 3$ yields 4 peaks with a fidelity of $F_H = 0.9989$ to the target GKP state, while the success probability was $P_g = 0.99$. Thus, we

may also reset the ancilla after each C_k . Such high success probability justifies using the measurements to keep ancilla errors in check (see Sec. V A).

c. Other GKP Lattice Finally, to achieve different GKP rectangular and hexagonal lattice based GKP codes, we will only need to change the lattice spacing l and the rotation angle θ according to the position of the deformed lattice peaks $k\alpha$, in the circuit components C_k .

$$C_k = \mathcal{U}\left(\frac{\pi}{4k}, \frac{l}{2}, \Delta_{k-1}\right) e^{-i\sqrt{2}\alpha\hat{p}\sigma_z} \quad (70)$$

Arbitrary GKP states (other than Pauli eigenstates) can be prepared using the gate-teleportation circuit discussed in Sec. V D. We also discuss state transfer from the perspective of entangling and unentangling gadgets in App. F.

Discussion We show a comparison of our scheme against two different GKP preparation methods [10, 60] in Fig. 6(b,c). It should be noted that our scheme is different from Ref. [41] where the authors propose to prepare GKP states using the same pattern of alternating conditional-displacements and momentum boosts, however, due to the lack of the non-abelian QSP pulse, in this case, the qubit needs to un-entangled using numerical schemes. The scheme in Ref. [41] starts with a large cat and then creates multiple superpositions by moving inwards towards the origin. The demerit of this scheme is that one needs additional numerical optimization to adjust the coefficient of each peak, in the absence of which, the GKP state has an external envelope of two Gaussian functions centered at the peaks of the cat state prepared in the first step. In addition, this means that our protocol uses smaller conditional displacements in one step. This is an important distinction since this incurs less error during one step, and so if post-selection upon qubit measurement after each step is used, our protocol will naturally yield a higher success probability. This direction has been discussed in detail in Sec. V A as mid-circuit ancilla error detection.

Another method to prepare the GKP states is by using a code space stabilization scheme followed by measurement of the Z_{GKP} operator on the cavity state. We find that our scheme is twice faster compared to the stabilization scheme *small-big-small* [16, 60], described later in detail in Sec. V. Finally, our circuit depth and fidelity (see table II and Fig. 6) are on par with the optimized ECD circuits in [10]. Importantly, our scheme gives us a way to make the scheme tolerant to circuit errors and achieve higher fidelity in the presence of faults, impossible for the long numerically optimized circuits in [10]. After each C_k , in the absence of errors, the qubit is in a known pure state untangled from the oscillator with a very high probability (> 0.99) as indicated by the low failure probability in Fig. 6(c). At this point, GKP states can be post-selected, given the qubit is found in the desired state. Thus, we can also keep qubit errors in check with this scheme.

D. Towards Universal State Preparation

The phase-space instruction set discussed in this work is more suited to oscillator states discussed above in terms of efficient circuits for preparation and control. However, this instruction set is universal, and thus, for completeness we discuss the preparation of rotationally symmetric states like N -legged cat states and Fock states. Finally, we will give insights into applications in the construction of arbitrary superposition of Fock states. We note that such states could be better prepared with the help of Fock-space instruction set [8] using the hybrid SNAP gates and unconditional displacement or momentum boosts of the oscillator.

1. Rotationally Symmetric Codewords

Here, we will discuss the preparation of four-legged cat states and their extension to N -legged cat states. N -legged cat states are superposition of N coherent states located at the vertices of an N -sided polygon, centered at the phase space origin. Superposition of N basis states requires a minimum of $\log_2 N$ conditional displacement applications, at the end of which the oscillator and qubit should be completely entangled. We again use QSP corrections to assist in un-entangling the ancilla qubit.

For example, in order to generate a 4-legged cat state, our first cat preparation circuit generates a two-legged cat state, and then the next circuit in the orthogonal direction generates a four-legged cat. The challenge is to un-entangle the qubit in this case where it is entangled with four oscillator states, all at $x \neq 0$ and $p \neq 0$.

Protocol: From the preparation of even cat states $|C_{i\beta}\rangle = \mathcal{N}(|i\beta\rangle + |i\beta\rangle)$ (where \mathcal{N} is the normalization constant), we proceed as follows,

$$\begin{aligned} \mathcal{U}(\theta, |\alpha|, 1) e^{-i2\alpha\hat{p}\sigma_x} |C_{i\beta}\rangle |g\rangle \\ = \mathcal{U}(\theta, |\alpha|, 1) [e^{-i2\alpha\hat{p}} |C_{i\beta}\rangle |+\rangle + e^{+i2\alpha\hat{p}} |C_{i\beta}\rangle |-\rangle] \end{aligned} \quad (71)$$

where $\mathcal{U}(\theta, |\alpha|, 1) \equiv \text{GCR or BB1}$. Here, $\theta = \frac{\pi}{2}$ and the un-entangling gadget \mathcal{U}_p rotates qubits based on their momentum eigenvalue (with uncertainty $\Delta = 1$). Fig. 7 summarizes the effects of both abelian and non-abelian QSP pulses discussed in our work.

a. GCR: We now need to simultaneously disentangle two displaced cat states, analogous to the case of displaced coherent states (see App. C 5). The effect of the disentanglement gadget on the two cat states in superposition is given by,

$$\begin{aligned} \mathcal{U}(\theta, |\alpha|, 1) e^{-i2\alpha\hat{p}\sigma_x} |C_{i\beta}\rangle |g\rangle \\ \approx [e^{i\alpha\frac{\pi}{4\beta}\sigma_x} e^{-i2\alpha\hat{p}} |C_{i\beta}\rangle + e^{-i\alpha\frac{\pi}{4\beta}\sigma_x} e^{i2\alpha\hat{p}} |C_{i\beta}\rangle] |g\rangle. \end{aligned} \quad (72)$$

Thus, the un-entanglement fails unless $\frac{\pi\alpha}{4\beta} = \frac{m\pi}{2} \implies \frac{\alpha}{\beta} = 2m$ where $m \in \mathbb{Z}$. Therefore, using the non-abelian QSP sequence we could only realize a four-legged

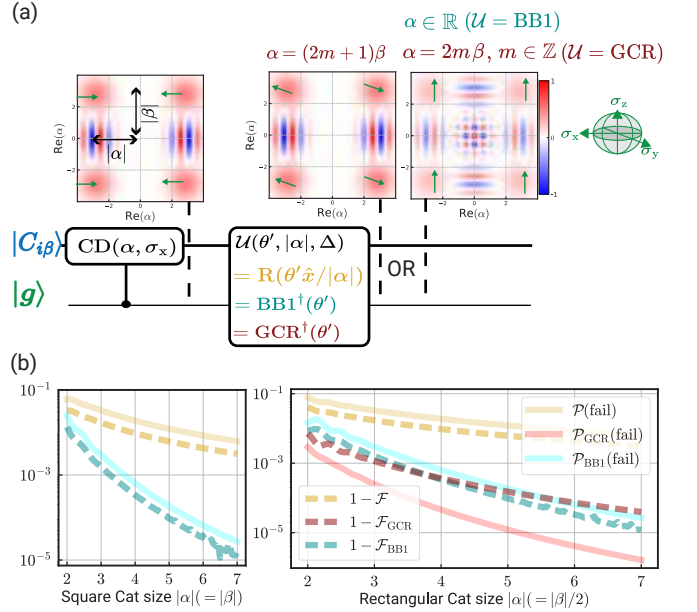


FIG. 7. **Circuit for preparation of Four-legged cat using QSP sequences.** (a) We use the two-legged cat preparation circuit in Fig. 5(a) starting in (perfect^a) momentum-cat state instead of vacuum. The green arrows in the Wigner plots shown here indicate the qubit spin polarization corresponding to each blob. Unless each blob has the arrow pointing in the same direction, the qubit is highly entangled with the oscillator. Given that this is necessary for deterministic preparation we observe the following. The non-abelian QSP sequence GCR can only prepare rectangular cat states where the aspect ratio ($|\beta|/|\alpha|$) is an even integer. On the other hand, the abelian sequence BB1 has no such restriction. (b) We plot performance of GCR and BB1 (only BB1) for rectangular (square) 4-legged cat states. The yellow curve marks the case of no QSP correction in both plots.

^a Note that the protocol does not require an initially unentangled two-legged cat state. We can instead start from vacuum and apply two conditional displacements, one along each quadrature direction, \hat{x} and \hat{p} . After these displacements, we obtain an entangled state similar to the one produced by \mathcal{U} , with the qubit spins aligned for blobs located along the same diagonal. The circuit shown here uses a cat state for simplification. Hence the use of perfect two-legged cat states in these simulations is justified.

cat state $|4C\rangle$ which is rectangular,

$$|4C\rangle \propto (|2\beta, i\beta\rangle - |2\beta, -i\beta\rangle) - (|-2\beta, i\beta\rangle + |-2\beta, -i\beta\rangle) \quad (73)$$

We could squeeze this state back to fix the gaps but that would squeeze the individual blobs and is not recommended. We show that with increasing α , our protocol gives an increase in fidelity to the rectangular four-legged cat state $|4C\rangle$. This specific example gives us some insight into how GKP states are ideal for GCR. For any logical Pauli state, the spacing between each blob in the grid is such that $\frac{\alpha}{\beta} = \frac{2m\sqrt{\pi}}{\sqrt{\pi}} = 2m$ where $m \in \mathbb{Z}$.

b. BB1: The above problem disappears if we use an abelian QSP sequence such as the BB1 scheme for the

un-entanglement $\mathcal{U}(\theta, |\alpha|, 1)$.

$$\begin{aligned} \mathcal{U}_p(\theta, |\alpha|, 1) e^{-i2\alpha\hat{p}\sigma_x} |C_{i\beta}\rangle |g\rangle \\ = \mathcal{U}_p(\theta, |\alpha|, 1) [e^{-i\alpha\beta/2} |\alpha + i\beta\rangle |+\rangle + e^{i\alpha\beta/2} |-\alpha + i\beta\rangle |-\rangle \\ e^{-i\alpha\beta/2} |\alpha - i\beta\rangle |+\rangle + e^{i\alpha\beta/2} |-\alpha - i\beta\rangle |-\rangle] \end{aligned} \quad (74)$$

$$= [|\alpha + i\beta\rangle + e^{i\alpha\beta} |-\alpha + i\beta\rangle] |g\rangle \quad (75)$$

All operations in $\mathcal{U} \equiv \text{BB1}$ are controlled momentum boosts, whose action depends on the position of the oscillator post $e^{-i2\alpha\hat{p}\sigma_x}$. So, the un-entanglement is the same as the two-legged cat state case except for the additional local phase $e^{i\alpha^2}$ on the blobs along $\frac{\hat{x} - \hat{p}}{\sqrt{2}}$ ⁷.

Discussion: Similar strategies can be applied for other rotationally symmetric codewords, that is, N -legged cat states for $N > 4$. However, we will not dive into these strategies and move on to discuss the more general rotationally symmetric states, Fock states. Since the Fock basis is a complete orthogonal basis for oscillator space this discussion takes a step forward towards universal state preparation using non-abelian QSP.

2. Fock state Preparation

For any instruction set to be universal, it should be able to generate the Fock Basis. Thus, this section is targeted at the generation of Fock states using the phase-space ISA. Although this preparation scheme may be inefficient given conditional displacements are more suited to states with translation symmetry, we give this construction for the sake of completeness. To this end, we first realize that Fock states can be approximately represented as a sum of coherent states as

$$|\psi_n\rangle = \frac{1}{\mathcal{N}} \sum_{j=0}^{m-1} e^{i\frac{2\pi n}{m} j} |\alpha e^{-i\frac{2\pi j}{m}}\rangle, \quad (76)$$

$$F_n = |\langle n|\psi_n\rangle|^2 = m^2 \frac{\alpha^{2n}}{n!} \frac{e^{-\alpha^2}}{\mathcal{N}^2}, \quad \alpha \in \mathbb{R}, \quad (77)$$

where F_n gives the fidelity of $|\psi_n\rangle$ with respect to the Fock state $|n\rangle$. Here m, α should be chosen such that the coherent states are on a ring completing an angle of 2π . To represent each Fock state $|n\rangle$ there is minimum requirement on m_n and the fidelity to the Fock states increases with increasing $m > m_n$.

Unlike our previous examples, Fock states are not superpositions of non-overlapping Gaussian wave functions. To prepare Fock states, a straightforward recipe is to use a trotterized circuit for the anti-Jayne Cummings Hamiltonian as described in App. G. Evolution under the Anti-JC Hamiltonian,

$$\text{AJC} = \hat{a}\sigma_- + \hat{a}^\dagger\sigma_+ = 2(\hat{x}\sigma_x - \hat{p}\sigma_y), \quad (78)$$

where $\sigma_\pm = \sigma_x \mp i\sigma_y$. This Hamiltonian allows the simultaneous addition (or removal) of a single photon to (or from) the qubit and the oscillator. Note that R.H.S. can be approximated using a conditional displacement and a conditional momentum boost. Further trotterization could yield even better approximations. App. G shows that Fock states prepared using this method are better than numerically optimized circuits [10] in terms of circuit duration for the preparation of Fock state $|1\rangle$. In addition, we can employ the Law-Eberly protocol [63] to prepare arbitrary superposition of Fock states.

In terms of circuit depth or gate counts (if for any scheme this is a useful quantity) the numerically optimized circuit is still unmatchable. In this section, we develop an alternative analytical scheme that matches the gate count, for the respective fidelity, of the numerically optimal circuits given in Ref. [10].

Protocol: Let us focus on the simplest case of Fock state $|n = 1\rangle$. To begin with, we realize that Eq. (76) gives us the Fock state $|1\rangle$ in the form of an odd small cat with m blobs in phase space. The smaller the α the better the fidelity to $|1\rangle$. However, using our small cat preparation circuit laid out in Sec. IV A, the probability of projecting onto small odd cat states is lower than small even cat states. This problem is explained in the context of two-legged cat states in App. E 2. We label the gate count as the number of conditional displacements and denote this quantity as N . The smaller the cat size, the smaller the probability of projecting the oscillator onto an odd cat state. Thus, there is an optimal α that can achieve the preparation of small odd cat states with low failure probability while maintaining a high fidelity with Fock state $|1\rangle$ for the case of $N = 1$.

a. $N = 1$: The optimal α for $\text{CD}(\alpha, \sigma_y)$, if we start with $|0, g\rangle$, that yields $|1, e\rangle$ is $\alpha = \frac{\pi}{2}$.

$$\begin{aligned} |0, g\rangle &\xrightarrow{\text{CD}(\alpha/2, \sigma_x)} |\alpha\rangle |+\rangle - |-\alpha\rangle |-\rangle \\ &= \mathcal{N}_{\text{odd}}(|\alpha\rangle - |-\alpha\rangle) |e\rangle + \mathcal{N}_{\text{even}}(|\alpha\rangle + |-\alpha\rangle) |g\rangle. \end{aligned} \quad (79)$$

Here, \mathcal{N}_{odd} ($\mathcal{N}_{\text{even}}$) are the normalization constants of the odd and even superpositions of $|\pm\alpha\rangle$ states. See App. E 2 for details. The probability increases of projecting the qubit onto $|e\rangle$ is given by $|\mathcal{N}_{\text{odd}}|^2/|\mathcal{N}_{\text{even}}|^2$ (see Eq. (E37) in App. E 2). The fidelity of this state with $|1\rangle$ is given by Eq. (77). The maximum product of these quantities lies at $\alpha = \pi/2$. This parameter is the same as the case of JC for $|0, g\rangle \rightarrow |1, e\rangle$ but with a single conditional displacement

b. $N = 2$: The optimal circuit for two CDs can be directly given by the first-order trotterized circuit for AJC. This circuit as explained in the App. G adds a photon to both the oscillator and the qubit, simultaneously, $|0, g\rangle \rightarrow |1, e\rangle$ at $\alpha = \pi/2$. In fact, for arbitrary Fock state $|n\rangle$, we have $\alpha = \pi/2\sqrt{(n+1)}$ for the evolution $|n, g\rangle \rightarrow |n+1, e\rangle$. This preparation is the same as the protocol for a small odd-cat state preparation discussed in Sec. IV A (also, see Apps. D, E 2) for $|\alpha| = \pi/2$.

⁷ There is no phase if $\alpha^2 = 2\pi$.

The fidelity with $|1, e\rangle$ at this stage is 0.70, slightly less than numerically optimized circuits [10].

See the Wigner function in Fig. 8 after $N = 1$ circuit. It represents two well-separated blobs which is a mixed state representing a large cat state (entangled with a qubit, traced out). Thus, in this case, it might be good to check if the large cat preparation circuit works better in this regime. We find that the second CD after $CD(\alpha/2, \sigma_y)$, in fact, yields better fidelity with $e^{i\frac{\pi}{4(\alpha/2)}\hat{x}^2}\otimes\sigma_y$. This is the un-entanglement sequence for large cat states, without any QSP correction, discussed in Sec. IVB (also, see Sec. IIB and App. E1). The hybrid fidelity after this $N = 2$ circuit is 0.84, the same as the numerical scheme.

The un-entanglement⁸ in this case involves a favorable back action in the momentum basis⁹. See the wave function and Wigner plots for the oscillator state in Fig. 8 after $N = 2$ circuit. The peaks in the momentum basis almost coincide with the peaks in the position basis, yielding a state close to Fock $|1\rangle$. The Wigner distribution of the position peaks overlaps with the momentum peaks yielding a near-circular quasi-probability distribution. Thus, the back action and overlapping peaks in the two bases, both aid in the preparation of a Fock state.

c. $N = 3$: Now, since $|\alpha|/2 > 2$ we can resort to QSP corrections for large cat states. We will, thus, use ideas from small cat state preparation. So far, in Sec. IV A, we have discussed this idea for creating a squeezed vacuum which is just even cat states. Now, we switch to the preparation of small odd cat states. The problem of using the same QSP correction with extremely small cat states is given in App. E2. Thus, a medium cat state is the best way to approach Fock states which resemble a small odd cat state. The case of cat state of size $|\alpha|/2 = \pi/4$ belongs to this class of states.

Given various preparation schemes discussed in previous sections and the JC Hamiltonian approach using this construction, we identify the following sequence (first used in Refs. [64]),

$$CD(\alpha_1, \sigma_y)CD(i\beta_1, \sigma_x)CD(\alpha_2, \sigma_y)CD(i\beta_2, \sigma_x)\dots \quad (80)$$

as the most general form of the non-abelian un-entanglement circuits. This sequence has implications in quantum random walk which we will discuss in Sec. VI. We have α_1, β_1 from the circuit to prepare a large cat state with

$$\alpha_1 = \frac{\pi}{2}, \beta_1 = \frac{\pi}{4}\left(\frac{\alpha_1}{2}\right). \quad (81)$$

⁸ Note that, since $|\alpha| < 2$ we cannot use a QSP correction here (see Fig. 2).

⁹ This feature is favorable for creating rotationally symmetric states such that due to the enhanced non-commutativity of displacement and momentum boosts at small amplitudes, $|\beta| \neq |\alpha|$ creates a perfect square inscribed inside the Wigner distribution of the Fock state

Now, for the next gate, we choose the momentum-controlled rotation or $CD(\alpha_2/2, \sigma_y)$ as follows. We note that the action of this gate on $\langle\sigma_y\rangle$, in the position basis, is

$$\langle\sigma_y\rangle_{\text{new}} = \langle\sigma_y\rangle_{\text{old}} \cos(-2\alpha_2 p) - \langle\sigma_z\rangle_{\text{old}} \sin(-2\alpha_2 p). \quad (82)$$

See Eq. (D14) in App. D for details. Following the small cat protocol, we note that for un-entanglement of the qubit, we need, $\langle\sigma_y\rangle_{\text{new}} = 0$, which yields the condition,

$$\tan(-2\alpha_2 p) = \frac{\langle\sigma_y\rangle_{\text{old}}}{\langle\sigma_z\rangle_{\text{old}}} \quad (83)$$

From Fig. 8, we notice that the circuit for $N = 2$ has created a large cat of size β_1 along the momentum quadrature, then we have (ignoring the local phase induced by the first gate)

$$\frac{\langle\sigma_y\rangle_{\text{old}}}{\langle\sigma_z\rangle_{\text{old}}} = \frac{\tanh 2\beta_1 p}{\text{sech} 2\beta_1 p} = \sinh 2\beta_1 p \quad (84)$$

Thus, we need to satisfy,

$$\tan 2\alpha_2 p = \sinh 2\beta_1 p \quad (85)$$

Since the state is not centered at the origin we cannot use the linearity condition, but we satisfy the equation at the maximas of the wave functions in p . Thus, imposing $\langle\sigma_y\rangle = 0$ at the maximas of $\psi(p)$, that is at $p = \alpha_1/2$ (see Fig. 8), we get,

$$\alpha_2 = \frac{1}{\alpha_1} \tan^{-1}(\sinh 2\beta_1 \alpha_1)/\alpha_1 = (\tan^{-1} \sinh(\pi/2)) \quad (86)$$

Thus, we have our third gate with this choice of α_2 ,

$$CD(\alpha_2/2, \sigma_y). \quad (87)$$

This $N = 3$ sequence further amplifies the hybrid state fidelity to 0.99. The sequence matches the fidelity and circuit duration of the numerically optimized circuits for depth $N = 3$ in Ref. [10]. In addition, when compared with the Law-Eberly Hamiltonian, this sequence has a higher operator fidelity to AJC Hamiltonian evolution compared to the symmetric second-order trotterized circuit in Eq. (80). We describe the above calculations pictorially in Fig. 8. This method can be generalized to obtain algorithms for arbitrary circuit depth N and Fock state $|n\rangle$. However, given the minimal use-case of this strategy in practical cases, we leave this discussion for future work addressing universal state preparation with the phase-space ISA.

Our work gives different strategies to approach the problem of universal state preparation using the phase space instruction set. Concluding this section, we point out that a single algorithm in this direction does not seem like the optimal solution, given the possibility of ancilla decay during a conditional displacement or momentum boost gate.

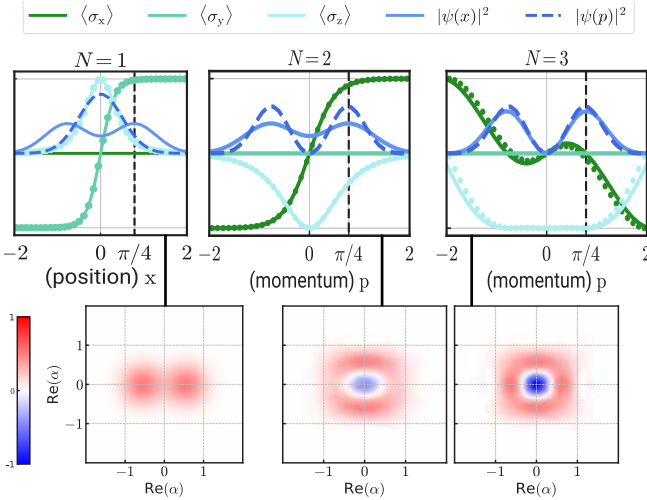


FIG. 8. Preparation of Fock state $|1\rangle$ using the GCR. We plot the wave functions in the position $\psi(x)$ and momentum basis $\psi(p)$ against x, p , respectively, to analyze the oscillator subspace. **(Left)** For the qubit subspace, we plot the expectation values $\langle\sigma_x\rangle, \langle\sigma_y\rangle, \langle\sigma_z\rangle$ as a function of oscillator position after the first gate $CD(\alpha_1, \sigma_y)$. At this point, the hybrid state fidelity is $F_H \sim 0.58$. The solid curves denote the simulated quantities while the dotted curves denote the analytical expressions derived for the case of small cats in Sec. D. However, the Wigner plot shows that the state is closer to a large cat (with maxima located at $\alpha_1/2$), and thus, will benefit from a (no-QSP) correction designed for this state such that $\beta_1 = \frac{\pi}{4}, \frac{\alpha_1}{2}$ in Eq. (80). **(Middle)** The expectation values $\langle\sigma_x\rangle, \langle\sigma_y\rangle, \langle\sigma_z\rangle$ as a function of oscillator-momentum after the second gate $CD(\beta_1, \sigma_x)$. At this point, the hybrid state fidelity is $F_H \sim 0.84$. Note that, the curves follow the expressions derived for small cats. These expressions are plotted in dotted curves and match well with the simulated solid curves. This indicates that for the next correction, we can use ideas from the small cat state preparation as discussed in the main text. **(Right)** The expectation values $\langle\sigma_x\rangle, \langle\sigma_y\rangle, \langle\sigma_z\rangle$ as a function of oscillator-momentum after the third gate $CD(\alpha_2, \sigma_y)$. The solid curves at this point follow the expression quoted for $\langle\sigma_{y,z}\rangle_{\text{new}}$ plotted in dotted curves in Eqs. (82,D14) and App. D. At this point, the hybrid state fidelity is $F_H \sim 0.99$. The Wigner plot shows a symmetric state that resembles Fock state $|1\rangle$. The fidelities obtained in this scheme match in circuit duration as well as fidelity with the numerically optimized circuits in Ref. [10].

V. UNIVERSAL CONTROL OF BOSONIC ERROR-CORRECTED QUDITS

The phase-space instruction set is most suited for the translationally invariant grid codes, or as acronymed, the GKP codes. These codes have shown promise in autonomous error correction achieving the record break-even gain, which has only been matched so far by the latest surface code experiment [39] using 49 DV qubits. While we can find applications in other error-correcting codes, we focus on the GKP codes because our framework of non-abelian QSP using the phase-space instruction set

gives access to high-fidelity universal control of finite-energy error-corrected GKP qudits [10, 23, 40, 60]. All our schemes are based on non-abelian sequence (GCR) using the phase-space instruction set [8]. Fast gates in this instruction set can be realized in the low dispersive-coupling regime [10] which has the advantage of reducing errors associated with higher-order Kerr effects [10] that cannot be efficiently corrected using GKP states. In this section we derive analytical schemes for (i) error-detected qudit state preparation, (ii) end-of-the-line logical qubit readout, and (iii) high-fidelity logical single-qubit and two-qubit universal gate set. All schemes presented here improve upon the performance of the state-of-the-art theoretical schemes and experimental demonstrations. Our schemes are generalizable for arbitrary lattice spacing, thus, yielding universal control for square, hexagonal, and rectangular GKP qubits, GKP qudits, and multi-mode GKP codes. Below we summarize our GKP control results before diving into the details.

The ancilla-assisted finite-energy GKP readout [45] and stabilization schemes [60] are tied together using our non-abelian GCR sequence in Sec. V B. The stabilization scheme used to achieve the record gain for beyond break-even logical lifetime in superconducting circuits [23], was derived using dissipation engineering techniques. We not only give the first analytical explanation for the numerically optimized readout scheme but also tie it together with the stabilization scheme. Our framework is helpful in understanding error correction to the right logical state in the GKP manifold using this qubit-based dissipation scheme, which was only engineered to avoid leakage and not logical errors. In addition, we give an end-of-the-line readout circuit in Sec. V C which could yield better readout fidelity for GKP qubits with correctable displacement errors using abelian QSP sequence BB1. In addition, in Sec. V C we give an end-of-the-line readout circuit based on the abelian QSP sequence BB1 that could yield better readout fidelity for GKP qubits with correctable displacement errors.

A crucial finding of this paper is a peaceable gate teleportation scheme discussed in Sec. V D. This is the first known scheme to correct errors during gate teleportation in a single system. The peaceable scheme then further takes advantage of this novel quality to mitigate the effects of ancilla dephasing errors. Thus, the piece-wise teleportation scheme yields high-fidelity universal single-qubit logical rotations in the presence of a biased-noise ancilla, such as cat qubits [55, 65–67]. This is the best-known scheme for implementing non-Clifford operation available for GKP qubits to date [42].

We restrict the derivation and discussion to the case of square GKP, where x and p are treated symmetrically, for Secs. V A–V D while discussing generalizations to other qubit and qudit lattices in Sec. V F. While we have already introduced the definition for GKP states and finite-energy stabilizers in Sec. F, here, we present a more general description for the mapping from ideal GKP codes to finite-energy GKP codes. This formalism

will help construct control sequences. An arbitrary logical GKP codeword was defined as the un-normalizable states,

$$|\psi\rangle_{\text{GKP}} = \alpha |0\rangle_{\text{GKP}} + \beta |1\rangle_{\text{GKP}} \quad (88)$$

$$|0\rangle_{\text{GKP}} = \sum_{n \in 2\mathbb{Z}} D(n\sqrt{\pi/2}) |0\rangle_x \quad (89)$$

$$|1\rangle_{\text{GKP}} = \sum_{m \in 2\mathbb{Z}+1} D(m\sqrt{\pi/2}) |0\rangle_x \quad (90)$$

$$\text{where } |0\rangle_x = S(\infty) |0\rangle \quad (91)$$

$$\text{and } D(\alpha) = e^{\alpha a^\dagger - \alpha^* a}, \quad (92)$$

$$S(r, \phi) = e^{-\frac{r}{2}(e^{i\phi} a^\dagger)^2 - e^{-i\phi} a^2} \quad (93)$$

Realistic quantum states are normalizable. One way to achieve a finite-energy version of the above code is to apply a Gaussian envelope $\hat{E} = e^{-\Delta^2 \hat{n}}$ such that any ideal GKP state and operator A on this subspace transforms as,

$$|\psi_\Delta\rangle_{\text{GKP}} = \hat{E} |\psi\rangle_{\text{GKP}}, \hat{A}_\Delta = \hat{E} \hat{A} \hat{E}^{-1}. \quad (94)$$

Note that \hat{E} is a non-unitary operation and hence, in experiments, we achieve this using dissipation-based methods. The practical envelopes are closer to a cosine envelope which is closer to the Eq. (69) given in Sec. IV C. Note that this envelope transforms delta functions to a Gaussian wave packet of uncertainty Δ . The envelope in itself has an uncertainty of $1/\Delta^2$.

Our non-abelian composite pulse GCR schemes reduce sensitivity to uncertainties in the position and momentum of finite-energy oscillator states. Thus, these schemes can be viewed as mappings from idealized, infinitely squeezed position and momentum eigenstates to realistic Gaussian states in superposition with finite uncertainty. This explains our findings in connection with GKP states. All GKP operations are well-defined for ideal GKP codes which are superpositions of infinitely squeezed states, our framework maps these operations to yield circuits that can come extremely close to the exact finite-energy GKP operations. In a previous work, an approach towards such finite-energy operations, in particular the logical entangling gates ($\text{CX}_{\text{GKP}}/\text{CZ}_{\text{GKP}}$), was suggested in [43] with a qutrit ancilla. In contrast, our construction for entangling gates yields comparable fidelity using two ancilla qubits. We also give decompositions to execute fast two-mode echoed Gaussian operations in the context of finite-energy GKP entangling operations in App. I 1. We owe this improvement to the simplicity provided by the description of our framework. Both these approaches are better than implementing the ideal gate followed by several rounds of stabilization. Most importantly, all our single-mode circuits use phase-space instruction set and the two-mode schemes use squeezing, beam-splitters, in addition to the gates mentioned in Eq. (1) for phase space IS. Proposals to realize these operations can be found in [33, 68]. This

indicates that our circuit construction is a closer approximation to the finite-energy GKP gates.

We compare all our results against state-of-the-art theoretical schemes in terms of fidelity and feasibility, in the absence of errors. We also show that our analytical schemes achieve universal control of the GKP code robust to ancilla and cavity errors, surpassing the best-known fidelities in the presence of such faults.

A. High-Fidelity Error-Detected State Preparation

Fault-tolerant preparation of logical GKP states is an important resource for bosonic quantum error correction. Previously in this work, we described a protocol that prepares GKP states in small steps $\mathcal{S}_k, \mathcal{C}_k$, at the end of which the ancillary qubit was left in a deterministic state. In this section, we will investigate the performance of this scheme in the presence of cavity and qubit noise. We will then compare this fidelity with the scheme in Ref [41] which can also benefit from mid-circuit error detection.

For the protocol presented in Sec. IV C we introduce mid-circuit detection on ancilla errors via post-selection upon outcome $|g\rangle$ after every round; resetting the qubit to $|g\rangle$ if the step has succeeded. During each gate in the circuit, we add photon loss at the rate $\kappa/2\pi = 1/1000 \mu\text{s}^{-1}$, ancilla decay at the rate $\gamma/2\pi = 1/200 \mu\text{s}^{-1}$, and ancilla dephasing at the rate $\gamma_\phi/2\pi = 1/200 \mu\text{s}^{-1}$. With this, we run the protocol for $\Delta = 0.34$ [23] for 10^5 rounds. For each preparation round, we execute the GKP state preparation circuit $\mathcal{C}_1 - \mathcal{C}_2$ shown in Fig. 6 with measurements after every \mathcal{C}_k . We throw away any round where we encounter a -1 outcome for a Z measurement on the ancilla qubit and start over with the oscillator in the squeezed state. The success probability (fraction of rounds that will not be thrown away) for this simulation is 0.94. Now, the average fidelity for this case was 0.96 in comparison to 0.9969 in the case of no errors. On the other hand, the numerical scheme in Ref. [10] reports a simulated (and experimental) fidelity of 0.85 for a numerically optimized circuit with the same Δ without post-selection. Post-selection with their circuit is possible but only at the end of the entire circuit whose length is comparable to our entire preparation circuit. Thus, the efficiency with which such a circuit can detect errors with post-selection would be low. Relative to Ref. [45], our scheme performs better due to a similar argument. In comparison to the first step of that protocol, the length of our snippet \mathcal{C}_1 is much smaller, reducing the probability of errors and thus improving the success probability and fidelity.

Thus, we have shown numerically that our scheme performs better than state-of-the-art schemes for GKP preparation using a DV ancilla, even in the presence of errors.

B. GKP protocols in the non-abelian QSP framework

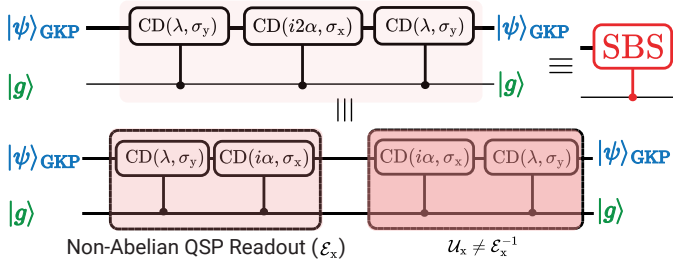


FIG. 9. **Finite-energy GKP readout** [45] and **stabilization** [60] **protocols in non-abelian QSP framework**. Interpretation of SBS circuit along the position quadrature as logical identity on the GKP codewords. The circuit is divided into the entangling and unentangling gadgets. The first half of this circuit \mathcal{E} is the GKP readout circuit. Here, $\alpha = \frac{\sqrt{\pi}}{2\sqrt{2}}$ and $\lambda = -\alpha\Delta^2$.

a. Analytical explanation for numerically-optimized readout scheme in Ref. [45]: Ref. [45] shows a numerically-optimized circuit for improved GKP readout over the ideal readout scheme. Ideal GKP readout scheme is explained in Sec. H. The ideal GKP readout circuit is rotation gadget which intends to rotate the state by 2π (π) if the logical codeword is $|0\rangle_{\text{GKP}}$ ($|1\rangle_{\text{GKP}}$) using $e^{i\sqrt{\frac{\pi}{2}}\hat{v}\otimes\sigma_x}$ with the qubit starting in $|g\rangle$. Thus, a readout circuit is nothing but an entanglement gadget. For finite-energy GKP, we can employ our entanglement gadget with the small GCR pre-correction $e^{i\sqrt{\frac{\pi}{2}}\Delta^2\hat{p}\otimes\sigma_y}$. Thus, we give the logical readout circuits for logical bases X ($\hat{v} = \hat{p}$), Y ($\hat{v} = \hat{x} + \hat{p}$), and Z ($\hat{v} = \hat{x}$).

$$\mathcal{E}_{\hat{v}}\left[\frac{\pi}{2}, \sqrt{\frac{\pi}{2}}, \Delta\right] = e^{i\sqrt{\frac{\pi}{2}}\hat{v}_\perp\Delta^2\sigma_y} e^{i\sqrt{\frac{\pi}{2}}\hat{v}\sigma_x}. \quad (95)$$

See Sec. II for the definition of \hat{v}_\perp . Notice that for a square GKP code defined in Eqs. 64,65 and Eq. (69), the displacement required to implement a logical Y operation is longer than the corresponding displacements required for logical X or Z operations by a factor of $\sqrt{2}$.

The GCR correction given here, which we obtained analytically from $\mathcal{E} = \text{GCR}$ following the discussion in Sec. IV B 1, is exactly the numerically-optimized correction in Ref. [45].

b. Dissipation-engineering based stabilization and correction of displacement errors: Dividing the stabilization circuit SBS from Ref. [60] into two halves (see Fig. 9), the first half can be identified exactly as the entangling gadget used for readout as described in Eq. (95). The second half satisfies the constraints identified for the un-entangling gadget $\mathcal{U}(\pi/2, \sqrt{\pi/2}, \Delta)$ in Sec. IV B since,

$$\pi/2 \text{ (from } \mathcal{E} \text{)} + \pi/2 \text{ (from } \mathcal{U} \text{)} = \pi, \quad (96)$$

as required by Eq. (52). And thus,

$$\text{SBS}_{\hat{v}} = \mathcal{E}_{\hat{v}}\left[\frac{\pi}{2}, \sqrt{\frac{\pi}{2}}, \Delta\right] \mathcal{U}_{\hat{v}}\left[\frac{\pi}{2}, \sqrt{\frac{\pi}{2}}, \Delta\right]. \quad (97)$$

Note that, here $\mathcal{U} \neq \mathcal{E}^{-1}$, and so, this circuit is a logical GKP identity and not a universal identity. The circuit has a non-trivial back action if the oscillator is not in the GKP state which is the key to its success for error correction.

The error correction properties of this circuit were experimentally verified and qualitatively discussed in [23]. Here, we provide a quantitative argument using our framework to compute the back action on the oscillator and its effects on the state when the state has a displacement error. As discussed before, the SBS circuit applies a deterministic logical Pauli when the oscillator is in codespace. However, when the state is not in the GKP codespace, the unentangling gadget needs to be apply the correction along a different axis, depending on the displacement error λ . Since this knowledge is not available to the stabilization circuit, it applies a back action on the oscillator depending on the qubit outcome.

This back action of the SBS circuit can be explained using non-abelian QSP as follows. In the event of a displacement error, say ϵ , the GKP states are positioned at $m\sqrt{2\pi} + \epsilon$, where m is any odd (even) integer for the peaks of $|0_\Delta\rangle_{\text{GKP}}$ ($|1_\Delta\rangle_{\text{GKP}}$). Now, the effect of the entangling part of SBS will be rotating the qubit by $e^{i\sqrt{\frac{\pi}{2}}(m\sqrt{2\pi} + \epsilon)\sigma_x}$. Thus, for an erroneous state $|\psi\rangle_\epsilon = \alpha|0\rangle_\epsilon + \beta|1\rangle_\epsilon$, where $|0\rangle_\epsilon, |1\rangle_\epsilon$ denote erroneous GKP states $|0_\Delta\rangle, |1_\Delta\rangle$ with displacement error ϵ , we have,

$$\mathcal{E}_{\hat{x}}|\psi\rangle_\epsilon|g\rangle \approx e^{i\epsilon\sqrt{\frac{\pi}{2}}\sigma_x}(\alpha|0\rangle_\epsilon|g\rangle + \beta|1\rangle_\epsilon|e\rangle) \quad (98)$$

$$\begin{aligned} &= -\alpha|0\rangle_\epsilon(\cos\epsilon\sqrt{\pi/2}|g\rangle + i\sin\epsilon\sqrt{\pi/2}|e\rangle) \\ &\quad + \beta|1\rangle_\epsilon(\cos\epsilon\sqrt{\pi/2}|e\rangle + i\sin\epsilon\sqrt{\pi/2}|g\rangle) \end{aligned} \quad (99)$$

We would like to remind the reader at this point that $\mathcal{U}_{\hat{x}}$, the second half of the circuit has a correction $e^{i2\lambda\hat{p}\sigma_y}$ (with $\lambda = \alpha\Delta^2$) which depends on the final qubit state. The un-entanglement routine \mathcal{U} will correctly rotate the qubit state back to $|g\rangle$ for the first terms in each row. However, for the second term, where the qubit will be rotated to $|e\rangle$, the sign of the finite-energy correction is wrong. And hence, here the finite energy correction of \mathcal{U} will apply a back action of $e^{i4\lambda\hat{p}\sigma_y}$. Thus, after $\mathcal{U}_{\hat{x}}$, the hybrid qubit-oscillator state takes the form,

$$\begin{aligned} &(\cos\epsilon\sqrt{\pi/2}|g\rangle + ie^{i4\lambda\hat{p}\sigma_y}\sin\epsilon\sqrt{\pi/2}|e\rangle)\alpha|0\rangle_\epsilon \\ &\quad - (\cos\epsilon\sqrt{\pi/2}|g\rangle + ie^{i4\lambda\hat{p}\sigma_y}\sin\epsilon\sqrt{\pi/2}|e\rangle)\beta|1\rangle_\epsilon \\ &= (\cos\epsilon\sqrt{\pi/2}|g\rangle + ie^{i4\lambda\hat{p}\sigma_y}\sin\epsilon\sqrt{\pi/2}|e\rangle)(\alpha|0\rangle_\epsilon - \beta|1\rangle_\epsilon). \end{aligned} \quad (100)$$

If $\epsilon = 0$, this hybrid state is equal $(\alpha|0\rangle_\epsilon - \beta|1\rangle_\epsilon)|g\rangle = |\bar{\psi}\rangle_\epsilon|g\rangle$, where a deterministic logical Pauli operation has been applied to $|\psi\rangle$. Note that this Pauli operation can be

tracked and hence does not play any role in stabilization. In the presence of error, as we can see, the probability for outcome $|g\rangle$ is not 1. At this point, if the qubit is measured, the probability of getting each possible outcome is,

$$P_g = \int_{-\infty}^{\infty} dp (\cos^2(\epsilon\sqrt{\pi/2}) + \sin^2(\epsilon\sqrt{\pi/2}) \sin^2(4\lambda p)) \times |\psi(p)|^2, \quad (101)$$

$$P_e = \int_{-\infty}^{\infty} dp \sin^2(\epsilon\sqrt{\pi/2}) \cos^2(4\lambda p) |\psi(p)|^2. \quad (102)$$

Now, the back action in the event that the qubit is projected to state $|g\rangle$ is given by W_{gg} (in the notation introduced in Sec. II) for the SBS state in this case,

$$(\cos(\epsilon\sqrt{\pi/2})I + i \sin(4\lambda\hat{p}) \sin(\epsilon\sqrt{\pi/2})) |\bar{\psi}\rangle_{\epsilon} \quad (103)$$

$$= (I + i4\lambda\epsilon\sqrt{\pi/2}\hat{p}) |\bar{\psi}\rangle_{\epsilon} + (\mathcal{O}(\epsilon^2) + \mathcal{O}(\lambda\epsilon^2)\hat{p} + \mathcal{O}(\lambda^2\epsilon)\hat{p}) |\bar{\psi}\rangle_{\epsilon} \quad (104)$$

$$\approx e^{i\pi\epsilon\Delta^2\hat{p}} |\bar{\psi}\rangle_{\epsilon} = D(-\pi\epsilon\Delta^2/2) |\bar{\psi}\rangle_{\epsilon}. \quad (105)$$

In the event of an error, this is a corrective displacement in the direction opposite to the error, as desired for the stabilization scheme. Thus, in the event of a +1 outcome, a single round of SBS partially corrects the error by applying a displacement of $-\pi\epsilon\Delta^2/2 \approx -0.18\epsilon$ for $\Delta = 0.34$.

Similarly, the back action in the event when the qubit is projected to state $|e\rangle$ is given by W_{eg} for the SBS unitary in this case,

$$\cos(4\lambda\hat{p}) |\bar{\psi}\rangle_{\epsilon} \quad (106)$$

This back action is independent of the error parameter ϵ , however, the probability of outcome increases with ϵ . This operator applies a symmetrized displacement along the position axis. In the momentum basis, this is equivalent to a cosine envelope on the state. To second order in \hat{p} , the cosine envelope can be approximated as a Gaussian,

$$\cos 4\lambda\hat{p} \approx e^{-8\lambda^2\hat{p}^2}, \quad (107)$$

where $8\lambda^2 = 8\alpha^2\Delta^4 = \pi\Delta^4$. We compare this envelope correction with the momentum part of the target Gaussian envelope $e^{-\Delta^2\hat{n}} = \exp[-\Delta^2(\hat{x}^2 + \hat{p}^2)]$ and note that an e outcome reduces the momentum uncertainty by 15%. Currently, we do not have an intuitive explanation for how this back action supports error correction or stabilization. The probability of both the back actions increases with an increase in the error ϵ , as should be the case for any autonomous error correction scheme. Importantly, the probability of correction is maximum at $\epsilon = \sqrt{\pi/2}$, at half the distance of the GKP code. At $\epsilon \geq \sqrt{2\pi}$ the displacement error causes a logical error in the GKP subspace and hence the stabilization scheme seems to slow down the correction as the error approaches

this value. Similarly, the stabilization of the logical X basis corrects displacement errors and envelope errors along the momentum axis.

In summary, we have shown that SBS is an example of probabilistic (or autonomous) error correction.

C. Logical Readout with Correctable Errors

At the end of any quantum circuit, the logical qubits must be measured to determine their state. In so-called dynamics circuits, such measurements may occur in the middle of the circuit so that a program branching decision ('measurement and feed forward') can be made. Inevitably, there can be residual correctable errors in the logical code states being measured. For the GKP encoding, such errors might be correctable random displacements, that is, $\sqrt{\pi/2}/2\sqrt{2}$. See the dashed curves in Fig. 10(a). These errors can lower the measurement fidelity since the ideal and finite-energy readout sequences are optimal at $\epsilon = 0$ only. For example, note how the probability of correct measurement decreases as a cosine for ideal energy readout and in a similar fashion for the finite-energy readout in Fig. 10(c) for the corresponding circuits given in Fig. 10(b). Fig. 10(a) shows the square wave pulse sequence (black dashed line) which would be ideal in the presence of correctable errors. In this section, we aim to use QSP sequences to approach this square response.

The problem at hand is described by Fig. 10(a) which suggests that we need to extract the one bit of information $\{0_{\text{GKP}}, 1_{\text{GKP}}\}$ where $|0\rangle_{\text{GKP}}$ ($|1\rangle_{\text{GKP}}$) corresponds to all states in the Hilbert space which are closer to logical $|0\rangle_{\text{GKP}}$ ($|1\rangle_{\text{GKP}}$) than to the opposite logical state. This can be understood from the readout sequence for infinite-energy states, and the argument carries over to all schemes. The infinite-energy sequence for logical Z measurement, described in App. H, follows

$$\text{CD}(i\alpha, \sigma_z) |\psi\rangle_{\text{GKP}} \otimes |+\rangle = \frac{1}{2}(D(i\alpha) \pm D(-i\alpha)) |\psi\rangle_{\text{GKP}} \otimes |\pm\rangle \quad (108)$$

$$= \frac{1}{2}D(i\alpha)(I \pm D(-i2\alpha)) |\psi\rangle_{\text{GKP}} \otimes |\pm\rangle \quad (109)$$

$$= \frac{1}{2}D(i\alpha)(I \pm e^{-i4\alpha\hat{x}}) |\psi\rangle_{\text{GKP}} \otimes |\pm\rangle \quad (110)$$

$$= D(i\alpha) \frac{I \pm Z_{\text{GKP}}}{2} |\psi\rangle_{\text{GKP}} \otimes |\pm\rangle. \quad (111)$$

Thus, this sequence applies a projective measurement modulo a displacement by $|\alpha|$. The definitions of infinite-energy GKP logical X/Z operators are given in App. H. However, for this infinite-energy GKP case, the readout fidelity follows a cosine curve (shown in panel (c) of Fig. 10) as a function of displacement ϵ . The fidelity value for the no-error case is less than unity when the infinite-energy readout scheme is applied to the finite-energy GKP state (see Fig. 10). The finite-energy readout, described in Sec. V B, yields a readout fidelity that

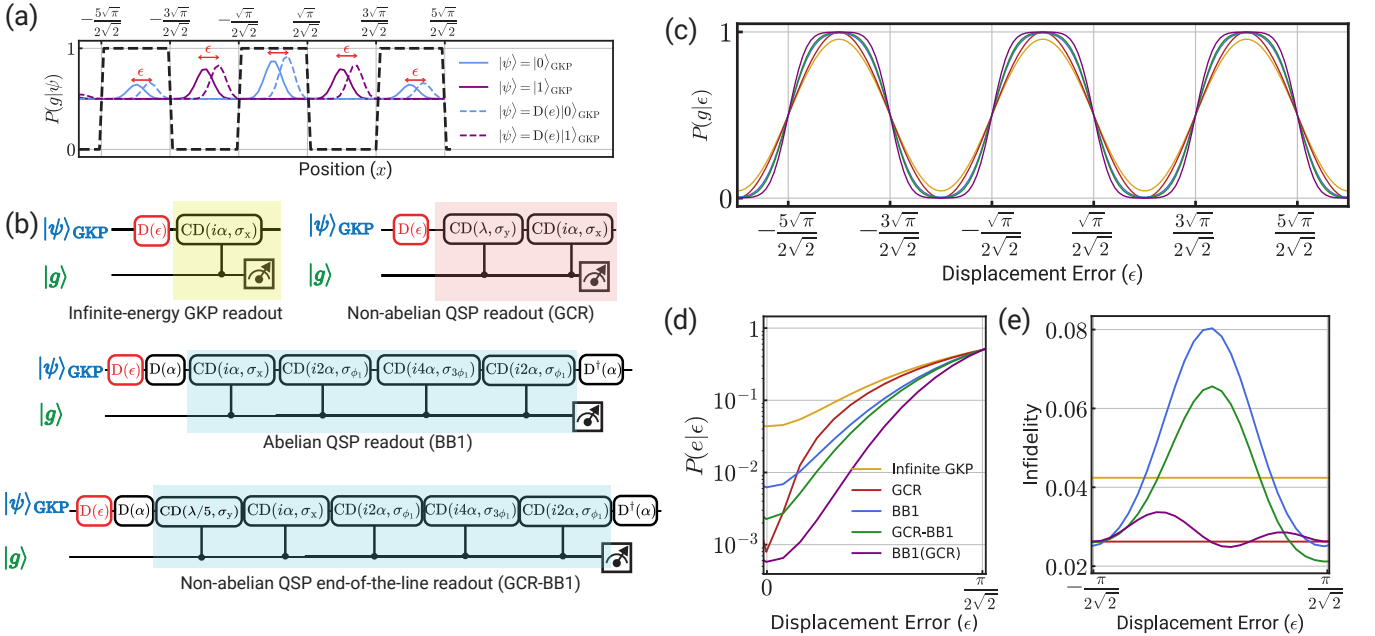


FIG. 10. Logical readout of GKP states with correctable errors. The readout procedure maps the GKP logical state onto the ancilla qubit states g, e which are then measured. (a) The solid curves denote GKP codewords while the dotted curves denote displaced GKP codewords. An ideal pulse for end-of-the-line GKP readout of a state with some correctable displacement error ϵ is a square wave, shown in the black dashed line here. It yields the probability $P(g|0, \epsilon)$ for the correct outcome $+1$ upon measurement of σ_z for all logical $|0, \epsilon\rangle$ states if the displacement error $|\epsilon| < \sqrt{\pi/2}$, and similarly for $P(e|1, \epsilon)$ for all logical $|1, \epsilon\rangle$ states. (b) GKP Readout schemes. The infinite energy readout scheme only takes care of the peak locations, the non-abelian QSP readout also found numerically in Ref. [45] yields corrections for the Gaussian width of finite-energy GKP peaks. Finally, an abelian QSP readout can handle the ambiguity in the location of the peak as per the binning shown in (a) due to the flattening of the cosine curve by the BB1(90) QSP pulse. (c) Probability of getting the right outcome $P(g|0, \epsilon)$ as a function of end-of-the-line errors (ϵ) for infinite-energy (no correction), GCR (correction for Gaussian uncertainty), and BB1 GKP readout (correction for errors in peak locations). Legend defining the colors is given in panel (d). (d) The zoomed-in version of (c) shows $1 - P(g|0, \epsilon)$ for the errors inside the Voronoi cell of square GKP codeword $|0\rangle$. The GCR – BB1 is a scheme where the BB1(90) readout is enhanced by pre-pending a single conditional displacement. On the other hand, BB1(GCR) is the sequence derived in Eq. (37) by composing GCR into BB1. For the circuit of BB1(GCR), we swap the blue region by the circuit for BB1(GCR). These sequences take care of the Gaussian uncertainty while yielding a square response. Here α, λ follow the notations used in Fig. 9. (e) Infidelity of the various readout sequences. The plot follows the same color coding as (b,d). These back actions are mostly due to an envelope error which can be fixed with further stabilization. Note that BB1 and GCR-BB1 can have the worst infidelity while finite-energy readout and BB1(GCR) have the least infidelity, and hence back action. The size of GKP states used to produce the curves in this figure is set by $\Delta = 0.34$.

follows a similar curve with a peak value closer to unity. In the presence of displacement errors ϵ , the qubit is rotated to a different basis other than the σ_z basis. Thus, for varying ϵ , the curves resemble a cosine. However, in the case of such residual (yet correctable) errors, we would like a readout sequence that yields a square wave response shown by the dotted black lines in Fig. 10(a).

a. Abelian QSP readout: We can achieve something close to the required square wave using our adaptation of BB1(90) in Eq. (11) for hybrid oscillator-qubit control. See circuit in Fig. 10(b). This circuit yields improved readout fidelity for all correctable error states compared to the finite-energy readout circuit, as shown by Fig. 10(c). A zoomed-in version is shown in Fig. 10(d) to assess the situation in the no error case of $\epsilon = 0$. Note that the Helstrom bound for the given value of $\Delta = 0.34$ is $\frac{1}{2}(1 - \sqrt{1 - |\langle 0|1 \rangle|^2}) \approx 10^{-4}$, far below the BB1 pro-

tocol readout error at $\epsilon = 0$. Hence, we do not need to account for the non-orthogonality of the GKP logical Pauli states.

b. Non-abelian end-of-the-line readout: The abelian end-of-the-line sequence works desirably well and is relatively robust for $\epsilon \neq 0$ case. However, its performance for the no error case $\epsilon = 0$ is worse than the finite-energy readout sequence. Thus, it might be a good idea to think of an end-of-the-line sequence where these finite-energy corrections are also taken care of. This is the exact problem we solved in Sec III while composing GCR into BB1. As shown above, this routine works on par with the finite-energy correction. We use the BB1(GCR(90)) with $|\alpha| = \sqrt{\pi}/2$ to achieve this optimal readout sequence. For low enough $\Delta = 0.34$, as used for GKP experiments, this sequence is not much longer compared to the BB1(90). Thus, our non-abelian QSP sequence yet again performs

a better end-of-the-line GKP readout.

However, the sequence still requires four additional gates with amplitude proportional to Δ^2 . Therefore we have also studied another sequence in which a single conditional displacement is prepended to BB1. The amplitude of this GCR-type correction ($\lambda/4$) is optimized numerically to take into account the finite-energy corrections of the four rotations in BB1 collectively. This sequence is termed GCR-BB1 in the figure above. Fig. 10 shows that GCR(BB1) is the best sequence among all readout sequences given correctable errors and finite-energy code words.

c. Back action: Note that during each readout sequence, the GKP state is displaced by an amount $|\alpha|$ along the quadrature orthogonal to the one being measured. However, this displacement is deterministic and can be accounted for. Thus, canceling this displacement, we compute the fidelity of the resulting state with the initial erroneous state. A large infidelity would indicate worse back action from the respective circuit. See Fig. 10(d) for the back action of all readout schemes discussed in this section. Note that ideally for an end-of-the-line readout sequence, we do not care about the back action on the state. However, if the back action is not very bad, the readout scheme can be repeated to increase measurement fidelity.

Given that the non-abelian end-of-the-line readout requires a larger circuit depth than the abelian readout, the theoretical improvement in fidelity may be difficult to realize in practice. We conjecture that the circuit depth could be reduced if we squeeze the oscillator quadrature that is being read out. If the squeezing parameter is r , squeezing will make all required conditional displacements smaller by a factor of e^{-r} . However, squeezing itself is a time-consuming process and could induce more errors. The question is if the reduction in ancilla errors during the shorter readout circuit overcomes the increase in oscillator errors during squeezing. This process requires a larger truncated Hilbert space to be simulated, and hence we have not numerically tested this idea.

D. Universal qubit rotations: Pieceable gate teleportation

Arbitrary operations on finite-energy GKP states are generally not easily available. Recall that Pauli operations are simple phase space translations. However logical rotations are exponentials of Pauli's which (by the Pauli-Euler identity) can be written as a coherent superposition of identity and a phase space translation. Unfortunately, it is not possible to apply a classical control pulse that is in a superposition of zero amplitude (to achieve identity) and non-zero amplitude (to achieve the phase space displacement). One method to circumvent this problem is to use ancillary systems to teleport gates into the GKP codespace by use of conditional displacements. However, this method limits the logical er-

ror due to the physical errors of the ancilla. Here, we devise a technique to teleport gates while simultaneously correcting errors in the oscillator. We devise a pieceable gate teleportation circuit that is protected against ancilla decay errors, yielding room for high-fidelity gate operations using a biased-noise ancilla. This protection against errors is different from the general path-independent mechanisms engineered for circuits using SNAP gates [32, 51, 52]. Our construction does not require any hardware engineering feats such as chi matching [32, 69] (though these might yield further improvements).

a. Error-corrected gate teleportation. The error-corrected gate teleportation sequence is constructed by realizing that the stabilization circuit $SBS = \mathcal{E}\mathcal{U}$ is composed of entangling and unentangling gadgets. See fig. 9. By introducing a qubit gate in between the two gadgets, we can construct a phase-transfer circuit, as illustrated in Fig. 11(a). For logical $Z(\theta)$ gate, the circuit obeys the following equations, up to a global phase,

$$|\phi\rangle_2 = \mathcal{E}_x |\phi\rangle_1 \quad (112)$$

$$= \mathcal{E}_x(a|0\rangle_{GKP} + b|1\rangle_{GKP}) \otimes |g\rangle \quad (113)$$

$$= a|0\rangle_{GKP} \otimes |g\rangle - b|1\rangle_{GKP} \otimes |e\rangle \quad (114)$$

$$|\phi\rangle_3 = ZZ(\theta)|\phi\rangle_1 \quad 2 = e^{-i\frac{\theta}{2}\sigma_z}|\phi\rangle_2 \quad (115)$$

$$= a|0\rangle_{GKP} \otimes |g\rangle - e^{-i\theta}b|1\rangle_{GKP} \otimes |e\rangle \quad (116)$$

$$|\phi\rangle_4 = \mathcal{U}_x|\phi\rangle_2 \quad (117)$$

$$= a|0\rangle_{GKP} \otimes |g\rangle - e^{i\theta}b|1\rangle_{GKP} \otimes |g\rangle \quad (118)$$

$$= [Z(\pi + \theta)_{GKP}(a|0\rangle_{GKP} + b|1\rangle_{GKP})] \otimes |g\rangle. \quad (119)$$

To perform logical $X(\theta)$ ($Y(\theta)$) rotations, one only needs to entangle the qubit with the logical X (Y) eigenstates of the GKP code. This circuit corresponds to the stabilization of a different stabilizer operator. For example, the same circuit becomes a logical $X(\theta)$ gate if $\mathcal{E}_x \rightarrow \mathcal{E}_p, \mathcal{U}_x \rightarrow \mathcal{U}_p$. Similarly, for logical $Y(\theta)$ gate we have, $\mathcal{E}_x \rightarrow \mathcal{E}_{x+p}, \mathcal{U}_x \rightarrow \mathcal{U}_{x+p}$. The circuit can be easily changed to use ancilla $X(\theta)$ gates, mutatis mutandis if this is an easier gate for the DV ancillary system. This is the so-called phase transfer circuit.

If we ignore qubit errors, these circuits will yield $|g\rangle$ corresponding to the desired gate operation. The fidelity of these gates in the absence of any physical errors is 99.88% while the probability of a successful logical gate operation is 0.9994.

b. Trivial gate teleportation: Note that the “error-corrected” feature of our sequence comes from the fact that it is constructed from the logical identity, $\mathcal{U}_{x/p/x+p}\mathcal{E}_{x/p/x+p}$, that is the SBS stabilization circuit, unlike trivial gate teleportation (where $\mathcal{U}_{x/p/x+p} = \mathcal{E}_{x/p/x+p}^{-1}$) where the two gadgets would form a universal identity. That is, the error-corrected gate teleportation circuit, in addition to applying the logical gate on logical GKP codewords, also applies a corrective back action on erroneous GKP states similar to the small-big-small

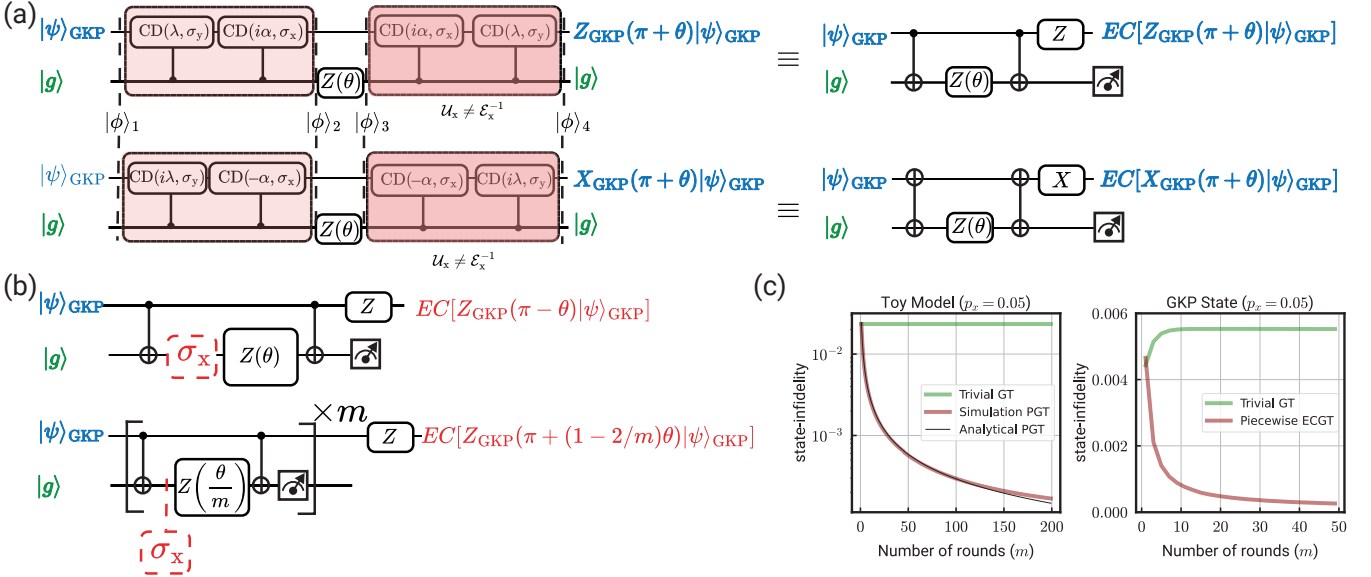


FIG. 11. **Error-suppressed GKP gate teleportation.** (a) Error-corrected gate teleportation of logical $Z(\theta)$ ($X(\theta)$) gate by an entangling-un-entangling sequence obtained from stabilizer of the logical $\{0,1\}$ ($\{+, -\}$) basis. (b) Toy model of a pieceable circuit to mitigate effects of biased-noise ancilla errors. (c) Comparison of trivial gate teleportation and pieceable gate teleportation for $\theta = \pi/4$ in the presence of ancilla errors. Here, the dotted line in the left panel presents the analytical curve for the state infidelity in the case of pieceable teleportation obtained from Eq. (120). The GKP state used for simulation results shown in the right panel simulation has an envelope size of $\Delta = 0.34$.

stabilization circuits discussed in Sec. V B.

c. *Protection from biased-ancilla errors:* Our teleportation circuit, however, is severely affected in the presence of ancillary errors (the same as any teleportation circuit). For our circuit, ancilla errors tend to occur during the (relatively long duration) controlled displacement gates acting on the cavity. In the case of a biased-noise ancilla, the circuit will only be affected by one type of ancillary error since the other errors are largely suppressed [66, 67]. For protection against a single type of ancillary error, we propose the pieceable circuit shown in Fig. 11(b). For example, without loss of generality, let us imagine a biased-noise ancilla where the dominant error is σ_x . The effect of this gate is shown in the top circuit of Fig. 11(b). The σ_x error on the ancilla propagates to the oscillator as a logical rotation angle error of 2θ on the GKP state. We propose to solve this problem by dividing the circuit into m pieces where each piece applies a rotation by $Z(\theta/m)$ as shown in the lower panel of Fig. 11(b). In this case, a single σ_x error will reduce the effect on the logical fidelity with increasing m . This circuit performs a random walk such that the average rotation of the gate is $\theta(1 - 2p_x)$ where p_x is the probability of σ_x errors. The standard deviation of the rotation angle of the gate produced by this random walk after m steps is $\sigma_m = \frac{|\theta|}{\sqrt{m}} 2\sqrt{p_x(1 - p_x)}$ which becomes small for large m . If the standard deviation increases at a slower speed compared to the decrease in fidelity, we get an overall increase in the fidelity of the output state. After m pieces of the circuits with rotations θ/m , the state is rotated

by the mean angle $\theta' = \theta(1 - 2p_x)$. The fidelity of the resulting state with a state rotated by θ' is given by,

$$\mathcal{F} = \sum_{k=0}^m \binom{m}{k} (1 - p_x)^{m-k} p_x^k \cos^2 [\theta(p_x - k/m)]. \quad (120)$$

We assume the fidelity for pure states is $\cos^2(\theta(1 - 2p_x) - \theta_k)$ where θ_k is the achieved rotation angle when k bit flip errors occur. The systematic error in the mean rotation angle can be compensated by choosing to use angle $\theta' = \theta/(1 - 2p_x)$. This calculation for the toy model assumes that the states are pure for analytical understanding. The metric used in the simulation of GKP states is the state fidelity computed using QuTiP [53]¹⁰. The curves in Fig. 11(c) show that the decrease in infidelity is proportional to $1/m$. In the toy model, we apply errors only just before the CZ_{GKP} gates with probability $p_x = 0.05$ to emulate the case of GKP states where the CD gates are longer and more erroneous compared to the qubit rotation $Z(\theta)$. In the GKP simulation, we apply a σ_x error at a rather large rate of $\gamma \sim 1/22\mu\text{s}^{-1}$ during all conditional displacements (to emulate the probability $p_x = 0.05$ during the large conditional displacements). We use the metric that a conditional displacement by a magnitude of 1 takes time $\tau = 1\mu\text{s}$ as outlined in App. D and use τ to make all rates dimensionless.

We compare the method just described above against single-shot trivial gate teleportation followed by $m - 1$

¹⁰ $\text{Tr}(\sqrt{\rho_A} \rho_B \sqrt{\rho_A})$ for the density matrices ρ_A, ρ_B of mixed states.

stabilization rounds in Fig. 11c. The initial bump in the infidelity is due to the uncorrected gate teleportation step. The error introduced in this step is not corrected with further stabilization steps since it is a logical error. Note that, in the case of trivial gate teleportation, one could use the measurement outcome to check for ancilla errors more efficiently¹¹, but that would make the protocol reliant on measurements which can be the slowest (or, most erroneous) part of the circuit. The pieceable circuit is not applied to the trivial gate teleportation since this circuit does not stabilize the GKP states. Thus, prolonged exposure to the trivial gate teleportation will decrease fidelity due to ancilla errors. However, as can be seen, this is not the case for our error-corrected gate teleportation (ECGT). Despite applying ECGT for multiple pieces (m), the logical error does not just stay constant but decreases. This indicates that ECGT has an error-correcting property. Thus, we have proven here that pieceable gate teleportation is a more efficient method to apply autonomously error-resilient single-qubit gate rotations in the presence of errors with a biased-noise ancilla.

Just as in the stabilization circuit, the qubit is reset to $|g\rangle$ at the end of every piece in the circuit. This reset could be erroneous and this error has not been accounted for explicitly in our simulations. If the reset leaves the qubit in state $|e\rangle$, it has the same effect as a σ_x error on the ancilla at the beginning of the first conditional displacement. Since such an error has been accounted for, it indicates that if the total effect of ancilla errors during reset and conditional displacements is low enough, we will see an improved fidelity for the pieceable error-corrected gate teleportation circuit.

E. Entangling GKP qubits: Extension of GCR to multi-modal operations

The two-qubit gates suggested in [56] for an ideal GKP code have poor fidelity and require a few stabilization rounds to improve the error rate [43].

a. Single-qubit-ancilla: For the finite-energy states, Ref. [43] derived the finite-energy version of the two-qubit entangling gate. This circuit, the same as the stabilization circuit, can be derived using the non-abelian QSP extension for two modes. We discuss this extension here. For ideal GKP codes with support at positions $m\sqrt{\pi/2}$, $m \in \mathbb{Z}$, the conditional SUM gate displaces the second mode by the position $\pm\hat{x}$ of the first mode with the sign of the displacement determined by the state of the ancilla. Equivalently, for each pair of peaks of the two GKP states, in the position (first mode) and momentum (second mode), respectively, the conditional SUM

gate ($e^{i2\hat{x}\otimes\hat{p}}$) rotates the qubit via $e^{il\pi\sigma_x}$ by angle $2l\pi$, where l is the product of the two integers defining the positions of the two peaks. This operation is equivalent to $(-1)^l I$ on the joint oscillator-qubit state, and it applies a CX_{GKP} gate on the two logical GKP codewords with the qubit going back to the original state ($|g\rangle$, in this case). The non-abelian correction for the entangling half of this operation $e^{i(\hat{x}\otimes\hat{p})\otimes\sigma_x}$ due to the envelope size $\Delta \neq 0$ with respect to the first (second) GKP qubit is given by, $e^{i\Delta^2\hat{p}\otimes\hat{p}\otimes\sigma_y}(e^{-i\Delta^2\hat{x}\otimes\hat{x}\otimes\sigma_y})$, assuming the ancilla starts in state $|g\rangle$. Thus, the GCR-type pre-correction due to both modes will be equal to,

$$S \equiv e^{-i\frac{\Delta^2}{2}(\hat{x}\otimes\hat{x}-\hat{p}\otimes\hat{p})\otimes\sigma_y} \quad (121)$$

The corresponding SBS-type circuit, where $B \equiv e^{i(2\hat{x}\otimes\hat{p})\otimes\sigma_x}$ and S is given by Eq. (121), will have rotated the qubit by an angle of 2π about σ_x . In doing so, however, the SUM gate applies a logical controlled Pauli operation, just as the SUM gate applies a logical Pauli operation. This operation, the same as the stabilization circuit SBS, is protected against biased-noise ancilla errors. However, the fidelity of the Bell states prepared using this circuit is ~ 0.90 for $\Delta = 0.34$ which indicates that this gate requires more terms in the non-abelian correction to reach higher fidelities.

The fast conditional two-mode operations required for this operation can be achieved using Gaussian operations and weak dispersive coupling between the oscillator and qubit. Ref. [43] suggests that this sequence takes more gates (5 conditional two-mode operations equivalent to a SUM gate). However, we claim that this circuit can be achieved in three gate sequences given we can obtain fast $e^{i\frac{\Delta^2}{2}(\hat{x}\otimes\hat{x}-\hat{p}\otimes\hat{p})\otimes\sigma_y}$ gates using a two-mode extension of the echoed conditional displacement [10, 23, 24]. This decomposition is given in Ref. [8] for entangling oscillator gates in the weak dispersive regime, and we present it in App. I1 in the context of two-qubit GKP operations.

Fast echoed conditional displacement was obtained using (weak) dispersive coupling in the displaced frame. Similarly, we can obtain a fast echoed conditional SUM gate using (weak) dispersive coupling in a two-mode squeezed frame. The two-mode squeezing required for this operation can be obtained from single-mode squeezing and beam-splitters using Bloch-Messiah decomposition [8]. Thus, this circuit involves two single-mode squeezing operations and two beam-splitters to go to the two-mode squeezing frame using $\text{TMS}(\alpha, \pi)$ (see definition in Ref. [8]). In this new frame, the circuit uses evolution under the dispersive interaction in this frame for the duration $t_{\text{CX}} \geq \frac{\Delta^2}{\chi \sinh 2\alpha} + \frac{2\Delta^2}{\chi}$ where χ is the strength of the weak dispersive coupling. Thus, by increasing α one can make this process much faster. Hypothetically, $\lim_{\alpha \rightarrow \infty} t_{\text{CX}} \geq \frac{2\Delta^2}{\chi}$ is allowed, however, in reality, we are limited to finite and much lower values of α due to unwanted state transitions in a nonlinear ancilla dispersively coupled to a resonator (oscillator) [10, 23, 67].

¹¹ the corrective back action renders the measurement outcomes less useful in terms of detecting errors.

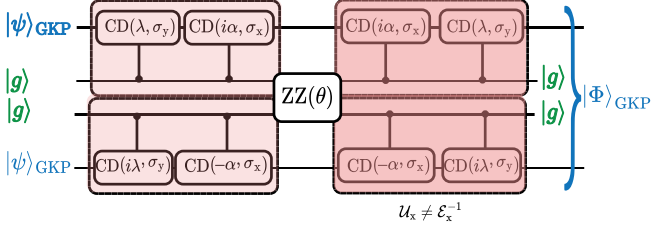


FIG. 12. **Pieceable GKP entangling operations.** Circuit for logical Pauli operations using two ancillae. Here, $|\Phi\rangle = EC[ZZ_{GKP}(\pi + \theta)|\psi, \psi\rangle_{GKP}]$. For $\theta = \pi/4$, we can prepare a Bell state if $|\psi, \psi\rangle_{GKP} = |++\rangle_{GKP}$. The fidelity of this Bell state preparation is 0.9997 (as per Sec. V D) and the success probability of the qubit outcome $|g, g\rangle$ is $P_g = (0.9997)^2 = 0.998$.

b. Two qubit ancillae: Our alternative circuit using two-qubit ancillae does not have the issue of engineering conditional Gaussian operations. This circuit only uses conditional displacements and qubit gates (again, protected from biased-noise ancilla error piecewise gate teleportation). An option to increase this fidelity in the absence of errors is using the error-corrected gate teleportation with two pairs of GKP oscillator state-DV qubit combinations. This circuit is similar to Fig. 11(a), except the middle gate can be a controlled Pauli operation between the two DV qubits given the initial states and final operation to be implemented. See App. I2. However, this circuit cannot be converted into a pieceable circuit to yield high-fidelity gates in the presence of ancilla errors.

Nevertheless, we can achieve pieceable circuits for two-qubit logical Pauli rotations $P_i P_j(\theta)$ ($P_i, P_j \in \{\sigma_x, \sigma_y, \sigma_z\}$). Fig. 12 gives the circuit construction for $P_i P_j(\theta) = ZZ_{GKP}(\theta)$. These gates are inspired by the single-qubit case discussed in Sec. V D and shown in Fig. 11(a), and thus, we can use the same arguments to perform two-qubit rotations in any basis, using the entangling and unentangling gadgets which apply SBS on both GKP qubits. This yields us two-qubit universality.

The pieceable version of this circuit is an error-corrected two-qubit entangling operation that is autonomously protected from ancilla errors and photon loss. In the absence of errors, this sequence yields a success probability of $P_g = 0.9987$. We believe that the state fidelity of this process will be the same as the single-qubit gate teleportation scheme. For example, computing the SBS state infidelity for a system with two truncated oscillators (each with Hilbert space dimension of 50) and two qubits is 0.98 (upper bounded by truncation issues and not the protocol). We achieve the same fidelity for the Bell pair. This fidelity is much lower than what is expected (0.998 from Sec. V D), and we believe this is due to the Hilbert space constraints. The error probability indeed increases with the use of two-qubit DV gates; however, the total error due to conditional displacement remains the same as the case of single-qubit gate teleportation analyzed in Sec. V D.

In addition, this operation only requires us to perform fast conditional displacements, a combination of weak dispersive coupling, unconditional displacements, and two-qubit ancilla rotations. Thus, the circuit is much faster compared to the combination of weak dispersive coupling and unconditional two-mode Gaussian operations. Even though Gaussian operations are interpreted to be an easy resource for oscillators, not much work has been done to improve the fidelity of non-number-preserving operations like two-mode and single-mode squeezing. Thus, in this manuscript, we have only considered unconditional displacements, phase space rotations, beam-splitters, and ancilla qubit rotations as the set of instructions for two-mode phase space ISA. Note that these operations have been demonstrated with high fidelity in hybrid oscillator-qubit systems [10, 24, 68, 70].

F. Generalization to multi-mode GKP codes and GKP qudits

Our high-fidelity control operations will not only be instrumental in realizing multi-mode operations between various GKP qubits but could be also used for the stabilization of multi-mode GKP codes. GKP qudits are encoded in an oscillator by changing the lattice spacing of the support (increasing the unit cell size in phase space to accommodate more than 2 code states) [40].

a. Error-detected State Preparation: The state preparation works by changing α to the required lattice spacing for qudits or an alternative qubit lattice.

b. Error-corrected gate teleportation: The pieceable gate teleportation is also extendable since these gates are derived from the GCR interpretation of the stabilization routine. The stabilization circuits are extendable to any qubit or qudit lattice by choosing appropriate α in the same circuit. Thus, the same argument extends all our gate teleportation circuits to arbitrary qubit and qudit lattices.

c. High-fidelity logical readout: The logical readout schemes for arbitrary lattices again follow from a change in α . However, for efficient qudit readout circuits that take the least amount of time, we need access to DV qudits. For example, each circuit used in Fig. 10 can be extended to qudits using an ancilla qudit of the same dimension for readout. This extension may not have the same readout fidelity and is left for future work to analyze.

VI. FURTHER APPLICATIONS

We have demonstrated the advantages of using non-commuting variables to construct composite pulse sequences, in the context of controlling hybrid CV-DV architectures. Using three different figures of merit, we verify the correctness and proof of our design. Finally, we have compared the scheme against the best known uni-

variate composite pulse sequence, BB1(90). Our composite pulse sequence is comparable to BB1(90) for a range of errors in the quantum control variables while being seven times shorter in circuit depth. This reduction in circuit depth makes our non-abelian-QSP-inspired scheme a more favorable candidate for the control of hybrid systems in the presence of noise. In this concluding section, we shed some light on some of the applications of our work in oscillator-based algorithms and discuss prospects.

A. Quantum Phase Estimation using Ancillary Oscillators

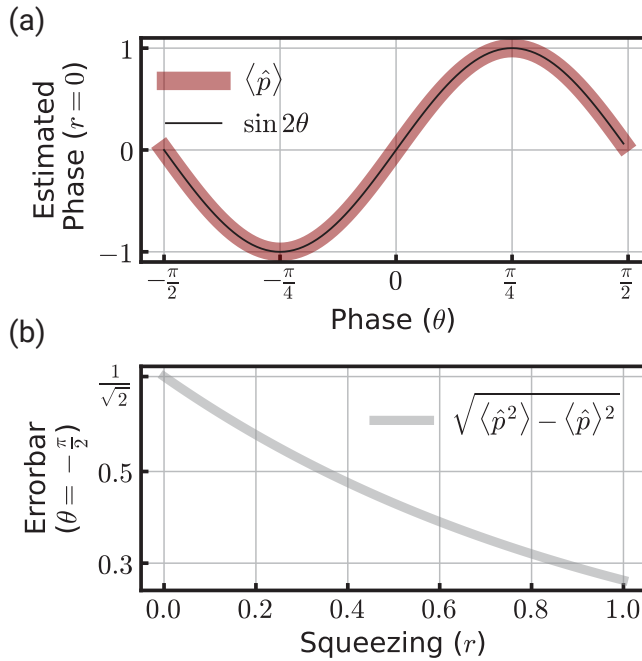


FIG. 13. **Quantum phase estimation in hybrid oscillator-qubit architecture.** (a) Phase estimation can be performed using the control sequence described in Sec. VI A as confirmed by this figure, for $\alpha = 1$ in Eqs. (124–127). (b) The error bar of this operation relies on the squeezing parameter r , upper bounded by $1/\sqrt{2}$ at $r = 0$. This upper bound can only be improved by repeated application of the protocol.

The eigenvalue of a unitary $U = e^{i\theta\hat{n}\cdot\vec{\sigma}}$ on an eigenstate $|\psi\rangle$ can be estimated in the hybrid oscillator-qubit architecture. In this section, we present an algorithm for this phase estimation with the help of an ancillary oscillator using the phase space instruction. For this purpose, we need to construct the following controlled-unitary CU operation $C_xU = e^{i\hat{f}(\theta)\hat{x}\otimes\hat{n}\cdot\vec{\sigma}}$, where $f(\theta)$ is a known polynomial in θ , using conditional displacements and qubit rotations (including U). Such an operation boosts the momentum of the oscillator state conditioned

on the qubit and $f(\theta)$. The measurement of momentum boost using techniques like homodyne measurement can then be used to determine the eigenvalue θ . This technique was outlined in [71] to find the eigenvalue of a Hamiltonian H ($= \theta\hat{n}\cdot\vec{\sigma}$). The authors construct the conditional gate $e^{i\hat{x}\otimes\hat{H}}$ by assuming the availability of elementary gates like $e^{i\hat{x}\otimes h_k}$ (i.e., $f(\theta) = \theta$) such that $\prod_k e^{ih_k} = e^{iH}$ and $[h_k, h'_k] = 0$. Building on Ref. [71], we construct the C_xU using *non-commuting gates* from the phase-space instruction architecture, assuming only the availability of U and leveraging *arbitrary conditional displacements and rotations* instead of specific hybrid gates. The precision of this phase estimation technique will thus not only depend on the squeezing of the bosonic mode (illustrated in Ref. [71]) but also on the approximation to which C_xU can be constructed using the instruction set.

For simplicity, we take $U = e^{i\theta\sigma_y}$, and the construction below, *mutatis mutandis*, follows for the case of arbitrary $\hat{n}\cdot\vec{\sigma}$ (see derivation in App. J).

$$e^{i\alpha\hat{x}\hat{n}\cdot\sigma_z}e^{i\theta\sigma_x}e^{-i\alpha\hat{x}\hat{n}\cdot\sigma_z}e^{-i\theta\sigma_x} = e^{i\hat{g}\hat{n}'\cdot\sigma} = C_xU \quad (122)$$

where,

$$\cos \hat{g} = 1 - 2 \sin^2(\alpha\hat{x}) \sin^2(\theta) \quad (123)$$

$$\cos \hat{c} = \cos \alpha\hat{x} \cos \theta \quad (124)$$

$$n'_z = \frac{\sin^2 \theta \sin 2\alpha\hat{x}}{\sin \hat{g} \sin^2 c} \quad (125)$$

$$n'_y = \frac{\sin 2\theta \sin 2\alpha\hat{x}}{2 \sin \hat{g}} \quad (126)$$

$$n'_x = \frac{\sin^2 \alpha\hat{x} \sin 2\theta}{\sin \hat{g} \sin^2 c}. \quad (127)$$

In Fig. 13 we show a proof of this calculation using a simulation that satisfies $\langle p \rangle = \alpha \sin 2\theta$. The figure also shows that the standard deviation for the protocol is upper bounded by $1/\sqrt{2}$ at no squeezing when $r = 0$, where r is the momentum-squeezing parameter. The precision of the homodyne measurement could be made better via repeated measurements, and the cost of this repetition should be compared against qubit and time overhead in DV phase-estimation circuits. Here, we could employ the GCR-composed BB1 schemes developed in Sec. III C to perform this task using qubits for bit-wise measurement of the mean position value of the squeezed oscillator state. We will not discuss the details of a circuit-depth analysis for this strategy in this work.

B. Summary and Future Prospects

The ultimate goal of our work is to enable high-fidelity control in hybrid oscillator-qubit architectures. To this end, we introduced a new class of quantum signal processing protocols, in which the qubit rotation angles are not classical control parameters but rather quantum operators associated with the position and momentum of

an oscillator. We have termed this non-abelian quantum signal processing, and proposed novel composite pulses within this class. Our primary composite pulse sequence, termed the Gaussian-Controlled-Rotation (GCR), is analytically and numerically benchmarked against the BB1 pulse sequence, widely used in classical NMR. We find that GCR achieves comparable performance with a $4.5\times$ shorter circuit depth, and due to this reduction, GCR outperforms BB1 in the presence of errors. Additionally, we construct a concatenated pulse, BB1(GCR), which produces a response function closer to a square wave than BB1 alone.

Using GCR, we provide completely analytical constructions for the deterministic preparation of squeezed states, cat states, GKP states, and Fock states. For squeezed and GKP states, we compare our analytical method with previous numerical and semi-analytical approaches, and show significant improvements in fidelity, surpassing prior results reported in Refs. [10, 41]. Importantly, our fully analytical approach has an intuitive physical interpretation and enables mid-circuit ancilla error detection. With this technique, we prepare a GKP logical $|0\rangle$ state with a fidelity of 0.96 and a success probability of 0.94, for experimentally realistic error parameters.

GCR further enables intuitive explanation of stabilization and logical readout protocols for the GKP code that were originally derived using dissipation engineering and numerical optimization, respectively. The GCR pulse unifies these protocols under a common framework of entangling and unentangling operations between a finite-energy GKP code and a qubit ancilla. This insight leads to an error-corrected gate teleportation (ECGT) scheme for both single- and two-qubit logical GKP gates. This ECGT scheme applies rotation on the logical GKP subspace while correcting errors in the oscillator. Our ECGT circuit can be chosen to further protect against either ancilla decay or dephasing errors using a novel pieceable approach, making the protocol fault-tolerant under biased-noise models. Thus, our non-abelian composite pulse scheme enables fault-tolerant universal control of GKP codes with a biased-noise ancilla.

A desirable feature of readout of logical codewords is that it is robust against errors as long as the state is still within the correctable subspace. Because BB1(GCR) produces a response closer to a square wave against the position or momentum of the oscillator, this composite pulse yields a logical readout of the GKP code that is more resilient than previous schemes to correctable errors.

Given the central role of the non-abelian composite pulse GCR, our work underscores the significance of non-abelian QSP for controlling hybrid CV-DV quantum processors. These results are a first example that motivate the development of a complete constructive theory of non-abelian QSP, a key future direction. This generalization could pave the way for non-abelian quantum singular value transformation (QSVT), in analogy

to the abelian QSVT that unifies quantum algorithms on qubit-only platforms. We anticipate that non-abelian QSVT may similarly unify hybrid CV-DV quantum algorithms. Moreover, the principles of non-abelian QSP may extend beyond hybrid systems to multi-qubit gate synthesis, broadening the impact of this framework. We believe that our work offers a foundational step toward this vision.

ACKNOWLEDGMENTS

SS and SMG were supported by the Army Research Office (ARO), under Grant Number W911NF-23-1-0051. The views and conclusions contained in this document are those of the authors and should not be interpreted as representing the official policies, either expressed or implied, of the Army Research Office (ARO), or the U.S. Government. The U.S. Government is authorized to reproduce and distribute reprints for Government purposes notwithstanding any copyright notation herein. BR was supported by the National Sciences and Engineering Research Council of Canada (NSERC), the Canada First Research Excellence Fund, as well as the Fonds de Recherche du Québec, Nature et Technologie (FRQNT). External interest disclosure: SMG receives consulting fees and is an equity holder in Quantum Circuits, Inc. We thank Liang Jiang for suggesting the term error-corrected for our teleportation scheme.

Appendix A: Quantum Phase Space Quadratures

Second quantization in quantum mechanics defines the position and momentum in the discrete space of oscillators using the non-hermitian operators \hat{a} and \hat{a}^\dagger . These definitions exist in various units, with $\hbar = 1$, where we use the following Wigner units,

$$\hat{x} = \frac{\hat{a} + \hat{a}^\dagger}{2}, \quad \hat{p} = \frac{\hat{a} - \hat{a}^\dagger}{2i}. \quad (\text{A1})$$

The definition implies the following. The commutation relation follows $[\hat{x}, \hat{p}] = \frac{i}{2} \implies \hat{p} = -\frac{i}{2} \frac{\partial}{\partial \hat{x}}$. The minimum uncertainty state, vacuum, is given by the derivation,

$$\hat{a} |0\rangle_{\text{vac}} = 0 \implies (\hat{x} + i\hat{p}) |0\rangle_{\text{vac}} = 0 \quad (\text{A2})$$

$$\implies (x + \frac{1}{2} \frac{\partial}{\partial x}) e^{-\frac{x^2}{\sigma}} = 0 \quad (\text{A3})$$

$$\implies x - \frac{x}{\sigma} = 0 \implies |0\rangle = \left(\frac{2}{\pi}\right)^{1/4} e^{-x^2}. \quad (\text{A4})$$

The minimum position uncertainty for this state is

$$\delta x = \sqrt{\langle \hat{x}^2 \rangle - \langle \hat{x} \rangle^2} = \left(\frac{2}{\pi}\right)^{1/4} \sqrt{\int_{-\infty}^{\infty} x^2 e^{-2x^2} dx} = \frac{1}{2} \quad (\text{A5})$$

Thus, we have $\delta x = \delta p = \frac{1}{2}$ for this state, and the minimum uncertainty principle is satisfied $\delta x \delta p = \frac{1}{4}$. Ignoring the normalization, we can define states with arbitrary position uncertainty as $\psi(x) = e^{-\frac{x^2}{\Delta^2}}$ such that $\Delta^2 = 4\delta x^2 = 1$ denotes the vacuum state. In these units, if we follow the definitions of a coherent state $|\alpha\rangle$ as $\hat{a}|\alpha\rangle = \alpha|\alpha\rangle$, the position representation of a squeezed coherent state is given by,

$$|\langle x|\alpha_\Delta\rangle|^2 = \left(\frac{2}{\pi\Delta^2}\right)^{1/4} e^{-\frac{2(x-\alpha)^2}{\Delta^2}} \quad (\text{A6})$$

For convenience of displacement units, we will use the unconventional conditional displacement operator definition,

$$\text{CD}(\beta, \sigma_\phi) = e^{(\beta\hat{a}^\dagger - \beta^*\hat{a}) \otimes \sigma_\phi} \quad (\text{A7})$$

In this convention, for purely real β , we have,

$$\langle x|\text{CD}(\beta, \sigma_\phi)|0_\Delta\rangle = \langle x, +\phi|e^{-i2\beta\hat{p} \otimes \sigma_\phi}|0_\Delta, +\phi\rangle \quad (\text{A8})$$

$$= \left(\frac{2}{\pi}\right)^{1/4} e^{-\frac{(x-\beta)^2}{\Delta^2}} \otimes |+\phi\rangle, \quad (\text{A9})$$

where $|+\phi\rangle$ is the eigenstate of σ_ϕ corresponding to the $+1$ eigenvalue. This is a state displaced along the position axis by $|\beta|$ to the left or right conditioned on the qubit state.

Appendix B: QSP Hierarchy for Optimal Universal Oscillator Control

In the following, multi-variate or multi-variable does not necessarily refer to having many oscillators each with their own \hat{x}, \hat{p} , but rather (for the case of a single oscillator at least) to having multiple directions in phase space along which displacements can be made.

a. Univariate QSP Here $[\hat{v}_i, \hat{v}_j] = 0$, that is, all the allowed vectors in phase space used for CD are parallel. Thus even though the rotation angles \hat{v}_j , are quantum operators, all the angles in the QSP sequence commute with each allowing us to directly utilize the univariate classical QSP methods introduced in [48]. Our BB1 analogue used for comparison above is an adaptation of this QSP class to quantum control variables. This formalism was also used for single-shot interferometry in [37] which introduced ‘Bosonic QSP’ independent of the present work.

b. Multivariate QSP with commuting variables The scheme is the primitive version of multivariate QSP introduced in [5, 50].

- *Bivariate QSP with commuting variables.* Here $\hat{v}_i \in \{\hat{v}_1, \hat{v}_2\}$ s.t. $[\hat{v}_1, \hat{v}_2] = 0$. In [50] the authors prove that it is possible to construct $U_{\vec{\phi}}$ for an arbitrary target Hamiltonian $\hat{H}(\hat{v}_1, \hat{v}_2)$, if $\deg_{\hat{v}_1}(\hat{H}) \leq 1$ or $\deg_{\hat{v}_2}(\hat{H}) \leq 1$. For state preparation defined above, $\langle x|U_{\vec{\phi}}|0\rangle = \psi(x)$, that is, it already satisfies the condition used in this

theorem. The theorem can be put to use towards oscillator state preparation if we restrict ourselves to the regime where $[[\hat{v}_1, \hat{v}_2]]$ is sufficiently small. The efficiency for universal control in the commuting variable regime is likely to be similar to Suzuki-Trotter decompositions.

- *Multivariate QSP (m – qsp) with commuting variables.* The adaptation of any composite pulse using quantum control variables is an example of a composite pulse which belongs to this QSP class, if it allows $|v_i| \neq |v_j|$ if $i \neq j$. In [5] authors introduce this QSP class towards control of single or multiple oscillators using operators which commute, for example $\hat{x}_1 = \hat{x} \otimes I, \hat{x}_2 = I \otimes \hat{x}$ on the joint space of two oscillators.

As before, if we restrict that pairwise products of the magnitudes $|v_i||v_j| = \mathcal{O}(\lambda) \forall i, j$, we can use CDs along arbitrary vectors in phase space to achieve state preparation using m-qsp even if $[v_i, v_j] \neq 0$. Such inputs will make QSP sequences more efficient to prepare states that have low mean photon number and are rotationally symmetric in phase space, for example, Fock state $|1\rangle$. However, unlike the abelian bivariate case, there is no constructive proof of an algorithm to generate $U_{\vec{\phi}}$ in this case.

- *Multivariate QSP with non-commuting variables* The scheme is lightly touched upon by [50].

• *Bivariate QSP.* Our scheme is the first example of a composite pulse that belongs to this QSP class. We have already seen the advantages of such schemes in achieving high-fidelity outputs for low circuit-depth via GCR. In addition, this class is necessary to achieve universal control which beats the efficiency of methods like Suzuki-Trotter.

• *Multivariate QSP.* This class lies at the top of the hierarchy and is the most efficient resource for optimal universal control of oscillators. The resource of multiple non-commuting variables was used with gradient-descent-based techniques to achieve highly efficient circuits for state preparation of various non-Gaussian states in [10]. The final goal towards universal control of CV-DV architectures will be to understand analytical constructions for this QSP class.

Appendix C: Error Analysis of Composite Pulse Sequences in Phase Space

In this appendix, we compute the error analysis for the univariate QSP sequence BB1(2 θ) and the bivariate non-abelian QSP sequence GCR(2 θ). We begin by describing the metrics used in the main text and the subsequent

appendices. The equations extracted in the latter sections of this appendix have been used in plots shown in Secs. III B.

1. Performance Metrics

This work focuses on extracting a single bit of information from the oscillators (CV systems) via qubits (DV systems). Here, we define the metrics which will be helpful in assessing the performance of the various sequences used towards this goal. One of the examples of this task is to distinguish between a $|\alpha_\Delta\rangle$ and $|- \alpha_\Delta\rangle$, where $|\pm \alpha_\Delta\rangle$ is a squeezed coherent state defined in Eq. (4). Let us suppose the QSP sequence used for this task is denoted by U has been applied to the hybrid oscillator-qubit system $|g\rangle \otimes |\pm \alpha_\Delta\rangle$. The most general statement we can write about this operation is as follows,

$$U(|g\rangle \otimes |\alpha_\Delta\rangle) = \beta_{+g} |\psi_{+g}\rangle |g\rangle + \gamma_{+e} |\phi_{+e}\rangle |e\rangle \quad (\text{C1})$$

$$U(|g\rangle \otimes |- \alpha_\Delta\rangle) = \gamma_{-g} |\phi_{-g}\rangle |g\rangle + \beta_{-e} |\psi_{-e}\rangle |e\rangle \quad (\text{C2})$$

We have two requirements here, (1) to determine whether the oscillator is in state $|\alpha_\Delta\rangle$ or $|- \alpha_\Delta\rangle$ with maximum fidelity, and (2) this measurement should be quantum non-demolition (QND) in that it has minimal back action on the oscillator state. We will assume that the two states are symmetric in that $\beta_{+g} = \beta_{-e} \equiv \beta$, $\langle + \alpha_\Delta | \psi_{+g} \rangle = \langle - \alpha_\Delta | \psi_{-e} \rangle \equiv \langle \alpha | \psi \rangle$ and $\gamma_{+e} = \gamma_{-g} \equiv \gamma$, $\langle + \alpha_\Delta | \phi_{+e} \rangle = \langle - \alpha_\Delta | \phi_{-g} \rangle \equiv \langle \alpha | \phi \rangle$. This indicates that $|\beta|^2$ decides the ability to successfully (unsuccessfully) deduce the sign of the mean position of the oscillator using the qubit outcome. Thus, we give the following two quantities.

- The *fidelity* of this measurement strategy,

$$\frac{|\beta_{+g}|^2 - |\gamma_{+e}|^2 + |\beta_{-e}|^2 - |\gamma_{-g}|^2}{2} \quad (\text{C3})$$

$$= |\beta|^2 - |\gamma|^2 = 1 - 2|\gamma|^2 = 1 - 2P_e(U), \quad (\text{C4})$$

where $P_e(U)$ is the probability of failure to rotate the qubit to the state(s) predicted by the mean position of the oscillator (for example, $|g\rangle$ ($|e\rangle$) if oscillator is in $|\alpha_\Delta\rangle$ ($|- \alpha_\Delta\rangle$) state).

- Another quantity is the *QNDness* of this measurement strategy which quantifies the back action of this strategy on the oscillator state,

$$\frac{|\beta_{+g}| \langle + \alpha_\Delta | \psi_{+g} \rangle|^2 + |\gamma_{+e}| \langle + \alpha_\Delta | \phi_{+e} \rangle|^2}{2} + \frac{|\beta_{-e}| \langle - \alpha_\Delta | \psi_{-e} \rangle|^2 + |\gamma_{-g}| \langle - \alpha_\Delta | \phi_{-g} \rangle|^2}{2} \quad (\text{C5})$$

$$= |\beta|^2 |\langle \alpha | \psi \rangle|^2 + |\gamma|^2 |\langle \alpha | \phi \rangle|^2. \quad (\text{C6})$$

The first (second) term represents the fidelity of the oscillator with the original state in the event of a

success (failure). Thus, this quantity presents the fidelity of the oscillator state in the event of a qubit reset, which we call the hybrid state fidelity F_H for the specific QSP sequence U .

Thus, based on these metrics, for each QSP sequence used in this work, we will quote the $P_e(U)$ and $F_H(U)$.

2. No QSP correction

Here, we start with a state $|\psi_1\rangle = |g\rangle \otimes |\alpha\rangle$ and analyze the effect of applying the conditional momentum boost $e^{-i\frac{\pi}{4\alpha}\hat{x}\sigma_x}$. Ignoring normalization factors, we have,

$$\langle x | \psi_1 \rangle = \left(\frac{2}{\pi}\right)^{\frac{1}{4}} e^{-(x-\alpha)^2} |g\rangle \quad (\text{C7})$$

$$\langle x | \psi_2 \rangle = \left(\frac{2}{\pi}\right)^{\frac{1}{4}} e^{-i\frac{\pi}{4\alpha}\hat{x}\sigma_x} e^{-(x-\alpha)^2} |g\rangle \quad (\text{C8})$$

Now, the task is to compute the overlap with the desired state $|-i\rangle \otimes |\alpha\rangle$ which is given by,

$$= \left(\frac{2}{\pi}\right)^{\frac{1}{2}} \int_{-\infty}^{\infty} dx \langle -i | e^{-i\frac{\pi}{4\alpha}x\sigma_x} e^{-2(x-\alpha)^2} |g\rangle \quad (\text{C9})$$

$$= \left(\frac{2}{\pi}\right)^{\frac{1}{2}} \frac{1}{2} \int_{-\infty}^{\infty} dx (e^{i\pi/4} e^{-i\frac{\pi}{4\alpha}x} + e^{-i\pi/4} e^{i\frac{\pi}{4\alpha}x}) e^{-2(x-\alpha)^2} \quad (\text{C10})$$

$$= \left(\frac{2}{\pi}\right)^{\frac{1}{2}} \frac{1}{2} \int_{-\infty}^{\infty} dx (e^{-i\frac{\pi}{4\alpha}(x-\alpha)} + e^{i\frac{\pi}{4\alpha}(x-\alpha)}) e^{-2(x-\alpha)^2} \quad (\text{C11})$$

$$= \left(\frac{2}{\pi}\right)^{\frac{1}{2}} \int_{-\infty}^{\infty} dx \cos\left(\frac{\pi}{4\alpha}(x-\alpha)\right) e^{-2(x-\alpha)^2} \quad (\text{C12})$$

$$= \left(\frac{2}{\pi}\right)^{\frac{1}{2}} \int_{-\infty}^{\infty} dx \left(1 - \frac{\pi^2}{32\alpha^2} y^2\right) e^{-2y^2} \quad (\text{C13})$$

$$= 1 - \left(\frac{2}{\pi}\right)^{\frac{1}{2}} \frac{\pi^2}{32\alpha^2} \int_{-\infty}^{\infty} dx y^2 e^{-2y^2} \quad (\text{C14})$$

$$= 1 - \frac{\pi^2}{128\alpha^2}. \quad (\text{C15})$$

Therefore, the hybrid state fidelity F_H for large $|\alpha|$ is equal to,

$$F_H(\text{no-QSP}) \approx \left|1 - \frac{\pi^2}{128\alpha^2}\right|^2 \approx 1 - \frac{\pi^2}{64\alpha^2}. \quad (\text{C16})$$

Since the operation $e^{i\frac{\pi}{4}x\sigma_x}$ applies no back action on the position basis, the probability of failure in this case is the same as the reset fidelity computed above.

3. Bivariate sequence: GCR(2θ)

Let us proceed with the calculation of $P_g = 1 - P_e$. For simplicity, we also define $y\Delta = (x - \alpha)$ and use $\lambda = \frac{\theta\Delta^2}{|\alpha|}$. Using the Taylor expansions from eqs. 29-31 to write,

$$\langle x|UV|\alpha_\Delta, g\rangle = \sum_{m=0}^{\infty} \frac{[i\theta(x-\alpha)\sigma_x]^m}{|\alpha|^m m!} \sum_{n=0}^{\infty} \left(-\frac{\lambda\sigma_y}{2\Delta}\right)^n \frac{1}{n!} H_n\left(\frac{x-\alpha}{\Delta}\right) \alpha_\Delta(x) |g\rangle \quad (C17)$$

$$= \sum_{m=4\mathbb{Z}, n=2\mathbb{Z}}^{\infty} \frac{(\lambda/\Delta)^{m+n}}{2^n n! m!} y^m \left[H_n(y) - \frac{(\lambda/\Delta)\sigma_y}{2(n+1)} H_{n+1}(y) \right] \alpha_\Delta(x) |g\rangle \quad (C18)$$

$$+ \sum_{m=4\mathbb{Z}+1, n=2\mathbb{Z}}^{\infty} \frac{i(\lambda/\Delta)^{m+n}}{2^n n! m!} y^m \left[H_n(y)\sigma_x - \frac{i(\lambda/\Delta)\sigma_z}{2(n+1)} H_{n+1}(y) \right] \alpha_\Delta(x) |g\rangle \quad (C19)$$

$$+ \sum_{m=4\mathbb{Z}+2, n=2\mathbb{Z}}^{\infty} \frac{-(\lambda/\Delta)^{m+n}}{2^n n! m!} y^m \left[H_n(y) - \frac{(\lambda/\Delta)\sigma_y}{2(n+1)} H_{n+1}(y) \right] \alpha_\Delta(x) |g\rangle \quad (C20)$$

$$+ \sum_{m=4\mathbb{Z}+3, n=2\mathbb{Z}}^{\infty} \frac{-i(\lambda/\Delta)^{m+n}}{2^n n! m!} y^m \left[H_n(y)\sigma_x - \frac{i(\lambda/\Delta)\sigma_z}{2(n+1)} H_{n+1}(y) \right] \alpha_\Delta(x) |g\rangle \quad (C21)$$

We have broken down the product terms $\langle x|UV|\alpha_\Delta, g\rangle$ into eight groups corresponding to the combinations of $m \in \{4\mathbb{Z}, 4\mathbb{Z}+1, 4\mathbb{Z}+2, 4\mathbb{Z}+3\}$ and $n, n+1$ s.t. $n \in 2\mathbb{Z}$. Now satisfying the requirements from our framework we have, $\sigma_y |g\rangle = i\sigma_x |g\rangle, \sigma_z |g\rangle = |g\rangle$,

$$\langle x|UV|\alpha_\Delta, g\rangle = \sum_{m=4\mathbb{Z}, n=2\mathbb{Z}}^{\infty} \frac{(\lambda/\Delta)^{m+n}}{2^n n! m!} y^m \left[H_n(y) - \frac{i(\lambda/\Delta)\sigma_x}{2(n+1)} H_{n+1}(y) \right] \alpha_\Delta(x) |g\rangle \quad (C22)$$

$$+ \sum_{m=4\mathbb{Z}+1, n=2\mathbb{Z}}^{\infty} \frac{(\lambda/\Delta)^{m+n}}{2^n n! m!} y^m \left[iH_n(y)\sigma_x + \frac{(\lambda/\Delta)}{2(n+1)} H_{n+1}(y) \right] \alpha_\Delta(x) |g\rangle \quad (C23)$$

$$+ \sum_{m=4\mathbb{Z}+2, n=2\mathbb{Z}}^{\infty} \frac{(\lambda/\Delta)^{m+n}}{2^n n! m!} y^m \left[-H_n(y) + \frac{i(\lambda/\Delta)\sigma_x}{2(n+1)} H_{n+1}(y) \right] \alpha_\Delta(x) |g\rangle \quad (C24)$$

$$+ \sum_{m=4\mathbb{Z}+3, n=2\mathbb{Z}}^{\infty} \frac{(\lambda/\Delta)^{m+n}}{2^n n! m!} y^m \left[-iH_n(y)\sigma_x - \frac{(\lambda/\Delta)}{2(n+1)} H_{n+1}(y) \right] \alpha_\Delta(x) |g\rangle \quad (C25)$$

It is clear from the above expression that the $m+n \in 2\mathbb{Z}+1$ terms reduce the probability of success, taking $|g\rangle \rightarrow |e\rangle$. Thus, we can rewrite the above expression as,

$$\langle x|UV|\alpha_\Delta, g\rangle = \sum_{m+n \in 2\mathbb{Z}} (-1)^{\nu_m} c_{n,m} y^m H_n(y) e^{-y^2} |g\rangle + i \sum_{m+n \in 2\mathbb{Z}+1} (-1)^{\mu_m} c_{n,m} y^m H_n(y) e^{-y^2} |e\rangle, \quad (C26)$$

$$\text{where } c_{n,m} = \frac{(\lambda/\Delta)^{m+n}}{2^n n! m!}, \quad \nu_m : \quad \text{mod } (m, 4) \geq 2, \quad \mu_m : \quad \text{mod } (m, 4) == (0 \text{ or } 3). \quad (C27)$$

Here, μ_m, ν_m are conditional variables that are equal to 1 if the condition representing them is true else they are 0. All terms yield a well-bounded Gaussian integral with decreasing contribution to the success probability for increasing $m+n$, assuming $\lambda/\Delta \ll 1$. Thus, the total error of the process is also bounded and we can focus on the leading order term. We will extract terms up to $\mathcal{O}(\lambda^6/\Delta^6)$ as these will contribute to the leading order terms in the failure probability, as shown below,

$$\langle x|UV|\alpha_\Delta, g\rangle = e^{-y^2} [c_{00} H_0(y) |g\rangle - i c_{10} H_1(y) |e\rangle + c_{20} H_2(y) |g\rangle - i c_{30} H_3(y) |e\rangle + c_{40} H_4(y) |g\rangle - i c_{50} H_5(y) |e\rangle + c_{60} H_6(y) |g\rangle - i c_{70} H_7(y) |e\rangle + c_{80} H_8(y) |g\rangle] \quad (C28)$$

$$+ i c_{01} y H_0(y) |e\rangle + c_{11} y H_1(y) |g\rangle + i c_{21} y H_2(y) |e\rangle + c_{31} y H_3(y) |g\rangle + i c_{41} y H_4(y) |e\rangle + c_{51} y H_5(y) |g\rangle + i c_{61} y H_6(y) |e\rangle + c_{71} y H_7(y) |g\rangle \quad (C29)$$

$$- c_{02} y^2 H_0(y) |g\rangle + i c_{12} y^2 H_1(y) |e\rangle - c_{22} y^2 H_2(y) |g\rangle + i c_{32} y^2 H_3(y) |e\rangle - c_{42} y^2 H_4(y) |g\rangle + i c_{52} y^2 H_5(y) |e\rangle - c_{62} y^2 H_6(y) |g\rangle - i c_{03} y^3 H_0(y) |e\rangle - c_{13} y^3 H_1(y) |g\rangle - i c_{23} y^3 H_2(y) |e\rangle - c_{33} y^3 H_3(y) |g\rangle - i c_{43} y^3 H_4(y) |e\rangle \quad (C30)$$

$$-c_{53}y^3H_5(y)|g\rangle \quad (C31)$$

$$+c_{04}y^4H_0(y)|g\rangle -ic_{14}y^4H_1(y)|e\rangle +c_{24}y^4H_2(y)|g\rangle -ic_{34}y^4H_3(y)|e\rangle +c_{44}y^4H_4(y)|g\rangle \quad (C32)$$

$$+ic_{05}y^5H_0(y)|e\rangle +c_{15}y^5H_1(y)|g\rangle +ic_{25}y^5H_2(y)|e\rangle +c_{35}y^5H_3(y)|g\rangle \quad (C33)$$

$$-c_{06}y^6H_0(y)|g\rangle +ic_{16}y^6H_1(y)|e\rangle -c_{26}y^6H_2(y)|g\rangle \quad (C34)$$

$$-ic_{07}y^7H_0(y)|e\rangle -c_{17}y^7H_1(y)|g\rangle \quad (C35)$$

$$+c_{08}y^8H_0(y)|g\rangle]+\mathcal{O}(\lambda^9/\Delta^9) \quad (C36)$$

As suggested earlier, the first order terms in y exactly cancel since $ic_{10}H_1(y) = ic_{01}yH_0(y)$, and hence there is no effect on the final state from terms that are degree 1 in λ/Δ . Defining $\chi = \lambda/\Delta$, we have

$$\langle x|UV|\alpha_\Delta,g\rangle = \mathcal{N} \left\{ 1 + \chi^2 \left[y^2 - \frac{1}{4} \right] + \chi^4 \left[-\frac{y^4}{6} - \frac{y^2}{4} + \frac{1}{32} \right] + \chi^6 \left[-\frac{y^6}{90} + \frac{y^4}{24} + \frac{y^2}{32} - \frac{1}{384} \right] + \chi^8 \left[\frac{y^8}{2520} + \frac{y^6}{360} - \frac{y^4}{192} - \frac{y^2}{384} + \frac{1}{6144} \right] + \mathcal{O}(\chi^{10}) \right\} e^{-y^2} |g\rangle \quad (C37)$$

$$+ \mathcal{N} \left\{ i\chi^3 \left[\frac{2y^3}{3} \right] - i\chi^5 \left[\frac{y^3}{6} \right] + \mathcal{O}(\chi^7) \right\} e^{-y^2} |e\rangle \quad (C38)$$

Here, \mathcal{N} is the normalization constant which will be computed using $\langle \psi | \psi \rangle = 1$.

a. *Figures of Merit*

• *Success Probability*.

The success probability of rotating the qubit by I is only affected by $\mathcal{O}(\chi^3)$ and $\mathcal{O}(\chi^5)$ terms in the expansion of UV . Using the variable transformation $dx = \Delta dy$ and $\int_{-\infty}^{\infty} dy y^{2n} e^{-2y^2} = \sqrt{\frac{\pi}{2}} \frac{(2n-1)!!}{(4)^n}$ effect of these terms can be approximated as ,

$$P_g = \int_{-\infty}^{\infty} dx |\langle x, g | UV | \alpha, g \rangle_{\Delta}|^2 \quad (C39)$$

$$= \mathcal{N}^2 \Delta \int_{-\infty}^{\infty} dy e^{-2y^2} \left(1 + \chi^2 \left[2y^2 - \frac{1}{2} \right] + \chi^4 \left[\frac{2y^4}{3} - y^2 + \frac{1}{8} \right] + \chi^6 \left[-\frac{16}{45}y^6 - \frac{y^4}{3} + \frac{y^2}{4} - \frac{1}{48} \right] + \chi^8 \left[-\frac{3}{140}y^8 + \frac{17}{180}y^6 + \frac{y^4}{32} - \frac{5}{192}y^2 + \frac{5}{3072} \right] + \mathcal{O}(\chi^{10}) \right) \quad (C40)$$

$$= \mathcal{N}^2 \Delta \sqrt{\frac{\pi}{2}} (1 - 5\chi^6/48 + 11\chi^8/768 + \mathcal{O}(\chi^{10})) \quad (C41)$$

where

$$1/\mathcal{N}^2 = P_g + \Delta \int_{-\infty}^{\infty} dy e^{-2y^2} \left(\frac{4}{9}\chi^6 y^6 - \frac{2}{9}\chi^8 y^6 + \mathcal{O}(\chi^{10}) \right) \quad (C42)$$

$$= \sqrt{\frac{\pi}{2}} \Delta (1 - 29\chi^8/768 + \mathcal{O}(\chi^{10})) \quad (C43)$$

Thus, we get the probability of making an incorrect rotation as the probability of ending in qubit state $|e\rangle$ at the end of UV ,

$$P_e = \frac{5\chi^6/48 - 5\chi^8/96}{1 - 29\chi^8/768} + \mathcal{O}(\chi^{10}) \quad (C44)$$

where $\chi = \frac{\pi\Delta}{4|\alpha|} = \frac{\theta\Delta}{|\alpha|}$, and 2θ is the angle by which the qubit is rotated on the Bloch sphere. Hence, the probability of making an erroneous rotation has been proved to scale as $\sim \chi^6/10$. In contrast to the traditional schemes for composite pulses with classical variables, the error terms for quantum control variables scale with Δ/α instead of error $e = |x - \alpha|$ due to the Gaussian-weighted distribution of error over this range. For a given state, the variables Δ, α are fixed, and hence the success probability is also fixed. As $\alpha \rightarrow 0$, the curve deviates since higher order terms start come into play. This is not an issue since neither the scheme nor the small χ approximation are well-suited for $\alpha \rightarrow 0$ limit.

• *Post-selected Fidelity*. Next, we quantify the back action on the oscillator state conditioned on the qubit being in the desired state using $\mathcal{F}_{\text{success}}$. The final oscillator state conditioned upon the qubit being in $|g\rangle$ state $\psi_{\text{final}}(x)$ is given by the Eq. (C37). This yields the fidelity upon success that is the fidelity of the oscillator state when the ancilla is in $|g\rangle$.

$$F_{\text{ps}} = |\langle \alpha | \psi_{\Delta} \rangle|^2 : \psi_{\Delta}(x) = \mathcal{N}_g \langle x, g | UV | \alpha, g \rangle_{\Delta}, \quad (C45)$$

where $1/\mathcal{N}_g^2$ is obtained from dividing Eq. (C41) by $\mathcal{N}^2 = \Delta \sqrt{\frac{\pi}{2}} (1 - 5\chi^6/48 + 11\chi^8/768) + \mathcal{O}(\chi^{10})$

$$|\langle \alpha_{\Delta} | \psi_{\text{final}} \rangle|^2 = \sqrt{\frac{2}{\pi}} \mathcal{N}_g^2 \Delta \left| \int_{-\infty}^{\infty} dy e^{-2y^2} \left\{ 1 + \chi^2 \left[y^2 - \frac{1}{4} \right] + \chi^4 \left[-\frac{y^4}{6} - \frac{y^2}{4} + \frac{1}{32} \right] + \chi^6 \left[-\frac{y^6}{90} + \frac{y^4}{24} + \frac{y^2}{32} - \frac{1}{384} \right] \right\} \right| \quad (C46)$$

$$\begin{aligned}
& + \chi^8 \left[\frac{y^8}{2520} + \frac{y^6}{360} - \frac{y^4}{192} - \frac{y^2}{384} + \frac{1}{6144} \right] \\
& + \mathcal{O}(\chi^{10}) \Big\} \\
& = \frac{|1 - \chi^4/16 + \chi^6/48 - \chi^8/1536|^2}{1 - 5\chi^6/48 + 11\chi^8/768} \\
& + \mathcal{O}(\chi^{10}) \quad (C46) \\
\therefore 1 - F_{\text{ps}} & = \frac{\chi^4/8 - \chi^6/8 + \chi^8/64}{1 - 5\chi^6/48 + 11\chi^8/768} + \mathcal{O}(\chi^{10}) \quad (C47)
\end{aligned}$$

- *Hybrid Fidelity.* If the failure probability is low enough, we can afford to ignore the outcome of the qubit and let it reset. In this case, the fidelity of the oscillator state is bounded as follows,

$$1 - F_{\text{H}} = |\langle \alpha, g | U V | \alpha, g \rangle_{\Delta}|^2 \quad (C48)$$

$$= \chi^4/8 - \chi^6/48 + \mathcal{O}(\chi^8) \quad (C49)$$

$$\begin{aligned}
|\psi_{\text{BB1}}\rangle &= R_{\phi_1} \left(-\frac{\pi}{|\alpha|} \hat{x} \right) R_{3\phi_1} \left(-\frac{2\pi}{|\alpha|} \hat{x} \right) R_{\phi_1} \left(-\frac{\pi}{|\alpha|} \hat{x} \right) R_0 \left(-\frac{2\theta}{|\alpha|} (\hat{x} - \alpha) \right) |\psi\rangle \otimes |g\rangle \quad (C50) \\
\langle x | \psi_{\text{BB1}} \rangle &= \left[\cos \frac{\pi\alpha}{2|\alpha|} I + i \sin \frac{\pi\alpha}{2|\alpha|} \sigma_{\phi_1} - \frac{\pi}{2\theta} \chi y \left(\sin \frac{\pi\alpha}{2|\alpha|} I - i \cos \frac{\pi\alpha}{2|\alpha|} \sigma_{\phi_1} \right) \right] \\
&\times \left[\cos \frac{\pi\alpha}{|\alpha|} I + i \sin \frac{\pi\alpha}{|\alpha|} \sigma_{3\phi_1} - \frac{\pi}{\theta} \chi y \left(\sin \frac{\pi\alpha}{|\alpha|} I - i \cos \frac{\pi\alpha}{|\alpha|} \sigma_{3\phi_1} \right) \right] \\
&\times \left[\cos \frac{\pi\alpha}{2|\alpha|} I + i \sin \frac{\pi\alpha}{2|\alpha|} \sigma_{\phi_1} - \frac{\pi}{2\theta} \chi y \left(\sin \frac{\pi\alpha}{2|\alpha|} I - i \cos \frac{\pi\alpha}{2|\alpha|} \sigma_{\phi_1} \right) \right] \\
&\times \left[\cos \frac{\theta\alpha}{|\alpha|} I + i \sin \frac{\theta\alpha}{|\alpha|} \sigma_x - \chi y \left(\sin \frac{\theta\alpha}{|\alpha|} I - i \cos \frac{\theta\alpha}{|\alpha|} \sigma_x \right) \right] R_0 \left(2\theta \frac{\alpha}{|\alpha|} \right) e^{-y^2} |g\rangle + \mathcal{O}(\chi^2). \quad (C51)
\end{aligned}$$

Simplifying this, using $\cos(\pi\alpha/|\alpha|) = -1$, $\cos(\pi\alpha/2|\alpha|) = 0$, $\sin(\pi\alpha/|\alpha|) = 0$, $\sin(\pi\alpha/2|\alpha|) = \alpha/|\alpha|$, we have

$$\langle x | \psi_{\text{BB1}} \rangle = \mathcal{N} \sum_{m=0}^{\infty} \frac{\sigma_{\phi_1}}{m!} \left[i \frac{\pi}{2\theta} \chi y \sigma_{\phi_1} \right]^m \sum_{n=0}^{\infty} \frac{1}{n!} \left[i \frac{\pi}{\theta} \chi y \sigma_{3\phi_1} \right]^n \sum_{o=0}^{\infty} \frac{\sigma_{\phi_1}}{o!} \left[i \frac{\pi}{2\theta} \chi y \sigma_{\phi_1} \right]^o \sum_{p=0}^{\infty} \frac{1}{p!} \left[i \chi y \sigma_x \right]^p e^{-y^2} |g\rangle. \quad (C52)$$

Here \mathcal{N} is the normalization constant. This expression simplifies as follows for terms up to third order, $\langle x | \psi_{\text{BB1}} \rangle =$

$$\begin{aligned}
& \mathcal{N} \left\{ 1 + i \chi y \left[\frac{\pi}{\theta} (\sigma_{\phi_1} + \sigma_{\phi_1} \sigma_{3\phi_1} \sigma_{\phi_1}) + \sigma_x \right] - \chi^2 y^2 \left[\frac{1}{2} + \frac{\pi^2}{\theta^2} + \frac{\pi^2}{2\theta^2} (\sigma_{\phi_1} \sigma_{3\phi_1} + \sigma_{3\phi_1} \sigma_{\phi_1}) + \frac{\pi}{\theta} (\sigma_{\phi_1} \sigma_x + \sigma_{\phi_1} \sigma_{3\phi_1} \sigma_{\phi_1} \sigma_x) \right] \right. \\
& - i \chi^3 y^3 \left[\frac{2\pi^3}{3\theta^3} + \frac{\pi}{2\theta} (\sigma_{\phi_1} + \sigma_{\phi_1} \sigma_{3\phi_1} \sigma_{\phi_1}) - \frac{\pi^3}{4\theta^3} \sigma_{\phi_1} \sigma_{3\phi_1} \sigma_{\phi_1} + \left(\frac{\pi^2}{\theta^2} + \frac{1}{6} \right) \sigma_x + \frac{\pi^3}{4\theta^3} \sigma_{3\phi_1} + \frac{\pi^2}{2\theta^2} (\sigma_{2\phi_1} + \sigma_{-2\phi_1}) \right] \\
& \left. + \mathcal{O}(\chi^4) \right\} e^{-y^2} |g\rangle \quad (C53)
\end{aligned}$$

$$\begin{aligned}
& = \mathcal{N} \left\{ 1 + i \chi y \left[\frac{\pi}{\theta} (\sigma_{\phi_1} + \sigma_{-\phi_1}) + \sigma_x \right] - \chi^2 y^2 \left[\frac{1}{2} + \frac{\pi^2}{\theta^2} + \frac{\pi^2}{2\theta^2} (e^{i2\phi_1\sigma_z} + e^{-i2\phi_1\sigma_z}) + \frac{\pi}{\theta} (e^{i\phi_1\sigma_z} + e^{-i\phi_1\sigma_z}) \right] \right. \\
& - i \chi^3 y^3 \left[\left(\frac{2\pi^3}{3\theta^3} + \frac{\pi}{2\theta} \right) (\sigma_{\phi_1} + \sigma_{-\phi_1}) - \frac{\pi^3}{4\theta^3} \sigma_{-\phi_1} + \left(\frac{\pi^2}{\theta^2} + \frac{1}{6} \right) \sigma_x + \frac{\pi^3}{4\theta^3} \sigma_{3\phi_1} + \frac{\pi^2}{2\theta^2} (\sigma_{2\phi_1} + \sigma_{-2\phi_1}) \right] + \mathcal{O}(\chi^4) \left. \right\} e^{-y^2} |g\rangle \quad (C54)
\end{aligned}$$

$$= \mathcal{N} \left\{ 1 + i \chi y \left[\frac{2\pi}{\theta} \cos \phi_1 \sigma_x + \sigma_x \right] - \chi^2 y^2 \left[\frac{1}{2} + \frac{\pi^2}{\theta^2} + \frac{\pi^2}{\theta^2} \cos 2\phi_1 + \frac{2\pi}{\theta} \cos \phi_1 \right] - i \chi^3 y^3 \left[\left(\frac{4\pi^3}{3\theta^3} + \frac{\pi}{\theta} \right) \cos \phi_1 \sigma_x \right. \right. \quad (C55)$$

Thus we see that the post-selected infidelity and reset infidelity both scale as $\chi^4/8$ for $\chi \ll 1$.

4. Univariate sequence: BB1(2θ)

We perform error analysis for the composite pulse sequence using quantum variables adapted from the well-known BB1(2θ) sequence [1]. Here, the fidelity needs to be computed for the Gaussian-weighted error terms obtained by Taylor expanding Eq. (11) when applied on the state $|\psi\rangle \otimes |g\rangle$ where $\langle x | \psi \rangle = e^{-\frac{(x-\alpha)^2}{\Delta^2}}$. We will continue to use the pre-defined shorthand notations $y\Delta = x - \alpha$, $\chi = \theta\Delta/|\alpha|$ from the main text. Note that, we have used the Taylor expansion $f(a + \varepsilon) = \sum_{n=0}^{\infty} \frac{\varepsilon^n}{n!} f^n(a)$, where $f^n(a)$ is the n^{th} derivative of the rotation $f(a) = \cos aI + i \sin a \sigma_{\phi}$. We want Eq. (C51) to be equivalent to identity upto $\mathcal{O}(\chi^k)$ where $k \geq 2$ determines the order of error cancellation.

$$-\frac{\pi^3}{4\theta^3}\sigma_{-\phi_1} + \left(\frac{\pi^2}{\theta^2} + \frac{1}{6}\right)\sigma_x + \frac{\pi^3}{4\theta^3}\sigma_{3\phi_1} + \frac{\pi^2}{\theta^2}\cos 2\phi_1\Big] + \mathcal{O}(\chi^4)\Big\} e^{-y^2} |g\rangle \quad (\text{C55})$$

For simplification we have used $\sigma_\phi = e^{-i\phi\sigma_z}\sigma_x$ to deduce that $\sigma_{\phi_1}\sigma_{3\phi_1}\sigma_{\phi_1} = \sigma_{-\phi_1}$. We observe that both first- and second-order terms cancel out with the choice of $\phi = \pm \cos^{-1}(-\theta/2\pi)$ and using $\cos 2\phi = 2\cos^2\phi - 1$.

$$\therefore \langle x|\psi_{\text{BB1}}\rangle = \mathcal{N}\left\{1 - i\chi^3 y^3 \left[\left(-\frac{\pi^2}{6\theta^2} + \frac{1}{24}\right)\sigma_x + \frac{\pi^3}{4\theta^3}(\sin 3\phi_1 + \sin \phi_1)\sigma_y\right] + \mathcal{O}(\chi^4)\right\} e^{-y^2} |g\rangle \quad (\text{C56})$$

$$= \mathcal{N}\left\{\left[1 + \mathcal{O}(\chi^4)\right]e^{-y^2} |g\rangle + \left[-i\chi^3 y^3 \left(-\frac{\pi^2}{6\theta^2} + \frac{1}{24} + i\frac{\pi^3}{2\theta^3}\cos \phi_1 \sin 2\phi_1\right) + \mathcal{O}(\chi^5)\right]e^{-y^2} |e\rangle\right\} \quad (\text{C57})$$

$$= \mathcal{N}\left\{\left[1 + \mathcal{O}(\chi^4)\right]e^{-y^2} |g\rangle + \left[-i\chi^3 y^3 \left(-\frac{\pi^2}{6\theta^2} + \frac{1}{24} + i\frac{\pi}{4\theta}\sqrt{1 - \frac{\theta^2}{4\pi^2}} + \mathcal{O}(\chi^5)\right) e^{-y^2} |e\rangle\right\} \quad (\text{C58})$$

For $\theta = \pi/2$, the failure probability of this error cancellation scheme is given by the probability of obtaining $|e\rangle$ in the outcome.

$$P_e = \int_{-\infty}^{\infty} dy \left| -\frac{\pi^2}{6\theta^2} + \frac{1}{24} + i\frac{\pi}{4\theta}\sqrt{1 - \frac{\theta^2}{4\pi^2}} \right|^2 \chi^6 y^6 e^{-2y^2} + \mathcal{O}(\chi^8) \quad (\text{C59})$$

$$= \left| -\frac{\pi^2}{6\theta^2} + \frac{1}{24} + i\frac{\pi}{4\theta}\sqrt{1 - \frac{\theta^2}{4\pi^2}} \right|^2 \left(\frac{15}{64}\right) \chi^6 + \mathcal{O}(\chi^8) \quad (\text{C60})$$

For $\theta = \pi/2$ i.e. BB1(180), we get,

$$P_e = \left| \frac{5}{8} - i\frac{\sqrt{15}}{8} \right|^2 \left(\frac{15}{64}\right) \chi^6 + \mathcal{O}(\chi^8) \\ = 0.15\chi^6 + \mathcal{O}(\chi^8) \quad (\text{C61})$$

For $\theta = \pi/4$ i.e. BB1(90), we get,

$$P_e = \left| \frac{63}{24} - i\frac{\sqrt{63}}{8} \right|^2 \left(\frac{15}{64}\right) \chi^6 + \mathcal{O}(\chi^8) \\ = 1.85\chi^6 + \mathcal{O}(\chi^8) \quad (\text{C62})$$

We see that the failure probability is worse for BB1(2 θ) compared to GCR(2 θ) for 2 $\theta = 90^\circ$ whereas it is comparable for both when 2 $\theta = 180^\circ$. For our purpose, we will primarily be using BB1(90).

Finally, the reset fidelity in both cases is also important when using our formalism. Note that in both cases, BB1 and GCR, the second order term disappears in the final integral. The reset fidelity expressions in Eqs. C63-C68 have been computed using the coefficient of χ^4, χ^6 in the Taylor expansion using Mathematica. For 2 $\theta = 90^\circ$, we have, the additional terms in the Taylor expansion are as follows,

$$\langle x, g|\psi_{\text{BB1}}\rangle = 1 - i\frac{\sqrt{15}}{8}\chi^4 y^4 - \frac{7}{9}\chi^6 y^6 + i\frac{5\sqrt{5}}{8\sqrt{3}}\chi^6 y^6 + \mathcal{O}(\chi^6) \quad (\text{C63})$$

This yields the hybrid state fidelity to be equal to for 2 $\theta = 180^\circ$,

$$F_H = \left| \int_{-\infty}^{\infty} dy \left[1 - i\frac{\sqrt{15}}{8}\chi^4 y^4 - \frac{7}{9}\chi^6 y^6 \right. \right. \\ \left. \left. + i\frac{5\sqrt{5}}{8\sqrt{3}}\chi^6 y^6 + \mathcal{O}(\chi^8) \right] e^{-2y^2} \right|^2 \quad (\text{C64})$$

$$= \left| 1 - i\frac{\sqrt{15}}{8}\left(\frac{3}{16}\right)\chi^4 - \frac{7}{9}\left(\frac{15}{64}\right)\chi^6 \right. \\ \left. + i\frac{5\sqrt{5}}{8\sqrt{3}}\left(\frac{15}{64}\right)\chi^6 + \mathcal{O}(\chi^8) \right|^2 \quad (\text{C65})$$

$$= 1 - \frac{105}{288}\chi^6 + \mathcal{O}(\chi^8) \quad (\text{C66})$$

$$1 - F_H = 0.37\chi^6 + \mathcal{O}(\chi^8), \quad (\text{C67})$$

Since the fourth-order term is purely imaginary there is no fourth-order term contributing to the infidelity of the state. Thus, in this case the infidelity scales as χ^6 . We can repeat this exercise for 2 $\theta = 90^\circ$, and find,

$$1 - F_H = 15.6\chi^6 + \mathcal{O}(\chi^6). \quad (\text{C68})$$

Hence, in this appendix, we have confirmed that the performance of GCR(2 θ) is on par with BB1(2 θ) in terms of success probability while yielding a lower fidelity, however, at a much lower circuit-depth, as claimed in Sec. III B. In Fig. 14, we plot the comparison of GCR(2 θ) for $\theta = \pi/2$ which can be contrasted with Fig. 2(a) for $\theta = \pi/4$.

5. Variations of GCR(θ): $\langle \hat{p} \rangle \neq 0, \langle \hat{x} \rangle \neq 0$ and $\Delta > 1$.

In Sec. III, we focused on the case of $\alpha \in \mathbb{R}$, however, our scheme is generalizable to arbitrary coherent states. For states in Eq. (4) where α is not real, i.e., the state is not located on the position axis of the oscillator phase space, or where $\Delta > 1$, i.e., a squeezed coherent state, GCR requires simple modifications as follows. For the latter, we simply choose $\hat{v}_1 = \hat{p}$ in Eq. (18). Let us

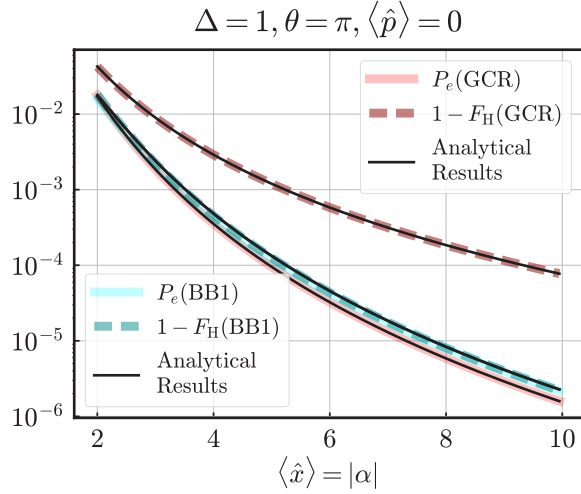


FIG. 14. Comparison of GCR(2θ) and BB1(2θ) schemes for $2\theta = \pi$. This scheme confirms our analytical understanding which shows that the failure probability for this case will be comparable for both the schemes. The figure can be contrasted against Fig. 2(a) where the two failure probabilities were off by an order of magnitude.

discuss the former case of $\langle \hat{p} \rangle \neq 0$ and $\langle \hat{x} \rangle \neq 0$. Up to a normalization constant and a phase factor,

$$\langle x | \alpha_\Delta, i\beta_\Delta \rangle = e^{i\beta\hat{x}} e^{-\frac{(x-\alpha)^2}{\Delta^2}} \quad (\text{C69})$$

Let us see how we can modify GCR(θ) to rotate the qubit using this state. We have,

$$\text{GCR}(\theta) |+\alpha_\Delta, i\beta_\Delta; g\rangle = \text{GCR}(\theta) e^{i\beta\hat{x}} |g, +\alpha_\Delta\rangle \quad (\text{C70})$$

$$= e^{i\beta\hat{x}} \text{GCR}(\theta) e^{-i\frac{\lambda}{2}\beta\sigma_y} |g, +\alpha_\Delta\rangle \quad (\text{C71})$$

$$= e^{i\beta\hat{x}} \text{GCR}(\theta) e^{-i\frac{\theta\Delta^2}{2|\alpha|}\beta\sigma_y} |g, +\alpha_\Delta\rangle \quad (\text{C72})$$

Therefore, for the correction to work in this case, we need to apply an initial rotation on the qubit equivalent to $e^{i\theta\Delta^2 \frac{\beta}{2|\alpha|}\sigma_y}$. In Fig. 2(b) we show the numerical results for this protocol as proof. This variation gives the generalization of GCR to coherent states located along arbitrary vectors in the phase space of a quantum oscillator.

Appendix D: Squeezing

Here, we look at the question of modifying δx of an oscillator state $\psi(x) = e^{-\frac{(x-\alpha)^2}{4\delta x^2}}$. Without loss of generality, we will use the vacuum state with $\alpha = 0, 4\delta x^2 = 1$. The action of squeezing this state along position is equivalent to,

$$S(\Delta) |\psi\rangle = \int_{-\infty}^{\infty} dp e^{-\frac{\delta^2 p^2}{4}} |p\rangle = \int_{-\infty}^{\infty} dx e^{-\frac{x^2}{4\delta x^2}} |x\rangle, \quad (\text{D1})$$

where $|p\rangle, |x\rangle$ are eigenstates of \hat{x}, \hat{p} and $4\delta x^2 > 1$.

a. *Squeezing in dB.* For comparison with [10] we use,

$$S(r) = 10 \log_{10}(e^{r/2}) S_p = S(\log 4\delta x^2) = S(\log 4\Delta^2) \quad (\text{D2})$$

$$S_x = S(\log 4/\Delta^2) \quad (\text{D3})$$

where r is the parameter used for the bosonic squeezing operation [8]. Here, $\delta x, \delta p$ are the uncertainties in position and momentum, respectively, as defined in App. A.

b. *Fisher Information.* Fisher information of a Gaussian state, such as, squeezed states is given by

$$F = 2 / (\langle \hat{x}^2 \rangle - \langle x \rangle^2) = 2/\delta x^2 \quad (\text{D4})$$

c. *Circuit-duration and circuit-depth.* We plot the squeezing curves with respect to circuit-duration, that is the time taken by the circuit instead of the gate count. It is because the error and speed of a conditional displacement gate depends on the length of the conditional displacement. This dependence is computed given access to the Hamiltonian $H_{\text{CD}} = \chi(\gamma_0 a^\dagger - \gamma_0^* a)$ where if $\frac{\chi}{2\pi} = 50$ kHz and $|\gamma_0| = 20$ it implies $T_{|\gamma_i|} = \frac{|\gamma_i|}{\chi|\gamma_0|}$. Note that, duration of the conditional displacements are lower bounded by $T_{|\gamma_i| < 0.024} = 48$ ns. This duration includes the necessary components for an echoed conditional displacement, an unconditional displacement $|\alpha_0|$ (24 ns) and a mid-circuit qubit rotation (24 ns). For details see Ref. [10].

d. *Sum of two Gaussian functions.* The sum of two Gaussian functions,

$$\mathcal{N}[e^{-\frac{(x-\alpha)^2}{\Delta^2}} + e^{-\frac{(x+\alpha)^2}{\Delta^2}}], \quad (\text{D5})$$

where $\mathcal{N} = (2/(\pi\Delta^2))^{1/4}/\sqrt{2(1+e^{-2\alpha^2/\Delta^2})}$. After each application of squeeze operator S , as described in Sec. IV A we create a superposition of Gaussian functions which resembles a wider (narrower) Gaussian function in position ($\mathcal{N}' e^{-x^2/\Delta'^2}$). We use the Python package `scipy.optimize()` to estimate the Δ corresponding to this output state. We can also directly use the function `variance()`, on the output state, in QuTiP [53]. Alternatively, there are other numerical methods such as Pade's approximation [72] which can be used here.

1. Squeezing with GCR

Our protocol outlined in Sec. IV A can be described as follows. Here we assume that vacuum is $\psi(x) = e^{-\frac{x-\beta}{\Delta^2}}$ such that $\Delta^2 = 1, \beta = 0$. After a $\text{CD}(\alpha, \sigma_x)$, we have,

$$\langle \sigma_z \rangle = \cos \theta = \frac{2e^{-(x-\alpha)^2/\Delta^2 - (x+\alpha)^2/\Delta^2}}{e^{-2(x-\alpha)^2/\Delta^2} + e^{-2(x+\alpha)^2/\Delta^2}} \quad (\text{D6})$$

$$= \frac{2}{e^{-4\alpha x/\Delta} + e^{4\alpha x/\Delta}} = \text{sech} 4\alpha x/\Delta^2 \quad (\text{D7})$$

$$\langle \sigma_y \rangle = \sin \theta \sin \phi = 0 \quad (\text{D8})$$

$$\langle \sigma_x \rangle = \sin \theta \cos \phi = 1 - \langle \sigma_z \rangle^2 = \tanh 4\alpha x / \Delta^2. \quad (\text{D9})$$

Now, if we maintain the slope to be small value then $\langle \sigma_x \rangle$ will be proportional to x for as long as the amplitude of $\psi(x)$ is significantly non-zero, say, $|x| \leq 2\delta x \leq \Delta$. Thus, for this range, applying a rotation $R_y(-4\alpha\hat{x}/\Delta^2)$, that is $e^{i\frac{2\alpha\hat{x}}{\Delta^2}\sigma_y}$ yields $\langle \sigma_x \rangle \sim 0$. This rotation basically takes care of the linear part and yields $\langle \sigma_x \rangle \rightarrow 0$ for the part where $\tanh \frac{4\alpha x}{\Delta^2}$ is linear in x . More precisely, the various expectation values take the following form after this corrective rotation,

$$\langle \sigma_z \rangle = \tanh \frac{4\alpha x}{\Delta^2} \sin \frac{4\alpha x}{\Delta^2} + \operatorname{sech} \frac{4\alpha x}{\Delta^2} \cos \frac{4\alpha x}{\Delta^2} \quad (\text{D10})$$

$$= 1 - \mathcal{O}(x^6) \quad (\text{D11})$$

$$\langle \sigma_y \rangle = 0 \quad (\text{D12})$$

$$\langle \sigma_x \rangle = \tanh \frac{4\alpha x}{\Delta^2} \cos \frac{4\alpha x}{\Delta^2} - \operatorname{sech} \frac{4\alpha x}{\Delta^2} \sin \frac{4\alpha x}{\Delta^2} \quad (\text{D13})$$

$$= \mathcal{O}(x^3) \quad (\text{D14})$$

The composite pulse sequence GCR(2 θ) described in App. III of the main text is exactly based on this principle since the $\frac{\theta}{|\alpha|}$ is small for large $|\alpha|$.

Choice of α : We need to cleverly choose α such that a linear slope is maintained throughout $|x| \leq 2\delta x \leq \Delta$. Since α decides the convergence of squeezing with each even cat step, it is important to make it as high as possible. However, we would also want the slope of $\langle \sigma_x \rangle$ against x ($4\alpha/\Delta^2$) to decrease accordingly with increase in Gaussian width Δ such that it is $\langle \sigma_x \rangle$ is linear range over which $\psi(x)$ has a significant amplitude. To be exact, the slope should be atleast

$$\frac{4|\alpha|}{\Delta^2} \ll \frac{1/\mathcal{N}}{\text{FWHM}} = \frac{(2/\pi\Delta^2)^{1/4}}{2\Delta\sqrt{\ln 2}} = \frac{0.53}{\Delta^{3/2}}, \quad (\text{D15})$$

$$|\alpha| \ll 0.13\Delta^{1/2} \quad (\text{D16})$$

where \mathcal{N} is the normalization constant and the maximum value $\psi(x)$ could achieve while FWHM is the full-width at half-maximum. Thus, we conclude that $|\alpha|_{k+1} \ll 0.13\Delta_k^{1/2}$ for \mathcal{S}_k to un-entangle efficiently. We can see that, as Δ_k increases, the upper bound on $|\alpha|_{k+1}$ decreases. Thus, in order to increase the fidelity these displacements need to be smaller with each step, which will decrease the rate of squeezing. We could make our process even faster if we go to the regime of $S_x \neq -S_p$ as Ref. [44]. We fit the $\langle \sigma_y \rangle$ for using \mathcal{S}_k with $|\alpha|_0 = 0.13$ and $|\alpha_k| = 0.06\Delta^2$ for $k \neq 0$. The curve fit yields the best correction for the approximately linear slope $\langle \sigma_y \rangle$. This method has been used to obtain Figs. 4(c,d).

2. Comparison with Previous Work

In [44] authors show that if large conditional displacements are allowed then by making a large odd cat one and then displacing towards vacuum while taking care of the

Gaussian envelope makes this process much faster. This happens because for large cat states the qubit can be easily unentangled and then by travelling towards origin one establishes the flattening in $\psi(x)$ while squeezing $\psi(p)$. This is the regime of non-commuting variables since the two conditional displacements clearly do not commute in this case [44]. Hence, this example also shines light on the power of non-abelian QSP framework. However, due to the lack of a well-known analytical scheme for non-abelian QSP this work used numerical optimizations for un-entanglement of the qubit and the oscillator. With this protocol, in the $L = 0.45$ (see Ref. [44]) limit, for a circuit duration of $4.7\mu\text{s}$ this state-of-the-art protocol yielded an infidelity of ~ 0.009 for a squeezing of $S_p = 8.5$ dB and an anti-squeezing of $S_x = -9.9$ dB. Note that $S_x \neq -S_p$.

On the other hand, with our protocol we were able to achieve squeezing of 8.5dB and anti-squeezing of -8.40dB with $\sum_i |\alpha_i| \sim 5.7\mu\text{s}$ with an infidelity of ~ 0.003 . We found that for the faster protocol our circuit duration also matches parameters from Ref. [44] (our protocol still being different from Ref. [44]). Instead, if we decrease the rate of squeezing by say, decreasing $k = 1/4$ we get improved fidelity for a squeezing of 6 dB using the same number of steps and sum of conditional displacement amplitudes. This interplay of infidelity and circuit-depth is captured in Fig. 4(e).

In contrast to our versatile scheme, the protocol in Ref. [44] can only engineer the former case of shorter circuit-depth with worse fidelity due to the bad approximation of odd cat states with a Gaussian wave function. The issue with this strategy is that the authors start in the large cat regime and use numerical methods to move towards the centre (contrast this with our scheme where we start with vacuum and approach a broader vacuum by making small odd cats). The problem with this strategy is two-fold. At some point the un-entanglement for this scheme is going to be inefficient given the overlapping Gaussian wave functions. Secondly, the envelope which has a maxima at the origin also needs to be taken care of numerically. This numerical optimization is evidently inefficient if one looks at the final state which has a dip at the centre (not a feature of squeezed states). This strategy if starting with large cats was because used there was no analytical scheme prior to our work (like GCR) for un-entangling qubits from oscillators with such high precision for small cats.

Finally, our scheme is on par with numerically optimized schemes shown in Ref. [10]. This comparison has been shown in our companion paper, Ref. [8]. For completeness, we also show this below in Fig. 15.

3. Comparison with Trotterization

Let us look at a sequence of CDs similar to GCR. This sequence is given by the following sequence using

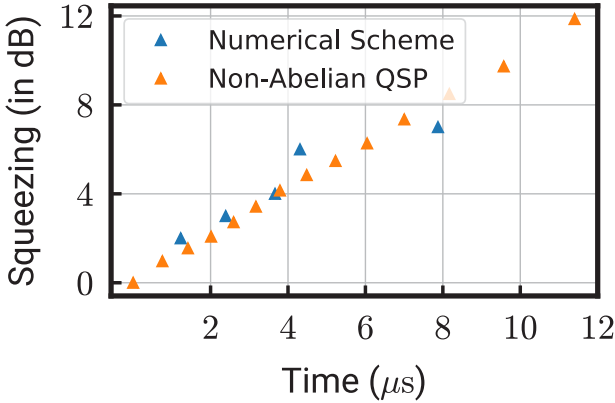


FIG. 15. Squeezing of vacuum achieved with fidelity $\mathcal{F} > 0.99$ using non-abelian QSP as discussed in Sec. IV A and the numerically optimal scheme in Ref. [10].

the BCH formula,

$$(e^{i\epsilon/Nx\sigma_x} e^{i\epsilon/Np\sigma_y} e^{-i\epsilon/Nx\sigma_x} e^{-i\epsilon/Np\sigma_y})^N |0, g\rangle \quad (D17)$$

$$= e^{i\epsilon^2(xp+px)\sigma_z} |0, g\rangle + \mathcal{O}(\epsilon^{4N}) \quad (D18)$$

$$= e^{i\epsilon^2(xp+px)} |0, g\rangle + \mathcal{O}(\epsilon^{4N}) \quad (D19)$$

For a squeezed state, this sequence can be changed to the following for $N=1$ WLOG,

$$e^{i(2\epsilon/\Delta^2)x\sigma_x} e^{i(2\epsilon p)\sigma_y} e^{-i(2\epsilon/(\Delta^2)x\sigma_x} e^{-i\epsilon p\sigma_y} |0, g\rangle \quad (D20)$$

$$= e^{i\epsilon^2/(\Delta^4)(xp+px)\sigma_z} |0, g\rangle \quad (D21)$$

$$= e^{i\epsilon^2/(\Delta^4)(xp+px)} |0, g\rangle, \quad (D22)$$

where Δ, ϵ for N^{th} patch of the sequence relies on Δ, ϵ from the N^{th} round. Here $\Delta > 1$, that is, we squeeze along the p quadrature for precision in p measurements.

Now, the unentanglement of the qubit depends on (1) the order of error cancellation in the BCH sequence (2) the magnitude of ϵ . Note that, increasing N and decreasing ϵ both decrease the acceleration of squeezing. The first because it effectively squeezes and anti-squeezes even if N is increased. The second one is obvious. Since with each step Δ increases, it is legitimate to increase ϵ carefully such that the overall un-entanglement is not affected. For this purpose we use $\epsilon = \delta p/2$ as long as we maintain that $\delta x = \Delta/2$ decreases by the same factor as the increase in δp . We use the factor of $1/2$ since we want to maintain that the small cat to be prepared is smaller than the width of the Gaussian (squeezed state) we started with. Note that, N should increase with ϵ in order to maintain a fixed fidelity. If we do not impose this then the fidelity decreases, however it does so gradually. The sequences using this idea prepare high-fidelity squeezing, however, this is achieved with large circuit duration. For example, for squeezing of 8.52dB , trotterization requires a circuit duration of $40.67\mu\text{s}$.

Appendix E: Cat State Preparation

Now, we compute fidelities of cat states against the output of the cat state preparation circuits in Fig. 5(a) for large cats and Fig. 4(a) for small cats. Cat states are described as superposition of two diametrically opposite conditions, for example, $|\text{Dead Cat}\rangle + |\text{Alive Cat}\rangle$ or $|0\rangle^{\otimes n} + |1\rangle^{\otimes n}$. In CV architecture, cat states are defined as superposition of states located diametrically opposite in phase space w.r.t the origin,

$$|C_{\pm\alpha}\rangle \approx \frac{(D(\alpha) \pm D(-\alpha))}{2} |0\rangle \approx \frac{|\alpha\rangle \pm |-\alpha\rangle}{\sqrt{2}} \quad (E1)$$

$$\psi(x) = \langle x|C_{\pm\alpha}\rangle = \left(\frac{2}{\pi}\right)^{1/4} (e^{-(x-\alpha)^2} \pm e^{-(x+\alpha)^2}) \sqrt{2} \quad (E2)$$

a. Non-deterministic preparation. Preparation of cat states $|C_{\pm\alpha}\rangle$ requires one to entangle the cavity state in vacuum ($|0\rangle$) and the qubit in $|g \pm ie\rangle$ state using $CD(\alpha, \sigma_z)$. We have flipped the Bloch sphere compared to the main text, for convenience in addressing both even and odd cat states together. Ignoring the normalization factors, we have,

$$|\psi 1\rangle = CD(\alpha, \sigma_x) |0\rangle |\pm\rangle \approx |\alpha\rangle |+i\rangle \pm |-\alpha\rangle |-i\rangle \quad (E3)$$

$$(E4)$$

Now, rotating the qubit state along σ_x axis by $\pm\pi/2$ will give us even and odd cats entangled with $|g\rangle$ and $|e\rangle$, respectively, if the qubit was initially in the state $|g + e\rangle$. Thus, again ignoring normalization constant we have,

$$|\psi 2\rangle = R_0(-\pi/2) |\psi 1\rangle = |\alpha\rangle |+i\rangle \pm |-\alpha\rangle |-i\rangle \quad (E5)$$

$$= (|\alpha\rangle \pm |-\alpha\rangle) |g\rangle - i(|\alpha\rangle \mp |-\alpha\rangle) |e\rangle \quad (E6)$$

On measurement of the qubit, the cavity will yield odd or even cats each with probability $\frac{1}{2}$.

b. Deterministic preparation. The above protocol is probabilistic with a success probability of $P_g = 0.5$. Ideally, we would like deterministic protocols which produce cat states with 100% probability in the absence of any error. An insightful way to look at this problem is shown in Fig. 5(a,b).

For a large cat peaked with $|\alpha|^2 > 4$, the qubit is unentangled from the cavity only when the spin of the qubit is polarized in a single direction globally, irrespective of the oscillator's position. This would require rotating the qubit entangled with cavity-state $|\pm\alpha\rangle$ by $\pm\frac{\pi}{2}$ about the σ_x axis or σ_y axis on the Bloch sphere. Note that, a momentum boost on this cavity-qubit state $e^{i\beta x\sigma_z}$ can be seen as a position dependent rotation by an angle $-2\beta\hat{x}$ about the σ_z axis. Using the identity $R_\phi(\theta) = R_{\pi/2-\phi}(-\pi/2)R_z(\theta)R_{\pi/2-\phi}(\pi/2)$, we have,

$$|\psi 4\rangle = R_{\pi/2}(-2\beta\hat{x}) |\psi 1\rangle \quad (E7)$$

$$= R_0(-\pi/2) R_z(-2\beta\hat{x}) R_0(\pi/2) |\psi 1\rangle \quad (E8)$$

$$= R_0(-\pi/2)R_z(-2\beta\hat{x})R_0(\pi/2)|\psi 1\rangle \quad (E9)$$

$$= R_0(-\pi/2)R_z(-2\beta\hat{x})|\psi 2\rangle \quad (E10)$$

$$= R_0(-\pi/2)e^{i\beta\hat{x}\sigma_z}|\psi 2\rangle \quad (E11)$$

$$= R_0(-\pi/2) \quad (E12)$$

The final rotation performs a global rotation about the σ_z axis and can be skipped. Let us call the state $|\psi 4\rangle$ minus this rotation as $|\psi 3\rangle$. In order to align the qubit state entangled with the cavity-state at peaks of the Gaussian, the momentum boost $e^{i\beta\alpha\sigma_z}$ should yield $R_z(\pi\alpha/(2|\alpha|))$ which implies $\beta = -\pi/4|\alpha|$. Cavity-qubit state $|\psi 4\rangle$ is shown in Fig. 5(a) where the initial qubit state is $|g\rangle$ such that the protocol prepares an even cat with $|\alpha|^2$. Notice that, $\langle\sigma_z\rangle = \cos\frac{\pi x}{2|\alpha|}$ and $\langle\sigma_x\rangle = \sin\frac{\pi x}{2|\alpha|}$ such that qubit polarization is $|+\rangle$ in the xz-plane at $x = \pm 3$ as intended.

1. Fidelity of deterministic preparation without QSP correction

Here, we rewrite the states $|\psi 1\rangle - |\psi 4\rangle$ in the position basis for the preparation of an even cat, ignoring normalization factors,

$$\langle x|\psi 1\rangle = e^{-(x-\alpha)^2}|g\rangle + e^{-(x+\alpha)^2}|e\rangle \quad (E13)$$

$$\langle x|\psi 2\rangle = e^{-(x-\alpha)^2}|-i\rangle - ie^{-(x+\alpha)^2}|+i\rangle \quad (E14)$$

$$\langle x|\psi 3\rangle = e^{-i\frac{\theta(x)}{2}\sigma_z}(e^{-(x-\alpha)^2}|-i\rangle - ie^{-(x+\alpha)^2}|+i\rangle) \quad (E15)$$

$$\langle x|\psi 4\rangle = e^{i\frac{\pi}{4}\sigma_x}e^{-i\frac{\theta(x)}{2}\sigma_z}(e^{-(x-\alpha)^2}|-i\rangle - ie^{-(x+\alpha)^2}|+i\rangle) \quad (E16)$$

where $\frac{\theta(x)}{2} = -\beta x$. We would have prepared an ideal cat if $\theta(x) = \frac{\pi}{2}\frac{|x|}{x}$ (for large cats where the overlap between the two Gaussian curves is insignificant),

$$|\psi_{\text{cat}}\rangle = e^{i\frac{\pi}{4}\sigma_x}(e^{-i\frac{\pi}{4}\sigma_z}e^{-(x-\alpha)^2}|-i\rangle - ie^{i\frac{\pi}{4}\sigma_z}e^{-(x+\alpha)^2}|+i\rangle) \quad (E17)$$

$$= e^{i\frac{\pi}{4}\sigma_x}(e^{-i\frac{\pi}{4}}e^{-(x-\alpha)^2}|+\rangle + e^{-i\frac{\pi}{4}}e^{-(x+\alpha)^2}|-\rangle) \quad (E18)$$

$$= e^{-(x-\alpha)^2}|+\rangle + e^{-(x+\alpha)^2}|-\rangle \quad (E19)$$

$$= |C_{+\alpha}\rangle|+\rangle \quad (E20)$$

Therefore, the overlap between $\langle x|\psi 4\rangle$ and $\langle x|\psi_{\text{cat}}\rangle$ can be computed approximately, neglecting the overlap between the two Gaussian curves, as

$$\approx \left(\frac{2}{\pi}\right)^{\frac{1}{2}}\frac{1}{2}\int_{-\infty}^{\infty}dx e^{-2(x-\alpha)^2}\langle+|e^{i\frac{\pi}{4}\sigma_x}e^{-i\frac{\theta(x)}{2}\sigma_z}|-i\rangle - ie^{-2(x+\alpha)^2}\langle+|e^{i\frac{\pi}{4}\sigma_x}e^{-i\frac{\theta(x)}{2}\sigma_z}|+i\rangle \quad (E21)$$

$$= \left(\frac{2}{\pi}\right)^{\frac{1}{2}}\frac{1}{2}\int_{-\infty}^{\infty}dx e^{i\frac{\pi}{4}}e^{-2(x-\alpha)^2}\langle+|e^{-i\frac{\theta(x)}{2}\sigma_z}|-i\rangle + e^{-i\frac{\pi}{4}}e^{-2(x+\alpha)^2}\langle+|e^{-i\frac{\theta(x)}{2}\sigma_z}|+i\rangle \quad (E22)$$

$$= \left(\frac{2}{\pi}\right)^{\frac{1}{2}}\frac{1}{2}\int_{-\infty}^{\infty}dx e^{-2(x-\alpha)^2}\cos\left(\frac{\pi}{4} - \frac{\theta(x)}{2}\right) + e^{-2(x+\alpha)^2}\cos\left(\frac{\pi}{4} + \frac{\theta(x)}{2}\right) \quad (E23)$$

$$= \left(\frac{2}{\pi}\right)^{\frac{1}{2}}\int_{-\infty}^{\infty}dx e^{-2(x-\alpha)^2}\left(1 - \frac{(\beta x - \pi/4)^2}{2}\right) \quad (E24)$$

$$= 1 - \frac{\pi^2}{32}\left(\frac{2}{\pi}\right)^{\frac{1}{2}}\int_{-\infty}^{\infty}dx e^{-2(x-\alpha)^2}\left(\frac{x}{\alpha} - 1\right)^2 \quad (E25)$$

$$= 1 - \frac{\pi^2}{32\alpha^2}\left(\frac{2}{\pi}\right)^{\frac{1}{2}}\int_{-\infty}^{\infty}dx e^{-2(x-\alpha)^2}(x - \alpha)^2 \quad (E26)$$

$$= 1 - \frac{\pi^2}{128\alpha^2} \quad (E27)$$

Eqs. E24 uses $\int_{-\infty}^{\infty}dx e^{-2(x-\alpha)^2}\cos(\beta(x - \alpha)) = \int_{-\infty}^{\infty}dx e^{-2(x+\alpha)^2}\cos(\beta(x + \alpha))$. Therefore, the fidelity for large cats is equal to,

$$\mathcal{F} \approx \left|1 - \frac{\pi^2}{128\alpha^2}\right|^2 \approx 1 - \frac{\pi^2}{64\alpha^2}. \quad (E28)$$

The cavity state $|\psi 4\rangle$ is not completely un-entangled from the qubit because the rotation angle varies continuously with x and has the correct values only at $x = \pm\alpha$. In an attempt to rotate the qubit in $|\psi 1\rangle$ by $\pm\frac{\pi}{2}$ at $x = \pm\alpha$ we have over- and under-rotations at $|x| \neq \alpha$. The fidelity can be increased for large cats if the magnitude of the position-dependent rotation could be fixed to $\frac{\pi}{2}$. Note that this error is same as the case of no-QSP correction for rotation gadgets computed in App. C2. Thus, this calculation indicates that the correction from GCR and BB1 will be similar to rotation gadgets and hence we will not repeat this calculation for preparation of cat states.

2. The Problem with Small Cat States

Cat states with a small number of photons do not obey the fidelity value given by Eq. (E28) mainly because $\langle\alpha| - \alpha\rangle \neq 0$. Given there is significant overlap for ‘small cats’, the qubit state polarization in $|\psi 1\rangle$ is no longer depicted by Fig. 5(b), that is, all $|+\rangle$ for $x > 0$ and all $|-\rangle$ for $x < 0$. Instead, the spin polarization is given by Fig. 4(b) in this case. We have given the expressions for these spin polarizations in App. D in reference to the squeezing gadgets. Here, we discuss the fidelity for the case of preparing odd and even cat states using this scheme.

For small cats, the fidelity of an odd cat will always be lower than the fidelity of an even cat with the same number of photons for smaller α . The reason for this difference in fidelity can be justified by analyzing the extra term that arises when $\langle\alpha| - \alpha\rangle \neq 0$.

a. *Small Cats with $\beta = -2\alpha$* The extra term in the overlap of $\langle x|\psi 4\rangle$ and $\langle x|\psi_{\text{cat}}\rangle$ for the analogue of Eq. (E22) when $\beta = -2\alpha$ is,

$$\sqrt{\frac{1}{2\pi}}\int_{-\infty}^{\infty}dx e^{-2(x^2+\alpha^2)}(\langle+|e^{i\frac{\pi}{4}\sigma_x}e^{-i\beta x\sigma_z}|+i\rangle$$

$$-i \langle +| e^{i\frac{\pi}{4}\sigma_x} e^{-i\beta x\sigma_z} | -i \rangle \quad (\text{E29})$$

$$\begin{aligned} &= \frac{e^{-2\alpha^2}}{\sqrt{2\pi}} \int_{-\infty}^{\infty} dx e^{-2x^2} \left(\cos\left(\frac{\pi}{4} - \frac{\theta(x)}{2}\right) \right. \\ &\quad \left. \pm \cos\left(\frac{\pi}{4} + \frac{\theta(x)}{2}\right) \right) \quad (\text{E30}) \end{aligned}$$

This correction is subtracted from the overlap of odd cats while it is added in the case of even cats. Now, computing the integral,

$$\begin{aligned} &\frac{e^{-2\alpha^2}}{\sqrt{2\pi}} \int_{-\infty}^{\infty} dx e^{-2x^2} \cos\left(\frac{\pi}{4} - \frac{\theta(x)}{2}\right) \\ &= \frac{e^{-2\alpha^2}}{\sqrt{2\pi}} \int_{-\infty}^{\infty} dx e^{-2x^2} \left(1 - \frac{(\beta x - \pi/4)^2}{2} \right) \quad (\text{E31}) \end{aligned}$$

$$\begin{aligned} &= \frac{e^{-2\alpha^2}}{2} - \frac{e^{-2\alpha^2}}{\sqrt{2\pi}} \frac{\beta^2}{2} \int_{-\infty}^{\infty} dx e^{-2x^2} (x^2 + \frac{\pi^2}{16\beta^2}) \\ &\quad (\text{E32}) \end{aligned}$$

$$= \frac{e^{-2\alpha^2}}{2} \left(1 - \frac{\alpha^2}{2} - \frac{\pi^2}{32} \right). \quad (\text{E33})$$

(E34)

Since $\frac{e^{-2\alpha^2}}{\sqrt{2\pi}} \int_{-\infty}^{\infty} dx e^{-2x^2} \cos\left(\frac{\pi}{4} - \frac{\theta(x)}{2}\right) = \frac{e^{-2\alpha^2}}{\sqrt{2\pi}} \int_{-\infty}^{\infty} dx e^{-2x^2} \cos\left(\frac{\pi}{4} + \frac{\theta(x)}{2}\right)$, and the normalization constant \mathcal{N} of the cat state including the overlap $\langle \alpha | -\alpha \rangle$ is given by,

$$\mathcal{N} = \left(\frac{1}{2\pi} \right)^{\frac{1}{4}} \frac{1}{\sqrt{1 + e^{-2\alpha^2}}}, \quad (\text{E35})$$

instead of just $\left(\frac{1}{2\pi} \right)^{\frac{1}{4}}$. Therefore the fidelity for even cats is,

$$\begin{aligned} \mathcal{F}_{\text{even}} &\approx \left| \frac{1}{\sqrt{1 + e^{-2\alpha^2}}} \left(1 - \frac{\alpha^2}{2} - 2\alpha^4 + \frac{\pi\alpha^2}{2} - \frac{\pi^2}{32} \right) \right. \\ &\quad \left. + \frac{e^{-2\alpha^2}}{\sqrt{1 + e^{-2\alpha^2}}} \left(1 - \frac{\alpha^2}{2} - \frac{\pi^2}{32} \right) \right|^2 \quad (\text{E36}) \end{aligned}$$

while for odd cats it is,

$$\begin{aligned} \mathcal{F}_{\text{odd}} &\approx \left| \frac{1}{\sqrt{1 + e^{-2\alpha^2}}} \left(1 - \frac{\alpha^2}{2} - 2\alpha^4 + \frac{\pi\alpha^2}{2} + \frac{\pi^2}{32} \right) \right. \\ &\quad \left. - \frac{e^{-2\alpha^2}}{\sqrt{1 + e^{-2\alpha^2}}} \left(1 - \frac{\alpha^2}{2} - \frac{\pi^2}{32} \right) \right|^2. \quad (\text{E37}) \end{aligned}$$

Here, the first addend represents the overlap when $\beta = -2\alpha x$ while the second addend is the correction due to the overlap. Thus, it is clear that the fidelity for odd cats is lower than even cats, and the difference becomes exponentially significant as α decreases.

Appendix F: GKP Logical Pauli States

Here, we derive the numerical circuit presented in Sec. IV C. From Eqs. 64 and 65, it is clear that we need

superposition of the finite energy basis states $|\alpha\rangle_{\Delta}$ where $\alpha = m\sqrt{\pi}$, $m \in 2\mathbb{Z}$ or $m \in 2\mathbb{Z} + 1$. This is indeed satisfied by the repeated cat state preparations. This circuit, however, prepares a state that is different from the GKP state. The Eqs. 64 and 65 have specific coefficients for each finite-energy basis state $|\alpha\rangle_{\Delta}$. In this appendix, we compare the coefficients of the final state with the desired GKP state to show the relationship between fidelity (F) and circuit depth (N) using only cat-state-transfer circuits. We also discuss how this motivates appending the stabilization scheme to the circuit in Fig. 6 to achieve the same fidelity F with lower circuit depth N .

a. State Fidelity v/s Circuit Depth: The coefficients of the superposition prepared via \mathcal{C}_k are obtained by recursively splitting a state using conditional displacements starting from the vacuum. These coefficients are related to Pascal's triangle (see figure 16), that is, after N cat-state transfer circuits, the coefficients of the m^{th} peak are equal to $\sqrt{\binom{N}{m}/2^N}$. The required coefficient for states peaked at $m\sqrt{\pi}$ in the GKP state is $ke^{-\pi\frac{m^2\Delta^2}{2}}$ where k is the normalization constant. We ignore the common factor of $(2/\pi)^{1/4}$. We can find an optimum even N for any given Δ and Z_{GKP} logical codeword μ as follows,

$$\sqrt{\binom{N}{m+\mu}/2^N} = \exp -\pi \frac{(2m + \mu - N/2)^2 \Delta^2}{4}, \quad (\text{F1})$$

for $m \in \mathbb{Z}$. Now, using Stirling approximation we have,

$$\Rightarrow \ln \left(\frac{N}{2} \right)^N \frac{1}{m^m (N-m)^{N-m}} = -2\pi(m - N/2)^2 \Delta^2, \quad (\text{F2})$$

$$\Rightarrow \frac{1/2}{\left(\frac{m}{N} \right)^{m/N} \left(1 - \frac{m}{N} \right)^{1-m/N}} = \exp -\frac{2\pi\Delta^2(m - N/2)^2}{N} \quad (\text{F3})$$

$$\Rightarrow \frac{x^{-x} (1-x)^{-(1-x)}}{2} = e^{-2N\pi\Delta^2(x-0.5)^2}, \quad (\text{F4})$$

$x = m/N$ where $x \leq 1$. The solution to the above equation involves a transcendental equation. Hence, one needs to resort to numerical methods to find $N = f(\Delta)$. Using the Newton-Raphson method we find that $N\Delta^2 = 0.32$ maximizes the overlap. Thus, we get the Table II for optimal N corresponding to reasonable finite-energy parameters Δ to reach $\mathcal{F} \geq 0.98$.

b. Un-entanglement: For un-entanglement after $k = 2$, the angle of rotation is not so straightforward as mentioned in the main text with the help of Fig. 6(a). To determine the optimal angle for un-entanglement with \mathcal{C}_k , let us define the following abstract fidelity and normalization functions in terms of a , the magnitude of conditional

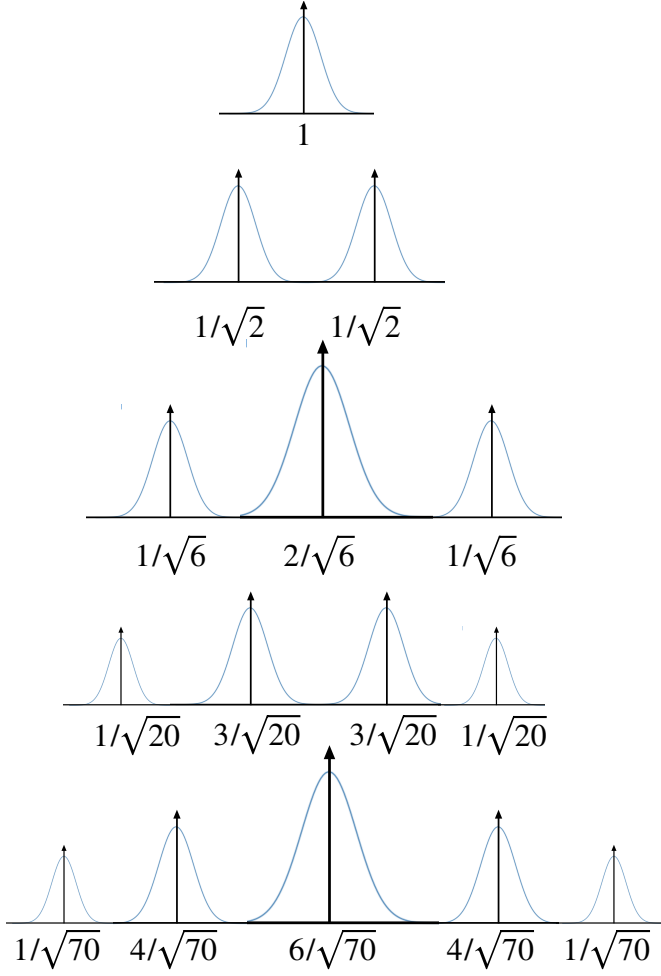


FIG. 16. The probability corresponding to the various finite-energy basis states in superposition generated after repeated cat state transfer circuit are related to Pascal's triangle as shown here. This defines the state prepared by the circuit shown in Fig. 6.

displacement used for rotation,

$$F = \frac{\left[\frac{\pi}{4} - a\sqrt{\pi}x\right]^2 + \sum_{i \in 2\mathbb{Z}}^{2 \leq i \leq x} \left[\binom{k}{i/2} a(x-i)\right]^2}{1 + \sum_{i \in 2\mathbb{Z}}^{2 \leq i \leq x} \binom{k}{i/2}^2}, \quad (\text{F5})$$

$$\text{where, } x = \frac{k+1}{2} + 1 \quad \text{if } k \in 2\mathbb{Z} + 1, \quad (\text{F6})$$

$$= \frac{k}{2} + 1 \quad \text{if } k \in 2\mathbb{Z}, \quad (\text{F7})$$

The fidelity function here only uses the left half since the effect from the right half will be the same. We also do not take into account the central peak if k is even just because the central peaks will not rotate the qubit at all. Thus, we need to minimize the following expression which measures the proximity of the qubit states entangled with

the centre of each peak to the target qubit state $|+\rangle$,

$$\min_a [1 - F] \quad (\text{F8})$$

$$(\text{F9})$$

The constraint is $a \leq \sqrt{\pi}/4k$. One can verify that the minima are indeed located at $a = \frac{\sqrt{\pi}}{4k}$ if $k \leq 3$.

c. Low circuit-depth scheme: The state generated by finite (N) cat state transfer circuits as seen above will not yield the correct coefficient, that is, the desired superposition. Yet, the state we achieve by a large enough N , say enough to get a significant number of peaks in superposition is sufficient to be appended by the SBS protocol. The state with incorrect superposition does not have the right grid in the Wigner representation of the state, (see the peaks at the end of the last Wigner graph in Fig. 6). This can be resolved by appending a few SBS rounds and thus, the resulting state will be higher in fidelity to the desired GKP state with a much smaller N compared to what's shown in the previous subsection here. The advantage of using the scheme is two-fold. Firstly, it prepares the state with a higher fidelity compared to when only using SBS followed by a logical Z_{GKP} measurement. Neither are we relying on ancilla measurement outcome (in the absence of errors) nor are we using the slow convergence of SBS (see Fig. 6(b)). This happens because we resort to SBS only after the overlap of the final state from our scheme with the target state in the GKP codespace is high enough such that ancilla measurement yields g deterministically after each SBS round. The second advantage is that since after each cat-state-transfer circuit the outcome is g with a very high probability, an e outcome indicates an error in the ancilla or the cavity with a very high probability. Thus, post-selection will make the scheme robust to errors during the GKP state preparation.

d. State Preparation from Vacuum: If we repeat the scheme described above with $\Delta = 1$, that is, vacuum in the oscillator, then we will prepare a momentum-squeezed state at the end of \mathcal{C}_4 . Post this, we determine the squeezing of the state-prepared δp . We use this finite-energy parameter to repeat the protocol in the momentum quadrature. This process prepares a magic state with fidelity 0.85 and success probability 0.90. The decrease in fidelity is because the unentangling gadget does yields a low success probability of 0.94 when generating a squeezed cat from a squeezed vacuum prepared in this manner (rather than resorting to the squeezing gadget). Note that, this circuit, however, would not need SBS to be appended. This circuit, while much faster, is worse in terms of hybrid fidelity than the circuit presented in Fig. 6(b) and should not be preferred.

e. Arbitrary GKP State: We have shown high-fidelity preparation of logical Pauli eigenstates of the GKP code space. The magic state from the vacuum is a good resource for non-Clifford operations, however, to demonstrate universal state transfer we also need to show the preparation of arbitrary GKP code words. This can

be done using a qubit-cavity state transfer technique restricted to GKP states. We start with $|0\rangle_{\text{GKP}}$ state in the cavity and the qubit in a desired state $a|+\rangle + b|-\rangle$. Next we can apply a finite-energy logical Z_{GKP} operation conditioned on the qubit state using $e^{i\sqrt{\pi/2}\hat{x}\sigma_z}$. Thus, we have the hybrid oscillator-qubit state,

$$|\psi\rangle = D(i\sqrt{\pi/2}\sqrt{2})[a|0g\rangle + b|1'e\rangle] \quad (\text{F10})$$

$$\text{where } |1'\rangle = D(i\sqrt{\pi/2})|0\rangle, \quad (\text{F11})$$

corresponds to an un-centered $|1\rangle_{\text{GKP}}$ state which can be re-centered using stabilization or adjusted for in the software.

Appendix G: Law-eberly Protocol for Preparation of Fock states.

An arbitrary conditional displacement $e^{i(\alpha\hat{x}+\beta\hat{p})\otimes\sigma_\phi}$ can be written in terms of ladder up and down operators $\{\hat{a}, \hat{a}^\dagger, \sigma_-, \sigma_+\}$ as follows,

$$\text{CD} = e^{i(\alpha\hat{x}+\beta\hat{p})\otimes\sigma_\phi} = e^{ir(\cos\theta\hat{x}+\sin\theta\hat{p})\otimes(\cos\phi\sigma_x+\sin\phi\sigma_y)} \quad (\text{G1})$$

where $r^2 = \alpha^2 + \beta^2$

$$\text{CD} = e^{ir/2(e^{i\theta}\hat{a}+e^{-i\theta}\hat{a}^\dagger)\otimes(e^{i\phi}\sigma_-+e^{-i\phi}\sigma_+)} \quad (\text{G2})$$

$$\begin{aligned} &= \exp\left[i\frac{r}{2}\underbrace{(e^{i(\theta+\phi)}\hat{a}\sigma_-+e^{-i(\theta+\phi)}\hat{a}^\dagger\sigma_+)}_{\text{AJC}}\right. \\ &\quad \left.+\underbrace{e^{i(\theta-\phi)}\hat{a}\sigma_++e^{-i(\theta-\phi)}\hat{a}^\dagger\sigma_-)}_{\text{JC}}\right] \quad (\text{G3}) \end{aligned}$$

The last equation underlines the terms that correspond to the Jaynes-Cummings (JC) and anti-JC (AJC) Hamiltonians. Let us look at the effect of the unitary $e^{i\gamma\text{AJC}}$ on $|n\rangle|g\rangle$.

$$(\text{Anti-JC})^n|n\rangle|g\rangle = e^{-i(\theta+\phi)}(2\sqrt{(n+1)})^n|n+1\rangle|e\rangle, \quad (\text{G4})$$

$$= (2\sqrt{(n+1)})^n|n\rangle|g\rangle, \quad n \in 2\mathbb{Z} \quad (\text{G5})$$

where $n \in 2\mathbb{Z} + 1$

$$\therefore e^{i\gamma\text{AJC}}|n\rangle|g\rangle = \sum_{j=1}^{\infty} \frac{(i\gamma)^n}{n!}(\text{Anti-JC})^n|n\rangle|g\rangle \quad (\text{G6})$$

$$\begin{aligned} &= \cos 2\gamma\sqrt{(n+1)}|n\rangle|g\rangle \\ &\quad + e^{-i(\theta+\phi)}\sin 2\gamma\sqrt{(n+1)}|n+1\rangle|e\rangle \quad (\text{G7}) \end{aligned}$$

Thus, if we only had AJC or JC then it would be easy to prepare arbitrary Fock states using qubit rotations with $\gamma = \frac{\pi}{4\sqrt{(n+1)}}$, starting from $|n=0\rangle|g\rangle$ with single photon consumption processes. Given we also have

the JC Hamiltonian, if we alternate between $\theta - \alpha = z$ and $\theta - \alpha = -z$ we can collectively cancel out the JC Hamiltonian. This can be easily achieved using $(e^{i\gamma x\sigma_y/N}e^{i\gamma p\sigma_x/N})^N$ in N steps where $\theta - \phi = -\frac{\pi}{2}$ for the first gate and $\theta - \phi = \frac{\pi}{2}$ for the second. Alternatively, this protocol can be seen as a trotterization to achieve the sum of two CD Hamiltonians to achieve $H = x\sigma_x - p\sigma_y = \text{AJC}$. The operator fidelity of the resulting operation with AJC Hamiltonian with respect to N has been studied in Ref. [8].

In the availability of the JC or AJC Hamiltonian evolution, we can prepare arbitrary superposition of Fock states, using the protocol defined by Law and Eberly in [63], and hence universal state transfer can be achieved. The efficiency of Fock state preparation using this scheme was also analyzed in Ref. [8], where the authors have shown that this trotterization-based scheme improves upon the numerical scheme in Ref. [10] in terms of circuit duration. However, in terms of circuit-depth the numerical scheme is still optimal, as expected.

Appendix H: GKP Logical Readout

a. Ideal Readout: The ideal logical GKP readout using a two-level system requires one to maximally entangle the GKP codespace with the two-level ancilla. One can translate this task into an entangling gadget for the logical GKP states. For the ideal GKP codewords $|0\rangle_{\text{GKP}}$ ($|1\rangle_{\text{GKP}}$) located at $x = \pm m\sqrt{2\pi}$ ($x = \pm(m+1/2)\sqrt{2\pi}$) where $m \in \mathbb{Z}$, this entanglement can be achieved simply using $e^{i\sqrt{\frac{\pi}{2}}\hat{x}\sigma_x}$. If the qubit starts in $|g\rangle$, this operation rotates the qubit by 2π about σ_x vector on the Bloch sphere if the oscillator is in $|0\rangle_{\text{GKP}}$ whereas it rotates the qubit by π if the oscillator is in $|1\rangle_{\text{GKP}}$. Similarly for ideal $|\pm\rangle_{\text{GKP}}$ basis states located at $p = \pm m\sqrt{\pi}$ the ideal readout circuit uses $e^{i\sqrt{\frac{\pi}{2}}\hat{p}\sigma_x}$. Following equation where $|\psi\rangle_{\text{GKP}} = \beta_1|0\rangle_{\text{GKP}} + \beta_2|1\rangle_{\text{GKP}} = \gamma_1|+\rangle_{\text{GKP}} + \gamma_2|-\rangle_{\text{GKP}}$ describes the process for an ideal GKP code where $\Delta = 0$.

$$e^{i\sqrt{\frac{\pi}{2}}\hat{x}\sigma_x}(|\psi\rangle \otimes |g\rangle) = -\beta_1|0\rangle_{\text{GKP}}|g\rangle + \beta_2|1\rangle_{\text{GKP}}|e\rangle \quad (\text{H1})$$

$$e^{i\sqrt{\frac{\pi}{2}}\hat{p}\sigma_x}(|\psi\rangle \otimes |g\rangle) = -\gamma_1|+\rangle_{\text{GKP}}|g\rangle + \gamma_2|-\rangle_{\text{GKP}}|e\rangle \quad (\text{H2})$$

Appendix I: Logical controlled-Pauli operations

1. Finite-energy SUM gate.

. The logical gates for GKP qubits are obtained via the non-unitary gate $\hat{E}_\Delta A \hat{E}_\Delta^{-1}$ where A is the gate for unrealistic infinite-energy GKP while \hat{E}_Δ is the envelope operator $e^{-\Delta^2\hat{n}}$ (see Sec. V). The entangling gate CX_{GKP} such that $A = e^{i2\hat{x}\otimes\hat{p}}$ takes the following form

$$\hat{E}_\Delta e^{i2\hat{x}\otimes\hat{p}} \hat{E}_\Delta^{-1}$$

$$= e^{i(2 \cosh \Delta^2 \hat{x} + i 2 \sinh \Delta^2 \hat{p}) \otimes (2 \cosh \Delta^2 \hat{p} - i 2 \sinh \Delta^2 \hat{x})} \quad (I1)$$

$$\approx e^{i(2\hat{x}_1\hat{p}_2 + 2\Delta^4\hat{p}_1\hat{x}_2 - i2\Delta^2(\hat{x}_1\hat{x}_2 - 2\hat{p}_1\hat{p}_2))} \quad (I2)$$

(Finite-energy CX_{GKP} gate)

These non-unitary gates can be approximated using an auxiliary qubit, where the approximations hold in the small Δ limit such that $\cosh \Delta^2 \approx 1$ and $\sinh \Delta^2 \approx \Delta^2$.

$$\text{CX}_{\text{GKP}} \approx e^{-i\Delta^2(\hat{x}_1\hat{x}_2 - \hat{p}_1\hat{p}_2)\sigma_y} e^{i(2\hat{x}_1\hat{p}_2 - 2\Delta^4\hat{p}_1\hat{x}_2)\sigma_x} \times e^{-i\Delta^2(\hat{x}_1\hat{x}_2 - \hat{p}_1\hat{p}_2)\sigma_y} |\psi\rangle_{\text{GKP}} |0\rangle \quad (I3)$$

We can use dissipation based methods followed by trotterization [43, 60] or realize this using GCR type correction techniques where $\sigma_x |g\rangle = -i\sigma_y |g\rangle$ to derive this sequence. Thus, for a two-mode equivalent of the SBS type circuit we have, $S \equiv e^{-i\Delta^2(\hat{x}_1\hat{x}_2 - \hat{p}_1\hat{p}_2)\sigma_y}$ and $B \equiv e^{i2(\hat{x}_1\hat{p}_2 - \Delta^4\hat{p}_1\hat{x}_2)\sigma_x}$. Now, we show a fast echoed conditional sequence to realize each gate in this sequence.

Let us first discuss S. Using the definition of TMS(r, ϕ) in Ref. [8], we first note that

$$\text{TMS}(\alpha, \pi) a \text{TMS}^\dagger(\alpha, \pi) = a \cosh \alpha + b^\dagger \sinh \alpha. \quad (I4)$$

This¹² in turn implies

$$\begin{aligned} & \text{TMS}(\alpha, \pi) e^{-i\chi t_S a^\dagger a \sigma_z} \text{TMS}^\dagger(\alpha, \pi) \\ &= \exp \left[-i\chi t_S \left(\cosh^2(\alpha) a^\dagger a + \sinh^2(\alpha) b b^\dagger \right. \right. \\ & \quad \left. \left. + \frac{1}{2} \sinh(2\alpha) (a^\dagger b^\dagger + ab) \right) \sigma_z \right] \quad (I5) \end{aligned}$$

The next steps of the method are inspired by the construction of echoed-conditional displacements (ECD) described above. Notice that the first two terms in Eq. (I5) do not change signs with α , whereas the last two will. Hence, running the pulse shown below yields an echoed two-mode squeezing, in close analogy with the echoed displacement gate previously discussed,

$$\begin{aligned} & \text{TMS}(\alpha, \pi) e^{-i\chi t_S a^\dagger a \sigma_z} \text{TMS}^\dagger(\alpha, \pi) \times \sigma_x \\ & \times \text{TMS}(-\alpha, \pi) e^{-i\chi t_S a^\dagger a \sigma_z} \text{TMS}^\dagger(-\alpha, \pi) \end{aligned} \quad (I6)$$

$$\approx e^{-i\chi t_S \sinh 2\alpha (a^\dagger b^\dagger + ab) \sigma_z} \quad (I7)$$

Now the qubit Bloch sphere can be rotated using $R_x(\pi/2)$ to transform this gate to S. The speed of the conditional two-mode squeezing gate, in this case, is decided by $t_S = \frac{\Delta^2}{\chi \sinh 2\alpha}$ instead of χt as in the case where this gate is synthesized with controlled parity gates (which would have required a high χ , not suitable for GKP states [10]).

As $\sinh 2\alpha$ is an unbounded function, we can in principle increase it to extremely large values by varying α . Thus, in the weak dispersive regime, we can achieve fast conditional oscillator-oscillator entangling gates by leveraging unconditional two-mode squeezing with large α as a resource. The two-mode squeezed frame used to actuate a large α can be achieved using single-mode squeezing and beam splitter via Bloch-Messiah decomposition. See Ref. [8].

Now, for the case of B, one could ignore Δ^4 term and directly use the Bloch-Messiah decomposition for the SUM gate [8]. However, we can achieve this gate exactly with the Δ^4 correction by going to the frame of $BS(\alpha, \pi)$. Using the definition of TMS(r, ϕ) in Ref. [8], we first note that

$$BS(\alpha, \pi) a BS^\dagger(\alpha, \pi) = a \cos \alpha / 2 + i b^\dagger \sinh \alpha / 2. \quad (I8)$$

Thus, we have

$$\begin{aligned} & BS(\alpha, \pi) e^{-i\chi t_B a^\dagger a \sigma_z} BS^\dagger(\alpha, \pi) \\ &= \exp \left[-i\chi t_B \left(\cos^2(\alpha/2) a^\dagger a + \sinh^2(\alpha/2) b b^\dagger \right. \right. \\ & \quad \left. \left. - \frac{1}{2} \sin(\alpha) (a^\dagger b - ab^\dagger) \right) \sigma_z \right] \quad (I9) \end{aligned}$$

The echoed conditional beam-splitter version is given by,

$$\begin{aligned} & BS(\alpha, \pi) e^{-i\chi t_B a^\dagger a \sigma_z} BS^\dagger(\alpha, \pi) \times \sigma_x \\ & \times BS(-\alpha, \pi) e^{-i\chi t_B a^\dagger a \sigma_z} BS^\dagger(-\alpha, \pi) \\ & \approx e^{-\chi t_B \sin \alpha (a^\dagger b - ab^\dagger) \sigma_z} \quad (I10) \\ & = e^{-i\chi t_B \sin \alpha (\hat{x}_1\hat{p}_2 + \hat{p}_1\hat{x}_2) \sigma_z}. \quad (I11) \end{aligned}$$

In order to extract B from Eq. (I11) we need to perform single-mode squeezing of one of the modes $S_a(r)$ such that $\hat{x}_a, \hat{p}_a \rightarrow e^r x_a, e^{-r} p_a$. Let $r > 0$ and $a = 1$, that is squeeze the position of the first mode. Thus, Eq. (I11) yields,

$$e^{-i\chi t_B e^r \sin \alpha (\hat{x}_1\hat{p}_2 + e^{-2r} \hat{p}_1\hat{x}_2) \sigma_z} \quad (I12)$$

Here $r = \frac{1}{2} \ln \Delta^{-4}$ is fixed. Lower the Δ , larger is the value of r . For example, $\Delta = 0.34$ requires $r \sim 2.15$. Thus, the speed of this gate is given by,

$$\chi t_B e^r \sin \alpha = 2 \quad (I13)$$

$$t_B = \frac{2\Delta^2}{\chi \sin \alpha} \quad (I14)$$

Thus, for lower Δ , this gate is much faster. Thus, for CX_{GKP}, we have,

$$t_S = \frac{\Delta^2}{\chi \sinh 2\alpha}, t_B \geq \frac{2\Delta^2}{\chi} \quad (I15)$$

Similarly, for CZ_{GKP}, we have,

$$t_B = \frac{2\Delta^2}{\chi \sinh 2\alpha}, t_S \geq \frac{\Delta^2}{\chi} \quad (I16)$$

¹² Such transformations are obtained using $e^A B e^{-A} = B + [A, B] + \frac{1}{2!} [A, [A, B]] + \frac{1}{3!} [A, [A, [A, B]]] \dots$

Note that even though the lower bound on t_S is half that of t_B in CX_{GKP}, total duration of the circuit is, $t_{\text{CX}}/\text{CZ} = 2t_S + t_B$. Thus, both gates come down to the same speed. Thus, we have given a new circuit decomposition for fast finite-energy SUM gate sequence for logical GKP entangling operations. This decomposition was derived using a two-mode extension of the echoed conditional displacements which we have derived, and have simultaneously provided in Ref. [8].

2. Error-corrected gate teleportation

The GKP CX operations could be done using the SUM gate $e^{i\hat{x}\otimes\hat{p}}$ in [56], however, these gates do not serve as logical operation to finite energy states since corresponding to $2m\sqrt{\pi}$ in the control qubit will displace the target qubit different from the peak at $x = 0$. Thus, neither does it preserve the envelope nor the periodicity, and the GKP envelope of the target would blow up disproportionately. This suggests that successive rounds of trimming $e^{i\hat{p}\otimes\hat{y}}$ will not be able to increase the gate fidelity. The significance of using qubits for GKP gates is that the rotation angles on qubits preserve the periodicity at for $\text{CD}(2\sqrt{\pi}, \sigma_\phi)$. It emulates a torus with the GKP unit cell as proposed in [56]. If we follow our previous formula of gate teleportation but this time use two GKP-qubit packages such that each qubit is used to stabilize its own GKP state. Now, if we entangle the GKP states and qubits using the x-entangling gadget on the control package and p-entangling gadget on the target package, perform CZ between the two qubits and then use the corresponding disentangling gadgets on both, we would have performed a CX on the two GKP states, $|\psi_1\rangle_{\text{GKP}} = a|0_1\rangle_{\text{GKP}} + b|1_1\rangle_{\text{GKP}}$, $|\psi_2\rangle_{\text{GKP}} = (c|+2\rangle_{\text{GKP}} + d|-2\rangle_{\text{GKP}})$.

$$\begin{aligned} \mathcal{E}_{x_1}\mathcal{E}_{p_2}[|\psi_1\rangle_{\text{GKP}} \otimes |g_1\rangle][|\psi_2\rangle_{\text{GKP}} \otimes |g_2\rangle] \\ = [(a|0_1\rangle_{\text{GKP}}|g_1\rangle - b|1_1\rangle_{\text{GKP}})|e_1\rangle] \\ [(c|+2\rangle_{\text{GKP}}|g_2\rangle - d|-2\rangle_{\text{GKP}})|e_2\rangle] \end{aligned} \quad (\text{I17})$$

$$\begin{aligned} &= |GKP_{CX1}\rangle \\ &C_1Z_2|GKP_{CX1}\rangle \\ &= [a|0_1\rangle_{\text{GKP}}|g_1\rangle [c|+2\rangle_{\text{GKP}}|g_2\rangle - d|-2\rangle_{\text{GKP}}|e_2\rangle] \\ &- b|1_1\rangle_{\text{GKP}}|e_1\rangle [c|+2\rangle_{\text{GKP}}|g_2\rangle + d|-2\rangle_{\text{GKP}}|e_2\rangle] \end{aligned} \quad (\text{I18})$$

$$= |GKP_{CX2}\rangle \quad (\text{I19})$$

$$\begin{aligned} \mathcal{E}_{x_1}\mathcal{E}_{p_2}|GKP_{CX2}\rangle \\ = a|0_1\rangle_{\text{GKP}}|g_1\rangle [c|+2\rangle_{\text{GKP}}|g_2\rangle - d|-2\rangle_{\text{GKP}}|g_2\rangle] \\ - b|1_1\rangle_{\text{GKP}}|g_1\rangle [c|+2\rangle_{\text{GKP}}|g_2\rangle + d|-2\rangle_{\text{GKP}}|g_2\rangle] \\ = a|0_1\rangle_{\text{GKP}}[c|+2\rangle_{\text{GKP}} - d|-2\rangle_{\text{GKP}}] \\ - b|1_1\rangle_{\text{GKP}}[c|+2\rangle_{\text{GKP}} + d|-2\rangle_{\text{GKP}}]|g_1\rangle|g_2\rangle \end{aligned} \quad (\text{I20})$$

If we start with the control GKP in $|-\rangle_{\text{GKP}}$ state, that is, $a = 1$, $b = -1$ and target GKP in $|1\rangle_{\text{GKP}}$ state, that is,

$c = 1, d = -1$; the final states of the two cavities will be in the entangled GKP Bell pair, $|0_10_2\rangle_{\text{GKP}} + |1_21_1\rangle_{\text{GKP}}$, with both the qubits decoupled and ready for the next round of stabilization or gate operation. The success probability of this gate is 0.9987 and the fidelity of the gate is 99.92%. However, these gates cannot be protected from any ancilla error. Thus, it will be a low-fidelity gate in the presence of any type of fault in ancilla.

Appendix J: Constructing Hybrid Unitary for Phase Estimation

The hybrid unitary C_xU is constructed as follows.

$$e^{i\alpha\hat{x}\otimes\sigma_z}S^\dagger US e^{-i\alpha\hat{x}\otimes\sigma_z}SUS^\dagger = e^{i\hat{g}\hat{n}'\cdot\sigma} = C_xU, \quad (\text{J1})$$

where, $S = \sqrt{\sigma_z}$ is the qubit phase gate. Note that, here, each expression can be presented as a quaternion where the four basis elements correspond to the Pauli vectors $\{I, \sigma_x, \sigma_y, \sigma_z\}$. The Pauli vectors follow the same algebra as quaternions, and hence, we now give derivation for the exact expression of g, \hat{n}' using the product formulas for quaternions.

$$e^{i\alpha\hat{x}\otimes\sigma_z}S^\dagger US e^{-i\alpha\hat{x}\otimes\sigma_z}SUS^\dagger \quad (\text{J2})$$

$$= e^{i\alpha\hat{x}\otimes\sigma_z}e^{i\theta\sigma_x}e^{-i\alpha\hat{x}\otimes\sigma_z}e^{-i\theta\sigma_x}. \quad (\text{J3})$$

For the product of quaternions (or qubit rotations)¹³,

$$e^{i\gamma\hat{k}\cdot\sigma} = e^{i\alpha\hat{x}\otimes\sigma_z}e^{i\theta\sigma_x} \quad (\text{J4})$$

$$e^{i\gamma'\hat{k}'\cdot\sigma} = e^{-i\alpha\hat{x}\otimes\sigma_z}e^{-i\theta\sigma_x}, \quad (\text{J5})$$

Defining $\hat{n}\cdot\vec{\sigma} = \sigma_z$, $\hat{m}\cdot\vec{\sigma} = \sigma_x$, we can use the vector identity, $(\hat{n}\cdot\vec{\sigma})(\hat{m}\cdot\vec{\sigma}) = (\hat{n}\cdot\hat{m})I + i(\hat{n}\times\hat{m})\cdot\vec{\sigma}$ to write,

$$\gamma = \gamma' = \cos^{-1}(\cos\alpha\hat{x}\cos\theta - (\hat{n}\cdot\hat{m})\sin\alpha\hat{x}\sin\theta) \quad (\text{J6})$$

$$\begin{aligned} \hat{k} = \frac{1}{\sin\gamma}(\hat{n}\sin\alpha\hat{x}\cos\theta + \hat{m}\sin\theta\cos\alpha\hat{x} \\ - (\hat{n}\times\hat{m})\sin\alpha\hat{x}\sin\theta), \end{aligned} \quad (\text{J7})$$

$$\begin{aligned} \hat{k}' = \frac{1}{\sin\gamma}(-\hat{n}\sin\alpha\hat{x}\cos\theta - \hat{m}\sin\theta\cos\alpha\hat{x} \\ - (\hat{n}\times\hat{m})\sin\alpha\hat{x}\sin\theta), \end{aligned} \quad (\text{J8})$$

For this case, $\hat{n}\cdot\hat{m} = 0$ and $(\hat{n}\times\hat{m})\cdot\vec{\sigma} = \sigma_y$. Thus,

$$\cos\gamma = \cos\alpha\hat{x}\cos\theta \implies \sin\gamma = \sqrt{1 - \cos^2\alpha\hat{x}\cos^2\theta}, \quad (\text{J9})$$

$$\hat{k}\cdot\vec{\sigma} = \frac{1}{\sin\gamma}(\sin\alpha\hat{x}\cos\theta\sigma_z + \sin\theta\cos\alpha\hat{x}\sigma_x - \sin\alpha\hat{x}\sin\theta\sigma_y), \quad (\text{J10})$$

¹³ Note that, such derivation for expressing the product of arbitrary rotations as another rotation is given in any elementary quantum information textbook.

$$\hat{k}' \cdot \vec{\sigma} = -\frac{1}{\sin \gamma} (\sin \alpha \hat{x} \cos \theta \sigma_z + \sin \theta \cos \alpha \hat{x} \sigma_x + \sin \alpha \hat{x} \sin \theta \sigma_y). \quad (\text{J11})$$

Thus, collectively, we can write,

$$\hat{k}_z = -\hat{k}'_z = \frac{\sin \alpha \hat{x} \cos \theta}{\sin \gamma} \quad (\text{J12})$$

$$\hat{k}_x = -\hat{k}'_x = \frac{\cos \alpha \hat{x} \sin \theta}{\sin \gamma} \quad (\text{J13})$$

$$\hat{k}_y = \hat{k}'_y = -\frac{\sin \alpha \hat{x} \sin \theta}{\sin \gamma}, \quad (\text{J14})$$

$$\gamma' = \gamma = \cos^{-1}(\cos \alpha \hat{x} \cos \theta). \quad (\text{J15})$$

Now, we repeat this procedure to compute the target operation $C_x U$ which is equal to,

$$e^{i\gamma \hat{k} \cdot \vec{\sigma}} e^{i\gamma \hat{k}' \cdot \vec{\sigma}} = e^{i\hat{g} \hat{n}' \cdot \vec{\sigma}} = \cos g I + i \sin g (\hat{n}' \cdot \vec{\sigma}). \quad (\text{J16})$$

Now, we have,

$$\cos g = \cos^2 \gamma - (\hat{k} \cdot \hat{k}') \sin^2 \gamma = 1 - 2 \sin^2 \alpha \hat{x} \sin^2 \theta, \quad (\text{J17})$$

$$\hat{n}' = \frac{1}{\sin g} (\hat{k} \sin \gamma \cos \gamma + \hat{k}' \sin \gamma \cos \gamma -$$

$$(\hat{k} \times \hat{k}') \sin \gamma \sin \gamma) \quad (\text{J18})$$

$$= \frac{1}{\sin g} ((\hat{k} + \hat{k}') (\sin 2\gamma)/2 - (\hat{k} \times \hat{k}') \sin^2 \gamma). \quad (\text{J19})$$

$$\Rightarrow \hat{n}' \cdot \vec{\sigma} = \frac{1}{\sin g} \left(\frac{\sin^2 \alpha \hat{x} \sin 2\theta}{\sin^2 \gamma} \sigma_x - \frac{\sin 2\alpha \hat{x} \sin 2\theta}{2} \sigma_y + \frac{\sin^2 \theta \sin 2\alpha \hat{x}}{\sin^2 \gamma} \sigma_z \right). \quad (\text{J20})$$

We need to choose $\alpha \rightarrow 0$ small enough such that we can ignore $\mathcal{O}(\alpha^2 \hat{x}^2)$ terms such that only terms linear in \hat{x} survive. In this limit, $\cos g \rightarrow 1$, $\frac{g}{\sin g} \rightarrow 1$, $\sin \gamma \rightarrow \sin \theta$ and,

$$\hat{n}'_x = 0 \quad (\text{J21})$$

$$\hat{n}'_y = -\alpha \hat{x} \sin 2\theta \quad (\text{J22})$$

$$\hat{n}'_z = 2\alpha \hat{x}. \quad (\text{J23})$$

If the qubit is in a particular eigenstate of σ_y , after application of $C_x U$, if the qubit is measured in the σ_y then the average displacement of the qubit will be $\alpha \hat{x} \sin 2\theta$.

[1] S. Wimperis, **Broadband, Narrowband, and Passband Composite Pulses for Use in Advanced NMR Experiments**, Journal of Magnetic Resonance, Series A 109 (2) (1994) 221–231.
URL <https://www.sciencedirect.com/science/article/pii/S1064185884711594>

[2] G. H. Low, I. L. Chuang, **Optimal Hamiltonian Simulation by Quantum Signal Processing**, Physical Review Letters 118 (1) (2017) 010501, publisher: American Physical Society.
URL <https://link.aps.org/doi/10.1103/PhysRevLett.118.010501>

[3] J. M. Martyn, Z. M. Rossi, A. K. Tan, I. L. Chuang, **Grand Unification of Quantum Algorithms**, PRX Quantum 2 (4) (2021) 040203, publisher: American Physical Society.
URL <https://link.aps.org/doi/10.1103/PRXQuantum.2.040203>

[4] D. Motlagh, N. Wiebe, **Generalized Quantum Signal Processing**, PRX Quantum 5 (2) (2024) 020368, publisher: American Physical Society.
URL <https://link.aps.org/doi/10.1103/PRXQuantum.5.020368>

[5] Z. M. Rossi, I. L. Chuang, **Multivariable quantum signal processing (M-QSP): prophecies of the two-headed oracle**, Quantum 6 (2022) 811, publisher: Verein zur Förderung des Open Access Publizierens in den Quantenwissenschaften.
URL <https://quantum-journal.org/papers/q-2022-09-20-811/>

[6] S. L. Braunstein, P. van Loock, **Quantum information with continuous variables**, Reviews of Modern Physics 77 (2) (2005) 513–577, publisher: American Physical Society.
URL <https://link.aps.org/doi/10.1103/RevModPhys.77.513>

[7] N. Liu, J. Thompson, C. Weedbrook, S. Lloyd, V. Vedral, M. Gu, K. Modi, **Power of one qumode for quantum computation**, Physical Review A 93 (5) (2016) 052304, publisher: American Physical Society.
URL <https://link.aps.org/doi/10.1103/PhysRevA.93.052304>

[8] Y. Liu, S. Singh, K. C. Smith, E. Crane, J. M. Martyn, A. Eickbusch, A. Schuckert, R. D. Li, J. Sinanan-Singh, M. B. Soley, T. Tsunoda, I. L. Chuang, N. Wiebe, S. M. Girvin, **Hybrid Oscillator-Qubit Quantum Processors: Instruction Set Architectures, Abstract Machine Models, and Applications**, arXiv:2407.10381 [quant-ph] (Aug. 2024).
URL <http://arxiv.org/abs/2407.10381>

[9] L. Brenner, L. Caha, X. Coiteux-Roy, R. Koenig, **Factoring an integer with three oscillators and a qubit**, arXiv:2412.13164 [quant-ph] (Dec. 2024).
URL <http://arxiv.org/abs/2412.13164>

[10] A. Eickbusch, V. Sivak, A. Z. Ding, S. S. Elder, S. R. Jha, J. Venkatraman, B. Royer, S. M. Girvin, R. J. Schoelkopf, M. H. Devoret, **Fast universal control of an oscillator with weak dispersive coupling to a qubit**, Nature Physics 18 (12) (2022) 1464–1469, publisher: Nature Publishing Group.
URL <https://www.nature.com/articles/>

s41567-022-01776-9

[11] S. Haroche, **Nobel Lecture: Controlling photons in a box and exploring the quantum to classical boundary**, *Reviews of Modern Physics* 85 (3) (2013) 1083–1102, publisher: American Physical Society.
URL <https://link.aps.org/doi/10.1103/RevModPhys.85.1083>

[12] A. Kumar, A. Suleymanzade, M. Stone, L. Taneja, A. Anferov, D. I. Schuster, J. Simon, **Quantum-enabled millimetre wave to optical transduction using neutral atoms**, *Nature* 615 (7953) (2023) 614–619, publisher: Nature Publishing Group.
URL <https://www.nature.com/articles/s41586-023-05740-2>

[13] S. D. Hogan, J. A. Agner, F. Merkt, T. Thiele, S. Filipp, A. Wallraff, **Driving Rydberg-Rydberg Transitions from a Coplanar Microwave Waveguide**, *Physical Review Letters* 108 (6) (2012) 063004, publisher: American Physical Society.
URL <https://link.aps.org/doi/10.1103/PhysRevLett.108.063004>

[14] S. Garcia, M. Stammmeier, J. Deiglmayr, F. Merkt, A. Wallraff, **Single-Shot Nondestructive Detection of Rydberg-Atom Ensembles by Transmission Measurement of a Microwave Cavity**, *Physical Review Letters* 123 (19) (2019) 193201, publisher: American Physical Society.
URL <https://link.aps.org/doi/10.1103/PhysRevLett.123.193201>

[15] C. D. Bruzewicz, J. Chiaverini, R. McConnell, J. M. Sage, **Trapped-ion quantum computing: Progress and challenges**, *Applied Physics Reviews* 6 (2) (2019) 021314.
URL <https://doi.org/10.1063/1.5088164>

[16] B. de Neeve, T.-L. Nguyen, T. Behrle, J. P. Home, **Error correction of a logical grid state qubit by dissipative pumping**, *Nature Physics* 18 (3) (2022) 296–300, publisher: Nature Publishing Group.
URL <https://www.nature.com/articles/s41567-021-01487-7>

[17] C. Flühmann, T. L. Nguyen, M. Marinelli, V. Negnevitsky, K. Mehta, J. P. Home, **Encoding a qubit in a trapped-ion mechanical oscillator**, *Nature* 566 (2019) 513–517, publisher: Nature Publishing Group.
URL <https://www.nature.com/articles/s41586-019-0960-6>

[18] M. O. Brown, S. R. Muleady, W. J. Dworschack, R. J. Lewis-Swan, A. M. Rey, O. Romero-Isart, C. A. Regal, **Time-of-flight quantum tomography of an atom in an optical tweezer**, *Nature Physics* 19 (4) (2023) 569–573, publisher: Nature Publishing Group.
URL <https://www.nature.com/articles/s41567-022-01890-8>

[19] A. L. Shaw, P. Scholl, R. Finkelstein, R. B.-S. Tsai, J. Choi, M. Endres, **Erasure-cooling, control, and hyper-entanglement of motion in optical tweezers**, arXiv:2311.15580 [quant-ph] (Aug. 2024).
URL <http://arxiv.org/abs/2311.15580>

[20] N. Ofek, A. Petrenko, R. Heeres, P. Reinhold, Z. Leghtas, B. Vlastakis, Y. Liu, L. Frunzio, S. M. Girvin, L. Jiang, M. Mirrahimi, M. H. Devoret, R. J. Schoelkopf, **Extending the lifetime of a quantum bit with error correction in superconducting circuits**, *Nature* 536 (7617) (2016) 441–445, publisher: Nature Publishing Group.
URL <https://www.nature.com/articles/nature18949>

[21] Z. Ni, S. Li, X. Deng, Y. Cai, L. Zhang, W. Wang, Z.-B. Yang, H. Yu, F. Yan, S. Liu, C.-L. Zou, L. Sun, S.-B. Zheng, Y. Xu, D. Yu, **Beating the break-even point with a discrete-variable-encoded logical qubit**, *Nature* 616 (7955) (2023) 56–60, publisher: Nature Publishing Group.
URL <https://www.nature.com/articles/s41586-023-05784-4>

[22] J. M. Gertler, B. Baker, J. Li, S. Shirol, J. Koch, C. Wang, **Protecting a bosonic qubit with autonomous quantum error correction**, *Nature* 590 (7845) (2021) 243–248, publisher: Nature Publishing Group.
URL <https://www.nature.com/articles/s41586-021-03257-0>

[23] V. V. Sivak, A. Eickbusch, B. Royer, S. Singh, I. Tsoutsios, S. Ganjam, A. Miano, B. L. Brock, A. Z. Ding, L. Frunzio, S. M. Girvin, R. J. Schoelkopf, M. H. Devoret, **Real-time quantum error correction beyond break-even**, *Nature* 616 (7955) (2023) 50–55, publisher: Nature Publishing Group.
URL <https://www.nature.com/articles/s41586-023-05782-6>

[24] P. Campagne-Ibarcq, A. Eickbusch, S. Touzard, E. Zalys-Geller, N. E. Frattini, V. V. Sivak, P. Reinhold, S. Puri, S. Shankar, R. J. Schoelkopf, L. Frunzio, M. Mirrahimi, M. H. Devoret, **Quantum error correction of a qubit encoded in grid states of an oscillator**, *Nature* 584 (7821) (2020) 368–372, publisher: Nature Publishing Group.
URL <https://www.nature.com/articles/s41586-020-2603-3>

[25] E. Crane, K. C. Smith, T. Tomesh, A. Eickbusch, J. M. Martyn, S. Kühn, L. Funcke, M. A. DeMarco, I. L. Chuang, N. Wiebe, A. Schuckert, S. M. Girvin, **Hybrid Oscillator-Qubit Quantum Processors: Simulating Fermions, Bosons, and Gauge Fields**, arXiv:2409.03747 [quant-ph] (Sep. 2024).
URL <http://arxiv.org/abs/2409.03747>

[26] N. Quesada, **Franck-Condon factors by counting perfect matchings of graphs with loops**, *The Journal of Chemical Physics* 150 (16) (2019) 164113.
URL <https://doi.org/10.1063/1.5086387>

[27] L. Hu, Y.-C. Ma, Y. Xu, W.-T. Wang, Y.-W. Ma, K. Liu, H.-Y. Wang, Y.-P. Song, M.-H. Yung, L.-Y. Sun, **Simulation of molecular spectroscopy with circuit quantum electrodynamics**, *Science Bulletin* 63 (5) (2018) 293–299.
URL <https://www.sciencedirect.com/science/article/pii/S209592731830063X>

[28] C. S. Wang, J. C. Curtis, B. J. Lester, Y. Zhang, Y. Y. Gao, J. Freeze, V. S. Batista, P. H. Vaccaro, I. L. Chuang, L. Frunzio, L. Jiang, S. Girvin, R. J. Schoelkopf, **Efficient Multiphoton Sampling of Molecular Vibronic Spectra on a Superconducting Bosonic Processor**, *Physical Review X* 10 (2) (2020) 021060, publisher: American Physical Society.
URL <https://link.aps.org/doi/10.1103/PhysRevX.10.021060>

[29] C. S. Wang, N. E. Frattini, B. J. Chapman, S. Puri, S. Girvin, M. H. Devoret, R. J. Schoelkopf, **Observation of Wave-Packet Branching through an Engineered Conical Intersection**, *Physical Review X* 13 (1) (2023) 011008, publisher: American Physical Society.
URL <https://link.aps.org/doi/10.1103/PhysRevX.13.011008>

[30] B. Royer, S. Singh, S. Girvin, **Encoding Qubits in Multimode Grid States**, PRX Quantum 3 (1) (2022) 010335, publisher: American Physical Society.
URL <https://link.aps.org/doi/10.1103/PRXQuantum.3.010335>

[31] S. Rosenblum, P. Reinhold, M. Mirrahimi, L. Jiang, L. Frunzio, R. J. Schoelkopf, **Fault-tolerant detection of a quantum error**, Science 361 (6399) (2018) 266–270, publisher: American Association for the Advancement of Science.
URL <https://www.science.org/doi/10.1126/science.aat3996>

[32] P. Reinhold, S. Rosenblum, W.-L. Ma, L. Frunzio, L. Jiang, R. J. Schoelkopf, **Error-corrected gates on an encoded qubit**, Nature Physics 16 (8) (2020) 822–826, publisher: Nature Publishing Group.
URL <https://www.nature.com/articles/s41567-020-0931-8>

[33] T. Tsunoda, J. D. Teoh, W. D. Kalfus, S. J. de Graaf, B. J. Chapman, J. C. Curtis, N. Thakur, S. M. Girvin, R. J. Schoelkopf, **Error-Detectable Bosonic Entangling Gates with a Noisy Ancilla**, PRX Quantum 4 (2) (2023) 020354, publisher: American Physical Society.
URL <https://link.aps.org/doi/10.1103/PRXQuantum.4.020354>

[34] J. D. Teoh, P. Winkel, H. K. Babla, B. J. Chapman, J. Claes, S. J. de Graaf, J. W. O. Garmon, W. D. Kalfus, Y. Lu, A. Maiti, K. Sahay, N. Thakur, T. Tsunoda, S. H. Xue, L. Frunzio, S. M. Girvin, S. Puri, R. J. Schoelkopf, **Dual-rail encoding with superconducting cavities**, Proceedings of the National Academy of Sciences 120 (41) (2023) e2221736120, publisher: Proceedings of the National Academy of Sciences.
URL <https://www.pnas.org/doi/10.1073/pnas.2221736120>

[35] N. Khaneja, T. Reiss, C. Kehlet, T. Schulte-Herbrüggen, S. J. Glaser, **Optimal control of coupled spin dynamics: design of NMR pulse sequences by gradient ascent algorithms**, Journal of Magnetic Resonance 172 (2) (2005) 296–305.
URL <https://www.sciencedirect.com/science/article/pii/S1090780704003696>

[36] R. W. Heeres, B. Vlastakis, E. Holland, S. Krastanov, V. V. Albert, L. Frunzio, L. Jiang, R. J. Schoelkopf, **Cavity State Manipulation Using Photon-Number Selective Phase Gates**, Physical Review Letters 115 (13) (2015) 137002, publisher: American Physical Society.
URL <https://link.aps.org/doi/10.1103/PhysRevLett.115.137002>

[37] J. Sinanan-Singh, G. L. Mintzer, I. L. Chuang, Y. Liu, **Single-shot Quantum Signal Processing Interferometry**, Quantum 8 (2024) 1427, publisher: Verein zur Förderung des Open Access Publizierens in den Quantenwissenschaften.
URL <https://quantum-journal.org/papers/q-2024-07-30-1427/>

[38] R. Acharya, I. Aleiner, R. Allen, T. I. Andersen, M. Ansmann, F. Arute, K. Arya, A. Asfaw, J. Atalaya, R. Babbush, D. Bacon, J. C. Bardin, J. Basso, A. Bengtsson, S. Boixo, G. Bortoli, A. Bourassa, J. Bovaard, L. Brill, M. Broughton, B. B. Buckley, D. A. Buell, T. Burger, B. Burkett, N. Bushnell, Y. Chen, Z. Chen, B. Chiaro, J. Cogan, R. Collins, P. Conner, W. Courtney, A. L. Crook, B. Curtin, D. M. Debroy, A. Del Toro Barba, S. Demura, A. Dunsworth, D. Eppens, C. Erickson, L. Faoro, E. Farhi, R. Fatemi, L. Flores Burgos, E. Forati, A. G. Fowler, B. Foxen, W. Giang, C. Gidney, D. Gilboa, M. Giustina, A. Grajales Dau, J. A. Gross, S. Habegger, M. C. Hamilton, M. P. Harrigan, S. D. Harrington, O. Higgott, J. Hilton, M. Hoffmann, S. Hong, T. Huang, A. Huff, W. J. Huggins, L. B. Ioffe, S. V. Isakov, J. Iveland, E. Jeffrey, Z. Jiang, C. Jones, P. Juhas, D. Kafri, K. Kechedzhi, J. Kelly, T. Khattar, M. Khezri, M. Kieferová, S. Kim, A. Kitaev, P. V. Klimov, A. R. Klots, A. N. Korotkov, F. Kostritsa, J. M. Kreikebaum, D. Landhuis, P. Laptev, K.-M. Lau, L. Laws, J. Lee, K. Lee, B. J. Lester, A. Lill, W. Liu, A. Locharla, E. Lucero, F. D. Malone, J. Marshall, O. Martin, J. R. McClean, T. McCourt, M. McEwen, A. Megrant, B. Meurer Costa, X. Mi, K. C. Miao, M. Mohseni, S. Montazeri, A. Morvan, E. Mount, W. Mruczkiewicz, O. Naaman, M. Neeley, C. Neill, A. Nersisyan, H. Neven, M. Newman, J. H. Ng, A. Nguyen, M. Nguyen, M. Y. Niu, T. E. O'Brien, A. Opremcak, J. Platt, A. Petukhov, R. Potter, L. P. Pryadko, C. Quintana, P. Roushan, N. C. Rubin, N. Saei, D. Sank, K. Sankaragomathi, K. J. Satzinger, H. F. Schurkus, C. Schuster, M. J. Shearn, A. Shorter, V. Shvarts, J. Skrzyni, V. Smelyanskiy, W. C. Smith, G. Sterling, D. Strain, M. Szalay, A. Torres, G. Vidal, B. Villalonga, C. Vollgraff Heidweiller, T. White, C. Xing, Z. J. Yao, P. Yeh, J. Yoo, G. Young, A. Zalcman, Y. Zhang, N. Zhu, Google Quantum AI, **Suppressing quantum errors by scaling a surface code logical qubit**, Nature 614 (7949) (2023) 676–681, publisher: Nature Publishing Group.
URL <https://www.nature.com/articles/s41586-022-05434-1>

[39] Google Quantum AI and Collaborators, **Quantum error correction below the surface code threshold**, Nature 638 (8052) (2025) 920–926, publisher: Nature Publishing Group.
URL <https://www.nature.com/articles/s41586-024-08449-y>

[40] B. L. Brock, S. Singh, A. Eickbusch, V. V. Sivak, A. Z. Ding, L. Frunzio, S. M. Girvin, M. H. Devoret, **Quantum Error Correction of Qudits Beyond Break-even**, arXiv:2409.15065 [quant-ph] (Oct. 2024).
URL <http://arxiv.org/abs/2409.15065>

[41] J. Hastrup, K. Park, J. B. Brask, R. Filip, U. L. Andersen, **Measurement-free preparation of grid states**, npj Quantum Information 7 (1) (2021) 1–8, publisher: Nature Publishing Group.
URL <https://www.nature.com/articles/s41534-020-00353-3>

[42] J. Hastrup, M. V. Larsen, J. S. Neergaard-Nielsen, N. C. Menicucci, U. L. Andersen, **Unsuitability of cubic phase gates for non-Clifford operations on Gottesman-Kitaev-Preskill states**, Physical Review A 103 (3) (2021) 032409, publisher: American Physical Society.
URL <https://link.aps.org/doi/10.1103/PhysRevA.103.032409>

[43] I. Rojkov, P. M. Röggla, M. Wagener, M. Fontboté-Schmidt, S. Welte, J. Home, F. Reiter, **Two-Qubit Operations for Finite-Energy Gottesman-Kitaev-Preskill Encodings**, Physical Review Letters 133 (10) (2024) 100601, publisher: American Physical Society.
URL <https://link.aps.org/doi/10.1103/>

PhysRevLett.133.100601

[44] J. Hastrup, K. Park, R. Filip, U. L. Andersen, **Unconditional Preparation of Squeezed Vacuum from Rabi Interactions**, Physical Review Letters 126 (15) (2021) 153602, publisher: American Physical Society.
URL <https://link.aps.org/doi/10.1103/PhysRevLett.126.153602>

[45] J. Hastrup, U. L. Andersen, **Improved readout of qubit-coupled Gottesman–Kitaev–Preskill states**, Quantum Science and Technology 6 (3) (2021) 035016, publisher: IOP Publishing.
URL <https://dx.doi.org/10.1088/2058-9565/ac070d>

[46] H. K. Cummins, G. Llewellyn, J. A. Jones, **Tackling systematic errors in quantum logic gates with composite rotations**, Physical Review A 67 (4) (2003) 042308, publisher: American Physical Society.
URL <https://link.aps.org/doi/10.1103/PhysRevA.67.042308>

[47] R. Tycko, H. M. Cho, E. Schneider, A. Pines, **Composite pulses without phase distortion**, Journal of Magnetic Resonance (1969) 61 (1) (1985) 90–101.
URL <https://www.sciencedirect.com/science/article/pii/0022236485902707>

[48] G. H. Low, T. J. Yoder, I. L. Chuang, **The methodology of resonant equiangular composite quantum gates**, Physical Review X 6 (4) (2016) 041067, arXiv:1603.03996 [quant-ph].
URL <http://arxiv.org/abs/1603.03996>

[49] G. H. Low, **Quantum signal processing by single-qubit dynamics**, Thesis, Massachusetts Institute of Technology, accepted: 2018-04-27T18:10:33Z (2017).
URL <https://dspace.mit.edu/handle/1721.1/115025>

[50] B. Németh, B. Kövér, B. Kulcsár, R. B. Miklósi, A. Gilyén, **On variants of multivariate quantum signal processing and their characterizations**, arXiv:2312.09072 [quant-ph] (Dec. 2023).
URL <http://arxiv.org/abs/2312.09072>

[51] W.-L. Ma, M. Zhang, Y. Wong, K. Noh, S. Rosenblum, P. Reinhold, R. J. Schoelkopf, L. Jiang, **Path-Independent Quantum Gates with Noisy Ancilla**, Physical Review Letters 125 (11) (2020) 110503, publisher: American Physical Society.
URL <https://link.aps.org/doi/10.1103/PhysRevLett.125.110503>

[52] W.-L. Ma, S.-S. Li, L. Jiang, **Algebraic structure of path-independent quantum control**, Physical Review Research 4 (2) (2022) 023102, publisher: American Physical Society.
URL <https://link.aps.org/doi/10.1103/PhysRevResearch.4.023102>

[53] J. R. Johansson, P. D. Nation, F. Nori, **QuTiP 2: A Python framework for the dynamics of open quantum systems**, Computer Physics Communications 184 (4) (2013) 1234–1240.
URL <https://www.sciencedirect.com/science/article/pii/S0010465512003955>

[54] B. d. Neeve, T.-L. Nguyen, A. Ferk, T. Behrle, F. Lancellotti, M. Simoni, S. Welte, J. Home, **Modular variable laser cooling for efficient entropy extraction**, arXiv:2408.16128 [quant-ph] (Aug. 2024).
URL <http://arxiv.org/abs/2408.16128>

[55] M. Mirrahimi, Z. Leghtas, V. V. Albert, S. Touzard, R. J. Schoelkopf, L. Jiang, M. H. Devoret, **Dynamically protected cat-qubits: a new paradigm for universal quantum computation**, New Journal of Physics 16 (4) (2014) 045014, publisher: IOP Publishing.
URL <https://dx.doi.org/10.1088/1367-2630/16/4/045014>

[56] D. Gottesman, A. Kitaev, J. Preskill, **Encoding a qubit in an oscillator**, Physical Review A 64 (1) (2001) 012310, publisher: American Physical Society.
URL <https://link.aps.org/doi/10.1103/PhysRevA.64.012310>

[57] M. Paris, J. Řeháček (Eds.), **Quantum State Estimation**, Vol. 649 of Lecture Notes in Physics, Springer, Berlin, Heidelberg, 2004.
URL <http://link.springer.com/10.1007/b98673>

[58] L. Sun, A. Petrenko, Z. Leghtas, B. Vlastakis, G. Kirchmair, K. M. Sliwa, A. Narla, M. Hatridge, S. Shankar, J. Blumoff, L. Frunzio, M. Mirrahimi, M. H. Devoret, R. J. Schoelkopf, **Tracking photon jumps with repeated quantum non-demolition parity measurements**, Nature 511 (7510) (2014) 444–448, publisher: Nature Publishing Group.
URL <https://www.nature.com/articles/nature13436>

[59] D. J. Wineland, **Nobel Lecture: Superposition, entanglement, and raising Schrödinger's cat**, Reviews of Modern Physics 85 (3) (2013) 1103–1114, publisher: American Physical Society.
URL <https://link.aps.org/doi/10.1103/RevModPhys.85.1103>

[60] B. Royer, S. Singh, S. Girvin, **Stabilization of Finite-Energy Gottesman–Kitaev–Preskill States**, Physical Review Letters 125 (26) (2020) 260509, publisher: American Physical Society.
URL <https://link.aps.org/doi/10.1103/PhysRevLett.125.260509>

[61] A. J. Brady, A. Eickbusch, S. Singh, J. Wu, Q. Zhuang, **Advances in bosonic quantum error correction with Gottesman–Kitaev–Preskill Codes: Theory, engineering and applications**, Progress in Quantum Electronics 93 (2024) 100496.
URL <https://www.sciencedirect.com/science/article/pii/S0079672723000459>

[62] T. Matsuura, H. Yamasaki, M. Koashi, **Equivalence of approximate Gottesman–Kitaev–Preskill codes**, Physical Review A 102 (3) (2020) 032408, publisher: American Physical Society.
URL <https://link.aps.org/doi/10.1103/PhysRevA.102.032408>

[63] C. K. Law, J. H. Eberly, **Arbitrary Control of a Quantum Electromagnetic Field**, Physical Review Letters 76 (7) (1996) 1055–1058, publisher: American Physical Society.
URL <https://link.aps.org/doi/10.1103/PhysRevLett.76.1055>

[64] J. Hastrup, K. Park, J. B. Brask, R. Filip, U. L. Andersen, **Universal Unitary Transfer of Continuous-Variable Quantum States into a Few Qubits**, Physical Review Letters 128 (11) (2022) 110503, publisher: American Physical Society.
URL <https://link.aps.org/doi/10.1103/PhysRevLett.128.110503>

[65] S. Puri, A. Grimm, P. Campagne-Ibarcq, A. Eickbusch, K. Noh, G. Roberts, L. Jiang, M. Mirrahimi, M. H. Devoret, S. Girvin, **Stabilized Cat in a Driven Nonlinear Cavity: A Fault-Tolerant Error Syndrome Detector**, Physical Review X 9 (4) (2019) 041009, publisher: American Physical Society.

URL <https://link.aps.org/doi/10.1103/PhysRevX.9.041009>

[66] A. Grimm, N. E. Frattini, S. Puri, S. O. Mundhada, S. Touzard, M. Mirrahimi, S. M. Girvin, S. Shankar, M. H. Devoret, *Stabilization and operation of a Kerr-cat qubit*, *Nature* 584 (7820) (2020) 205–209, publisher: Nature Publishing Group.
URL <https://www.nature.com/articles/s41586-020-2587-z>

[67] A. Z. Ding, B. L. Brock, A. Eickbusch, A. Koottandavida, N. E. Frattini, R. G. Cortinas, V. R. Joshi, S. J. d. Graaf, B. J. Chapman, S. Ganjam, L. Frunzio, R. J. Schoelkopf, M. H. Devoret, *Quantum Control of an Oscillator with a Kerr-cat Qubit*, arXiv:2407.10940 [quant-ph] (Jul. 2024).
URL <http://arxiv.org/abs/2407.10940>

[68] B. J. Chapman, S. J. de Graaf, S. H. Xue, Y. Zhang, J. Teoh, J. C. Curtis, T. Tsunoda, A. Eickbusch, A. P. Read, A. Koottandavida, S. O. Mundhada, L. Frunzio, M. Devoret, S. Girvin, R. Schoelkopf, *High-On-Off-Ratio Beam-Splitter Interaction for Gates on Bosonically Encoded Qubits*, *PRX Quantum* 4 (2) (2023) 020355, publisher: American Physical Society.
URL <https://link.aps.org/doi/10.1103/PRXQuantum.4.020355>

[69] Q. Xu, P. Zeng, D. Xu, L. Jiang, *Fault-Tolerant Operation of Bosonic Qubits with Discrete-Variable Ancillae*, *Physical Review X* 14 (3) (2024) 031016, publisher: American Physical Society.
URL <https://link.aps.org/doi/10.1103/PhysRevX.14.031016>

[70] Y. Lu, A. Maiti, J. W. O. Garmon, S. Ganjam, Y. Zhang, J. Claes, L. Frunzio, S. M. Girvin, R. J. Schoelkopf, *High-fidelity parametric beamsplitting with a parity-protected converter*, *Nature Communications* 14 (1) (2023) 5767.
URL <https://www.nature.com/articles/s41467-023-41104-0>

[71] N. Liu, J. Thompson, C. Weedbrook, S. Lloyd, V. Vedral, M. Gu, K. Modi, *Power of one qumode for quantum computation*, *Physical Review A* 93 (5) (2016) 052304, publisher: American Physical Society.
URL <https://link.aps.org/doi/10.1103/PhysRevA.93.052304>

[72] G. A. Baker, P. Graves-Morris, *Padé Approximants*, 2nd Edition, Encyclopedia of Mathematics and its Applications, Cambridge University Press, Cambridge, 1996.
URL <https://www.cambridge.org/core/books/pade-approximants/A98B8DD2AFC0AF094EB6BF96C5C77A06>